Probing Flocculation of Polyaromatic Compounds and Asphaltene Subfractions Using DLS

by

Xi Wang

A thesis submitted in partial fulfillment of the requirements for the degree of

Master of Science

in

Chemical Engineering

Department of Chemical and Materials Engineering

University of Alberta

Abstract

In this research, flocculation of fractionated asphaltenes was studied using dynamic light scattering (DLS). Three asphaltene fractions were obtained based on its adsorption characteristics onto calcium carbonate. The DLS results showed that the irreversibly-adsorbed asphaltenes (Irr-Ads), containing the highest number of polar groups, was the fraction responsible for the observed flocculation of whole asphaltenes. To better understand the aggregation behavior of asphaltenes, flocculation of three polyaromatic compounds (PAs), N-(1-hexylhepyl)-N'-(5-carboxylicpentyl)-perylene-3, 4, 9, 10-tetracarboxilicbisimide (C5Pe), N-(1-undecyldodecyl)-N'-(5-carboxylicpentyl)-perylene-3,4,9,10-tetracarboxylbisimide (C5PeC11) and N,N'-bis(1-undecyldodecyl)perylene-3,4,9,10-tetracarboxylbisimide (BisAC11) was further studied using DLS. The findings corresponded well with the results of studying nanoaggregation using electron spray ionization mass spectroscopy (ESI-MS). The flocculation of polyaromatic compound was found to be enhanced by increasing heptane content in the solvent. Among the three polyaromatic compounds studied, C5PeC11 showed similar flocculation kinetics to the Irr-Ads asphaltenes. Experiments using mixed PA compounds showed reduced flocculation tendency of C5PeC11 under otherwise identical solution conditions. The presence of polar groups in polyaromatic compounds was shown to be important in accelerating the flocculation of PA compounds beyond nano-scales. The results from molecular dynamics simulation study suggests that π-π stacking between polyaromatic cores, hydrogen bonds from polar groups and tail-tail interactions among aliphatic chains are all important to aggregation of PA (asphaltene) molecules. Taken together, this study provides a scientific basis for future manipulations of polyaromatic compounds aggregation and sheds light on understanding the flocculation onset of asphaltenes in crude oil.

Preface

The research conducted for this thesis forms part of a research collaboration, led by Professor Zhenghe Xu at University of Alberta and Professor Johan Sjoblom at NTNU. Asphaltene fractionation methods were developed by Sjoblom group at NTNU. Asphaltene fractions and all synthesized model compounds were provided by Sjoblom group. Dr. Lan Liu provided mass spectroscopy data in Chapter 5. Rongya Zhang provided MD simulation data in Chapter 5. I conducted all DLS optimization, experiments and data analysis in Chapters 4 and 5. The concluding analysis in Chapters 4 and 5 are my original work, as well as the literature review in Chapters 1, 2 and 3.

Parts of the thesis in Chapters 4 and 5 are being considered for two publications. I was responsible for the DLS data collection and analysis as well as the manuscript composition. Professor Zhenghe Xu was the supervisory author and was involved in revision of the manuscripts.

Acknowledgements

I would like to thank my supervisor Dr. Zhenghe Xu for his guidance and support throughout my M.Sc. project. I would like to thank Dr. Erica Pensini, Dr. Lan Liu, Dr. Simon Ivar Andersen, Dr. M. Sharath Chandra and Dr. Zuoli Li for their insightful suggestions, which facilitated the progress of this project.

I am very thankful to Dr. Johan Sjöblom and Dr. Sebastien Simon at NTNU for providing the asphaltene model compounds and fractionated asphaltenes. I appreciate the help from Mr. Jim Skwarok, Ms. Jie Ru and Ms. Lisa Carreiro for their assistance with my work. My appreciation also goes to the entire Oil Sands Extraction research group for their help and suggestions with my work. I would like to thank the NSERC Industrial Research Chair in Oil Sands Engineering for financial support.

To my beloved grandmother the late Xiangzao Bie, without your love, prayers and support, I would not be the person I am today.

Table of Contents

List of Figures

List of Tables

Chapter 1 Introduction

1.1 Canadian Oil Sands Overview

Crude oil production has been playing a pivotal role in fueling world economy and technology development. Despite the protracted downturn in oil prices, Canada remains the sixth largest oil producer in the world, hitting 3.5 Mbbl/d production rate in 2015.[1]

Oil sands are a form of petroleum in a semi-solid state, whose existence has been known for centuries. In 2014, more than half of Canadian crude oil and liquids fossil fuels production came from oil sands deposits and the number is expected to grow in the future.[2] There are three major oil sands deposits located in western Canada: Athabasca, Cold Lake and Peace River covering a total of 140,200 square kilometers.[3] Together these oil sands deposits account for 97% of oil reserves in Alberta.

The crude bitumen contained in Canadian oil sands is a highly viscous mixture of hydrocarbons.[4] Similar to other types of unconventional hydrocarbon resources, bitumen is rich in complex heavy organic molecules. In its natural state, bitumen is not recoverable using traditional production methods due to its extremely viscous nature.[5] Currently two methods are used predominately in oil sands extraction: traditional open pit mining for shallow formation and in-situ thermal production such as steam assisted gravity drainage (SAGD) for deeper formations.[2] In 2014, about 42% of bitumen produced from Canadian oil sands was by the open-pit mining method.

In surface mining operations, water- in-bitumen emulsions (also known as froth) are obtained. Froth treatment is then required to separate the aqueous and solid contaminants from the emulsion or froth to produce clean and diluted bitumen products. There are two major technologies used for froth treatment. In the conventional method, naphtha is used as the diluent to assist separation of solid and emulsified water from diluted bitumen. With a relatively low solvent-to-bitumen ratio (typically ~ 0.7), the separation can be further enhanced through chemical or demulsifier addition at elevated temperatures (~ 80 °C). The diluted bitumen product contains 2-5 wt% water and 0.5-1 wt% solids. Due to the high level of contaminants, the obtained bitumen product is usually not suitable for pipelining or direct refining. Further upgrading (high temperature cracking) is performed using a coker unit and/or hydrotreating to produce synthetic crude oil. [6][7]

The second method is the paraffinic froth treatment, which was developed only recently in 1990. Twice amount of paraffinic diluent is added to bitumen froth for viscosity and density reduction. During this process, approximately 1/3 of the asphaltenes contained in bitumen precipitate out, achieving partial upgrading of bitumen. Meanwhile, emulsified water droplets and fine solids are also phased out together with asphaltene precipitates acting as flocculants. In the paraffinic froth treatment, the quality of the resultant bitumen products is greatly enhanced. Compared with the naphthenic treatment, bitumen product from paraffinic froth treatment contains only ~ 550-800 ppmw (parts per million weight) solids and 100-300 ppmw water. [8] In addition, the content of asphaltene, which contributes to high viscosity in bitumen can also be significantly lowered.

Though new technologies have dramatically increased the efficiency in oil sands processing, numerous challenges remain in order to meet the global demand for fossil fuel energy and petrochemical products. To develop better methods and tackle the emerging problems associated

with crude oil extraction, a more comprehensive and systematic understanding of the inherent properties and interactions between various crude oil components is required.

1.2 Bitumen Characterization

The ballooning interest in detailed and quantitative measurements of bitumen or crude oil has spawned a new field of 'petroleomics', which identifies constituents in naturally occurring crude oil. [9] The recent development in high resolution analytical instruments such as GC-GC, FT-ICR-MS, NMR, ESI-MS, DLS, etc. facilitates the identification of elemental components in complexed mixtures.[10][11] These techniques have contributed significantly to advancing the knowledge in connecting the inherent structural and chemical property of bitumen components to bulk and interfacial behaviors such as aggregation and precipitation propensity, emulsion stability, and solubility characteristics. To further advance the field by performing such analysis, a basic separation (fractionation) of heavy oil has been practiced. One of the well-known separation protocols based on the varying polarizability and polarity of different components is the SARA (Saturates, Aromatics, Resins, Asphaltene) analysis. The general schematic diagram of SARA fractionation is shown on Fig. 1.1.

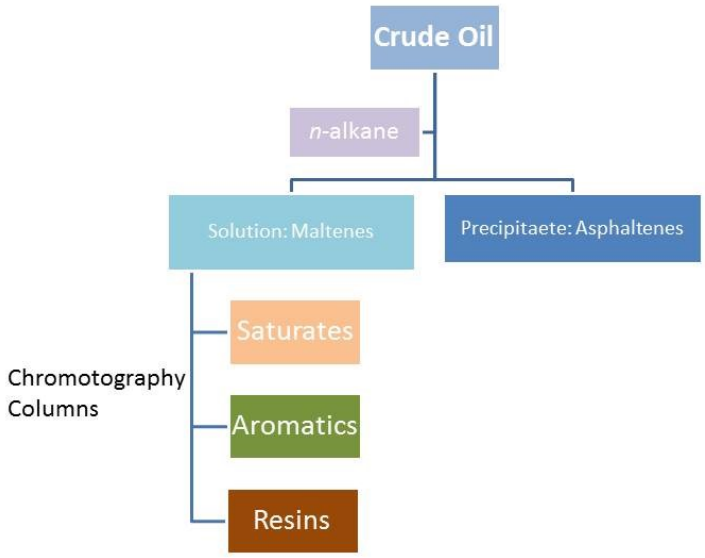

Figure 1.1 Schematic flow chart of SARA analysis. The standard protocol is described in ASTM D6560-00.

Based on SARA analysis, asphaltenes are classified as the fraction in bitumen that are insoluble in paraffinic solvents such as heptane, hexane or pentane but soluble in aromatic solvents such as toluene. Therefore, as seen in the paraffinic froth treatment, when paraffinic solvents are added into the crude bitumen, asphaltenes are the first to precipitate out.[12] The remaining de-asphalted bitumen is referred to as maltenes. The column chromatography is used for further separation of the remaining components into resins, aromatics and saturates. It should be noted that, for SARA analysis, the amount and properties of separated asphaltenes are dependent on the choice of the solvent as well as separation protocols. For Alberta Athabasca bitumen, typical SARA analysis results reported in literature are shown in Table 1.1.

Table 1.1 SARA Composition of Alberta Athabasca Bitumen [13][14]

SARA Fraction	Contain (wt%)
Asphaltenes	12.7-17.5
Aromatics	34.8-39.8
Resin	26.4-38
Saturates	14.5-17.3

Since asphaltene is defined as a solubility class, they consist of thousands of chemical species whose properties are not very well defined. It is known that asphaltenes are composed of condensed polyaromatic rings with aliphatic side chains and heteroatoms such as oxygen, nitrogen, sulfur and metals (primarily nickel and vanadium).[15] Structural building blocks such as fluorenes, cyclic sulfides, *n*-alkyl chains, alkyl benzenes, etc. have also been identified. [16] Despite their complex molecular properties and undefined chemical structures, asphaltenes are an important crude oil fraction due to their propensity to aggregate. In particular, the complex properties of asphaltenes render them one of the most enigmatic components in crude oil. [17]

1.3 Asphaltenes in Crude Oil Production

The propensity of asphaltenes to aggregate, flocculate, precipitate and adsorb onto various surfaces has posed great challenges to oil processing industries. However, it should be noted that the mere presence of asphaltenes does not necessarily portend aggregation related problems. Heavy oil, for example, containing the highest asphaltene concentrations, for example, is usually

stable during production stages and does not lead to pipeline clogging issues.[17] In fact, asphaltene-induced precipitation is more commonly observed in lighter oils. During the various stages of crude oil processing, fluid properties such as pressure, temperature, and composition vary greatly. As a result, asphaltene precipitate may build up along production systems, adhering to formation grains, pumps, tubulars, safety valves and flowlines. Eventually thick deposit of asphaltenes could lead to problems in well production, pipeline transfer, and land-and sea-based transportations.[17] In downstream oil refining stages, the flocculated asphaltenes accumulate during visbreaking and catalytic hydrocracking processes, resulting in the formation of sludge and sedimentations. Asphaltene adsorption onto cracking beds can also reduce the efficiency of both catalytic cracking and hydro-pyrolysis.

In addition, asphaltene nanoaggregates at the oil/water interface is responsible for the formation of rigid interfacial films resulting in stabilized water-in-oil emulsions.[18] The rigid skin-like structures at the interface can survive from multiple washings and have high compressional energy, decreasing the probability of water droplets coalescence. The dissolved salts in the emulsified water droplet can cause catalysts poisoning of downstream refining, scaling and pipeline corrosion.[19] Stable water-in-oil emulsions also incur higher costs in the transportation and refining processes due to increased volume to handle. Therefore many researches have been devoted to understanding the molecular association of asphaltenes to better predict and mitigate their negative impacts on petroleum production.

1.4 Thesis Objective and Organization

Previous research has found photon correlation spectroscopy also known as dynamic light scattering (DLS) a suitable technique to monitor the aggregation and flocculation properties of asphaltenes in crude oil. [20] However the complex and heterogeneous composition of asphaltenes render their aggregation and colloidal behaviors non-uniform.[21] In this research, asphaltenes were fractionated based on their adsorption onto calcium carbonate. [22] The flocculation behaviors of three asphaltene sub-fractions were studied using DLS. In addition, well- defined model systems containing single polyaromatic compound were also tested.[23] The aim of this research is to study the aggregation behaviors of various asphaltene sub-fractions and model compounds C5Pe/ C5PeC11 / BisAC11 with well-defined molecular structures. By comparing their physiochemical properties, it is the objective of this study to achieve the main goal of petroleomics while making a link between the inherent molecular structure and observed flocculation behaviors. Polydispersity effects were investigated by studying binary and tertiary mixtures of polyaromatic model compounds. Furthermore, the effects of asphaltene aggregation inhibitors such as DBSA were also studied.

Chapter 1 gives a brief introduction of the production of Canadian oil sands. Basic knowledge of crude oil fractionation and asphaltene properties are provided. Adverse effects of asphaltene aggregation encountered in various stages of crude oil processing are discussed.

Chapter 2 reviews the literature on the reported asphaltene model compounds and asphaltene aggregation kinetics. The use of light scattering technique in studying crude oil aggregation and colloidal properties is reviewed.

Chapter 3 gives a more precise review of the DLS technique used for the thesis. However it is not the intention of this study to dig into the theoretical background of DLS instrumentation. Since all measurements were conducted using a commercially available DLS, theories related to its use will only be presented in part for the purpose of data analysis required in this work.

Chapter 4 describes the materials and setups of experiments conducted in this study. Asphaltene fractionation methods developed by Prof. Sjöblom group at NTNU are briefly discussed. For DLS measurements, various experimental conditions were screened including measurement time, light scattering angle, solution concentrations, etc. to optimize the experimental condition to be used for the bulk of this research. All experiments followed the same optimized conditions unless otherwise stated.

Chapter 5 presents the dynamic aggregation behaviors for both asphaltene sub-fractions and model compounds. Results on the effects of solvent, aggregation inhibitors and polydispersity are discussed and compared between asphaltene sub-fractions and model compounds.

Chapter 6 provides a general summary of the work presented in this thesis and recommendations for future study in related areas.

Chapter 2 Literature Review

2.1 Asphaltene Aggregation

As mentioned before, asphaltene aggregation has caused great problems in oil industries. Production shutdown is often required in the field to remediate asphaltene deposition issues.

However, in many circumstances, shutdown in production only proved to be partially effective.[24] Therefore, the economic and technology incentives behind the prediction and prevention of deposit formation are enormous. In order to obtain a better understanding of the factors that promote asphaltene aggregation, basic concepts are first reviewed.

2.1.1 Asphaltene Molecular Structure

Due to the complex nature of asphaltenes, accurate molecular structures are difficult to be determined. So far, two competing models have been proposed to describe the molecular architectures in asphaltenes. In the archipelago model, different aromatic moieties or polycyclic aromatic hydrocarbon structures (PAHs) bridge together via aliphatic chains. In contrast, the island model suggests structures of a single aromatic core (constructed with several interconnected aromatic rings) together with aliphatic side chains on the peripheral. Figure 2.1 provides two examples of proposed model compounds with archipelago (a) and island (b) structures respectively.

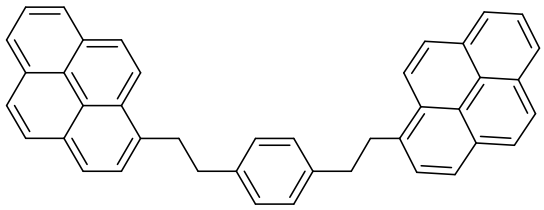

(a) Archipelago Model Compound
1,4-Bis(2-Pyren-1-yl-thyl)-benzene

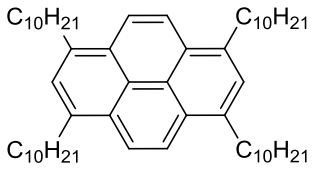

(b) Island Model Compound
1,3,6,8-tetradecyl pyrene

Figure 2.1 Examples of Archipelago (a) and Island (b) model compounds reported in previous literature. [25]

Previous studies based on bulk decomposition experiments of asphaltenes have concluded that the archipelago model compounds are possibly more representative of real asphaltenes. [26] More specifically, the small aromatic groups detected during decomposition can only be generated from highly condensed aromatic moieties. [27–30] More recent results also suggest the common pyrolysis/ cracking conditions are suitable for addition reactions which yield aryl-aryl linkages or larger fused ring products. As a result, islands-like model compounds can be easily converted to archipelago structures under pyrolysis reaction conditions. [31]

In addition, the presence of island structures in asphaltenes has been proved using various techniques. Time resolved fluorescence depolarization (TRFD) studies have shown the fast rotational diffusion of asphaltene chromophores, confirming lower degree of cross linkages.[32,33] Laser desorption laser ionization mass spectra results showed similar fragmentation behaviors of asphaltene and island model compounds. [34]Microscopic imaging such as scanning tunneling microscopy[35], high-resolution electron transmission microscopy[36] and Raman spectroscopy [37] have all reviewed the island structures being the dominant structure in asphaltene molecules. In addition, island structures are believed to be more stable compared to archipelago structures, which can be decomposed at elevated temperatures or at bio-degradation conditions. Therefore in recent years, the island structures of asphaltene molecules have been more wildly accepted.

One of the important parameters for asphaltene characterization is its average molecular weight. Though various techniques have been used, limitations exist that hamper more accurate measurements. Some of the previous reported methods are listed below.

Vapor pressure osmometry (VPO) has been wildly used for molecular weight determination in light hydrocarbon compounds. The principle behind VPO is based on the number concentration of the species of interest in a particular solution. However, to obtain accurate MW of asphaltene molecules, a more concentrated solution is required which induces nanoaggregation at the same time. As a result, the value obtained from VPO is more consistent with the MW for asphaltene nanoaggregates under particular concentrations.[17] Another commonly used technique for molecular weight measurements especially for large bio molecules such as DNA and protein is the size exclusion chromatography (SEC) or gel permeation chromatography (GPC). However the direct application of such techniques to asphaltene molecules results in some serious problems. Since asphaltene aggregation states within the column are unknown, the measured values cannot be assigned as that of single asphaltene molecules. In addition, no standard procedures exist for asphaltenes to convert their column retention time to molecular weights directly.[38,39] Therefore inconsistent MW values have been reported for asphaltenes using chromatography techniques. [40]

Recently, new instrumentations are employed for asphaltene MW measurements. The two main techniques are mass spectrometry and molecular diffusion. In mass spectrometry, ionization of molecules produces the charge-to-mass ratio distributions, which is used for MW calculations. The most successful example is the use of laser desorption/ ionization mass spectroscopy (LDI MS). However, unreliable and inconsistent results are obtained due to gas-phase aggregation induced by experimental conditions. [41,42] On the other hand, for the molecular diffusion method, asphaltene MW were estimated indirectly by comparing its diffusion properties with that of model compounds. Despite many efforts that have been devoted, current technology limitations have become the bottleneck debilitating more accurate determinations of asphaltene

molecular weights. In light of the solubility classification of asphaltenes, a more comprehensive picture starts to emerge that includes valuable results from several different measurement sources. [17] Currently a universally accepted asphaltene molecular weight is around 750 g/mol with a range of 300 to 1400 g/mol, which is consistent with a molecule containing seven or eight fused aromatic rings. [43,44]

2.1.2 Asphaltene Aggregation

When dissolved in organic solvents, asphaltene molecules interact with each other to form more complicated structures. The polyaromantic hydrocarbon (PAH) cores sit at the center of asphaltene molecules and are primary sites for intermolecular attractions, which originate from various sources such as London dispersion forces, π-π stacking, etc. On the other hand, the alkane chains on the peripheral of the PAH cores interact with each other resulting in steric repulsions. As a result, the net interactions obtained as a balance between intermolecular attractions and repulsions determine asphaltene aggregation behaviors.[45] This is consistent with the Yen model proposed fifty years ago where the stacking structures of asphaltenes are suggested.[46]

Studies using X-ray scattering (SAXS) and small-angle neutron scattering (SANS) have confirmed that in its natural state, asphaltenes are dispersed as nano-sized particles in crude oil. [47,48] High quality (high-Q) ultrasonic studies were the first to experimentally measure the critical nanoaggregation concentration of asphaltenes dissolved in toluene solutions (CNAC). The transition concentration for asphaltenes from a true molecular solution to nanoaggregates is narrow (~ 10^{-4} mass fraction) with small aggregate numbers. [49] Later, direct current (DC)

conductivity measurements confirm the results from high-Q ultrasonic studies. A comparison of conductivity at concentrations below and above CNAC indicates that the aggregation number is possibly small (<10).[50] To confirm the results, NMR measurements were conducted and a change in the rotational relaxation at CNAC concentrations can be observed.[51] Centrifugation experiments also show an increase in the fraction of sedimentation at above CNAC concentrations.[52,53] Other analysis such as SANS, Langmuir-Blodgett film studies, atomic force microscopy measurements and surface-compression analysis of asphaltenes in toluene confirm the estimate of 10 as the nanoaggregation number.[54,55]

It is believed at concentrations below CNAC, asphaltene molecules in toluene are dispersed as a true solution. When asphaltene concentration increases above the CNAC, molecules start to stick together to form nanoaggregates or nanometer sized molecules. [56] However, it should be noted that the CNAC value depends on the characteristics of both asphaltenes as well as the solvent used for their stabilization. Asphaltenes obtained from different sources may have different CNAC values.

Upon the formation of small nanoaggregates, secondary aggregation process takes off at significantly higher concentrations than CNAC. This stage is usually referred to as the clustering of nanoaggregates, where asphaltene nanoclusters are formed. In this stage, it is believed that the presence of π-stacking renders the nanoaggregates relatively tightly bound. However, for larger clusters formed of nanoaggregates, π-stacking is less common due to steric hindrance. [40]

Photon correlation spectroscopy studies show for this secondary aggregation process, a critical clustering concentration (CCC) exists, at which dramatic changes in flocculation kinetics occur. Below the asphaltenes/toluene concentration of several grams per liter, asphaltene flocculation

induced by heptane addition is governed by the diffusion-limited aggregation (DLA). At higher concentrations, flocculation process undergoes a transition to reaction limited aggregation kinetics (RLA).[57] DC conductivity experiments confirm that at CCC, a break in the conductivity curve can be observed.[51] This is also in agreement with asphaltene flocculation determinations using near-infrared spectroscopy.[58]

The onset point of asphaltene flocculation depends primarily on the refractive index of the solution or molecular polarizations within different systems. [40] Therefore, it can be concluded that the dominant forces governing asphaltene precipitation is the London dispersion contributing to the van der Waals forces. [59] This is consistent with the hierarchical asphaltene aggregation model in the modified Yen-Mullin model as shown in Fig. 2.2. In this model, asphaltene nanoaggregates are composed of six asphaltene molecules, where asphaltene clusters contain up to eight nanoaggregates. [60]

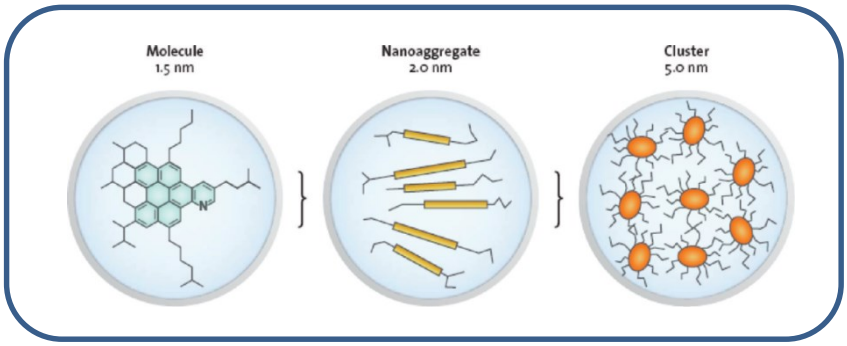

Figure 2.2 The previously reported Yen-Mullins model. The proposed nanoaggregate and cluster structures are shown in this model. This model proposes that the "island" molecular architecture dominates with one large aromatic ring system per asphaltene molecule. Aggregation numbers for nanoaggregates as well as clusters are small (<10) in this model. [60][45][61][34][46]

2.1.3 Asphaltene Precipitation

The nanocolloidal suspension of asphaltenes is usually stable in crude oil. However during reservoir production, the sudden change in temperature, pressure, solvent combination could render this suspension destabilized, resulting in asphaltene precipitation. The common reference to predict such precipitation is known as the asphaltene precipitation envelope (APE). In fact, asphaltene precipitation is most likely to occur when light crude oils that are highly unsaturated with gas are suddenly depressurized.[62] Typically, the amount of precipitated asphaltenes increase as the reservoir pressure drops, reaching a maximum at the bubble-point pressure.[17] It has been found that the flocculated asphaltenes differ greatly in properties. When pressure is set only slightly below the onset pressure, small asphaltene flocs of 0.9 microns are formed. These flocs are essentially stable in Brownian motion. In contrast, when pressure drops much below the onset point, large flocs (~3 microns) form which settle fast. These big flocs are detrimental since they are sticky due to high glass transition temperature and tend to fall out first. [63,64]

Laboratory studies of crude oil precipitation have been going on for a long time. Techniques such as gravimetric precipitation, acoustic resonance and filtration have been employed to determine the onset pressure of asphaltene precipitation.[65] Other techniques such as optical microscopy, refractive index measurements, UV-Vis spectroscopy, NIR spectroscopy have been used to study the mechanism behind the precipitation processes.[66–68]

When studying the mechanisms behind asphaltene precipitation, time allowed for solution to reach equilibration is important. Earlier studies were performed based on the assumption that the solution equilibrates shortly after precipitant addition. Therefore, the crude oil is considered stable if no flocculation of asphaltene was detected immediately after precipitant addition.

Meanwhile, the concentration of alkane solvent at which asphaltenes precipitate out is defined as the onset concentration.[69–71] In contrast with the instant equilibration assumption, some believe asphaltene equilibration can be a slow process. Experiments conducted by Maqbool *et al.* using optical microscopy and centrifugation-based separation have demonstrated that the time required to precipitate asphaltenes can actually vary from a few minutes to several months, depending on the precipitant concentration used. Therefore, no single concentration can be identified as the critical precipitant concentration for asphaltene precipitation.[72] Both mechanisms are useful in determining the precipitation behaviors of asphaltenes and various models have been proposed to account for the onset of precipitation processes.

In general, there are two approaches to model the asphaltene precipitation process. The solubility approach assumes that asphaltenes are dissolved in crude oil and the precipitation occurs when solubility falls below the threshold level.[73] The colloidal theory approach assumes that asphaltenes exist as colloidal particles stabilized by resins adsorbed on the surface. It is the distribution of resins between the colloidal surface and the surrounding medium that controls the ultimate asphaltene solubility.[74]

Among the two, solubility model is the most accepted one for the prediction of asphaltene precipitation. This approach is mostly based on the assumption that crude oils are consist of two distinct components, asphaltenes and de-asphalted oils. Scatchard or Hildebrand equations are generally used to calculate asphaltene solubility parameters,[75] and cubic EoS theories are employed to predict the properties of de-asphalted oils. Various models were developed based on regular solution theory, Flory-Huggins theory, Scott-Magat theory and etc. One of the earliest models was developed by Hirschbert *et al.* in 1984. In this model, the vapor-liquid equilibrium calculation was first performed to split the crude into vapor and liquid phases. The Flory-Higgins

theory was then employed to calculate asphaltene precipitation amount. [70] This model was based on the assumption that the precipitated asphaltenes do not change the vapor/ liquid equilibrium. [76] The Hirschbert model was successful when predicting the stability of asphaltenes undergoing tertiary CO_2 injection.[77] However, it fails in the prediction of asphaltene precipitation when *n*- alkane was added into the crude. [78]

Another disadvantage of the Hirschbert model is that it does not give the exact asphaltene precipitation amount. In order to obtain a more accurate prediction, Yarranton and Masliyah proposed a model where asphaltenes were treated as a mixture of subfractions with different densities and molar masses. The mixture's solubility was then modeled by the solid-liquid equilibrium.[79] The Yarranton-Masliyah model successfully predicts the asphaltene precipitation quantity and onset point. Later, this model was further modified by Alboudwarej *et al.*[80] In the modified model, asphaltenes were assumed to be macromolecular aggregates of monomers. The molecular mass distributions of asphaltene aggregates follow various distribution functions, such as Schultz-Zimm. The modified model was used successfully to predict asphaltene precipitation for Llyodminster bitumen. In addition, this model also correctly predicts that higher asphaltene precipitates could be obtained upon the addition of *n*-C_8 than *n*-C_7 solvent. However, data obtained using this model was found to deviate from experimental results at high temperatures (100 °C).

The colloidal model is less popular compare to the solubility model. The core concept in this model is the existence of asphaltenes in a colloidal form. According to Pfeiffer and Saal,[81] the heaviest asphaltenes with the greatest molecular weight and the most pronounced aromatic nature are arranged at the center forming a micelle structure. When there're sufficient light constituents such as resins to form the outer regions of the structure, asphaltenes are said to be

peptized. However, when there's a shortage of resins, the mutual attractions between the colloid cores will lead to asphaltene aggregates formation. One of the first models that falls into this category was proposed by Leontaritis and Mansoori in 1987.[82] This thermodynamic model employs a vapor-liquid equilibrium calculation to estimate the liquid phase composition at which asphaltene flocculate. This model is applicable to solutions where asphaltene dissociation occurs and makes good predictions for hexadecane and dodecane solvents. However, the predictions for heptane fitted runs with this model are poor. [82][73] Other thermodynamic models such as Victorov and Firoozabadi model, Pan and Firoozabadi model were also developed. However, compare to the solubility models, the colloidal models were found to be less accurate, but more complex and computationally demanding in nature. [73]

In the past 30 years, both solubility and colloidal models have made great progress in modeling and predicting asphaltene precipitations. Comparisons between various modeling techniques have concluded the use of PC-SAFT EoS is the most promising.[73] Using modeling techniques to predict asphaltene bulk behaviors is becoming more and more important in the industry of crude oil production.

2.1.4 Asphaltene Aggregation Inhibitors

Due to the problems caused by asphaltene aggregation and precipitation, various techniques have been tested for inhibition performance or control of asphaltene precipitation processes. Physical methods such as the change in temperature and pressure require implementation of new infrastructures and therefore are usually not practical for current oil industry. Various kinds of chemical treatments have been studied.

Aromatic based solvents such as toluene or xylene have been used to dissolve asphaltene deposits. Due to the large amount of solvents required, this method is deemed economically infeasible. In addition, periodic solvent injections might alter the physiochemical properties of crude oil.[83] On the contrary, chemical inhibitors are more effective and easier to add, therefore have been regarded as more suitable candidates. These chemical inhibitors have similar properties as petroleum resins and can adsorb to asphaltene surfaces to inhibit further aggregation formations. In general, the common inhibitors have an amphiphilic structure with polar heads and non-polar hydrocarbon chains.

Chang *et al.* investigated a series of alkylbenzene- derived amphiphiles in apolar alkane solvents as the asphaltene stabilizers. Their results showed that the polarity of the amphiphile's head groups and the length of alkyl tails primarily control the effectiveness of asphaltene stabilization. Increasing the acidity of the amphiphile's head groups promote their abilities to stabilize asphaltenes by increasing the acid-base interactions between asphaltenes and amphiphiles. Decreasing amphiphile's tail length increased the asphaltene-amphiphile attraction. However, a minimum tail length needs to be maintained in order for amphiphiles to form stable steric layers around asphaltenes. Change *et al.* revealed that dodecyl benzene sulfonic acid (DBSA) can strongly attach to asphaltene molecules making it one of the most effective aggregation inhibitors.[84,85] In addition, Miller *et al.* suggested ethercarboxylic acid as an effective asphaltene inhibitor in crude oil.[86] Hydrocarbyl-substituted aromatics were used by Gochin and Smith for asphaltene precipitation control.[87] Kraiwattanawong *et al.* compared the effects of dodecyle resorsinol (DR), dodecyle phenol and DBSA with other commercial inhibitors on asphaltene aggregation growth. Their results indicate commercial inhibitors are more effective in stabilizing colloidal asphaltenes, slowing down the growth and formation of flocs.[88] [89] It is

important to note that besides the inherent physiochemical properties of various inhibitors, asphaltene characteristics, solvent conditions, as well as inhibitor structures play important roles in the performance of asphaltene aggregation inhibition.

For example, Leon *et al.* studied the adsorption of alkyl benzene-derived amphiphiles on asphaltene particles and concluded a direct correlation exists between the maximum surface excess concentrations of the amphiphiles and their activity as stabilizers. According to this, the higher the inhibitor concentrations adsorbed on the asphaltene surface, the larger the volume of *n*-heptane is needed to start asphaltene flocculation.[90] However, the activity of inhibitors cannot always be correctly predicted. Even for the exact same system, two different inhibitors behave differently. They can act as stabilizers, enhance flocculation or have no effect at all. [91]

One such example is concerned with resins. It is not clear why in some cases the resins and dispersants not only cause precipitation, but also promote it. Some studies have shown the self-assembly of inhibitor molecules induced by lyophilic or lyophobic interactions may account for the declined inhibitors' efficiency.[92] [93] Other studies conclude inhibitors may significantly reduce the number of asphaltenes per aggregate without reducing the aggregates' sizes. Therefore, an optimal inhibitor concentration exists for each system that can best prevent asphaltene flocculation formation.[91] However current studies are not able to clarify why the interactions between asphaltenes and inhibitors can drive/ delay the agglomeration process. More research needs to be conducted in this area to shed light on the possible mechanisms that control inhibitor activities on asphaltene aggregation. [91]

2.2 Asphaltene Model Compounds

Due to the complex nature of asphaltene molecules, the understanding of their behaviors and properties in crude oil is limited. Proper model compounds with well-defined structures are helpful to improve our understanding of real asphaltenes. Various model compounds were proposed while studies were carried out to understand whether they are able to mimic asphaltene behaviors in various solvent systems.

In 2005, Akbarzadeh *et al.* synthesized a series of model compounds based on the aromatic compound pyrene. The molecular association for this representative model structure was measured via vapor-pressure osmometry in *o*-dichlorobenzene at 75-130 °C as well as with small angle neutron scattering in toluene. The structure of the model compound was designed to provide interactions between aromatic cores, alkyl chains as well as selected functional groups through π-π interactions, hydrogen bonding and polar group interactions. The results indicate that polar groups contribute to the associative behaviors. However only dimer formation was observed in solution. The lack of further extensive association suggests pyrene derivatives lack the central features to mimic asphaltene behaviors in solution.

Rakotondradany *et al.* reported the synthesis and characterization of alkylated hexabenzocoronens (HBC) as model compounds for bitumen residue fractions. In their studies, the associative properties of the thirteen-ring pericondensed HBC derivatives were determined using a variety of techniques including vapor-pressure osmometry (VPO), ^{1}H NMR, differential scanning calorimetry, thermogravimetric analysis, hot-stage polarized microscopy, scanning electron microscopy, X-ray and small-angle neutron scattering. Together, these studies showed C_6-HBC tends to self-associate and form dimers in dilute solutions and at temperatures as high as

400 °C, resembling the behaviors of asphaltenes. Computer simulation results support these observations and suggest that the self-association of C_6-HBC is due to the favorable interplay of alkyl-alkyl and π-π stacking interactions.[94]

Gray *et al.* synthesized and characterized bridged structure 4, 4'-bis-(2-pyren-1-yl-ethyl)-[2, 2'] bipyridinyl (PBP) as a model compound for petroleum asphaltenes. PBP contains two pyrene structures bridged together by a bipyridyl spacer and exhibits similar solubility and chromatographic properties to some asphaltene fractions. Self-association properties of PBP were also studied using nuclear magnetic resonance, steady state fluorescence and vapor pressure osmometry. The results showed the onset aggregation concentration of PBP in solution was similar to that of asphaltenes.[95] Dimer formation was observed when the model compound was dissolved in toluene, which differs from asphaltene behaviors. The authors attribute the dimer formation phenomena to the π-π stacking interactions involving both pyrene rings and the bipyridine spacer.

In order to find model compounds that better mimic the association/ aggregation behaviors of real asphaltenes in crude oil, molecular simulation studies were carried out. Kuznicki *et al.* studied the aggregation and partitioning of four different model compounds: continental(C), violanthrone-79(VO-79), anionic continental (AC), and thiophenic anionic continental (TAC). MD simulations were able to elucidate the aggregation and partitioning of model asphaltenes in a binary solvent system and relate these behaviors to the model compounds molecular structures.[96,97] Their work showed interfacial activity of model compounds depends more on the terminal groups than the polyaromatic core. In addition, they also revealed while the ionized asphaltene model compounds remain at toluene-water interface, the uncharged ones prefer to

aggregate in the bulk toluene phase, indicating the importance of charge and pH of the target systems.

Recently Gray *et al.* studied the thermal cracking of both pyrene based and substituted cholestane-benzoquinoline asphaltene model compounds.[98,99] The later structure incorporated a biomarker of 5α-cholestane. For the pyrene based archipelago model compounds, the initial cracked fragments recombine to form larger structures. Results also showed that the presence of heteroatoms was responsible for the higher coke yield and varying selectivity of the cracked products. The cracking of cholesterane-benzoquinoline compounds consist mainly dehydrogenation reactions together with demethylation and steroid chain fragmentation. No significant ring openings were observed from the steroid units. [23]

2.2.1 Perylene Model Compounds

In 2008, a new group of asphaltene model molecules were proposed by Johan Sjöblom *et al.* in studies of interfacial tension, film properties and emulsion stability of real asphaltene molecules.[100–103] The design of these asphaltene model compounds incorporates hydrophobic aromatic cores with branched alkyl chains attached. Different functional groups were introduced through the alkyl chains to yield asymmetric model molecules with both polar and non-polar moieties. Therefore, these molecules can be considered polyaromatic surfactants with high interfacial activity. In addition, due to the observed pH dependence of asphaltenes, acidic functional groups were also included into the model compounds to increase the interfacial activity of charged species when the molecules come in contact with alkaline solutions. [102] Furthermore, the number of aromatic rings and molecular weights of the designed polyaromatic

compounds are consistent with that of asphaltene monomers.[23] Structures of the synthesized model compounds are shown in Fig. 2.3.

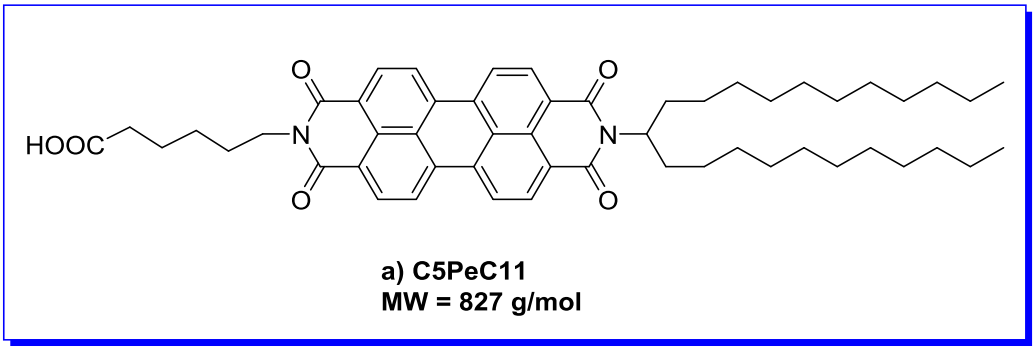

a) C5PeC11
MW = 827 g/mol

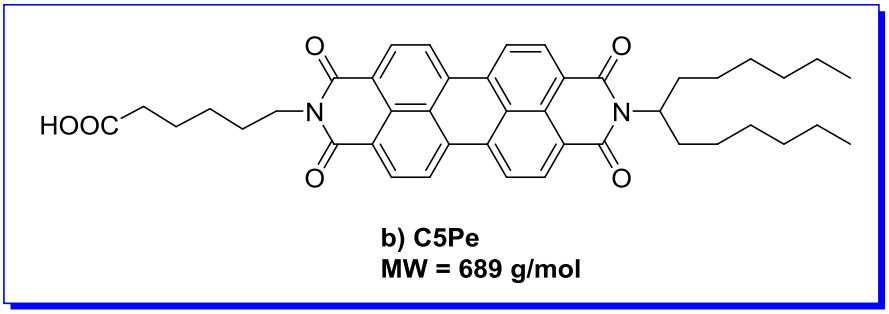

b) C5Pe
MW = 689 g/mol

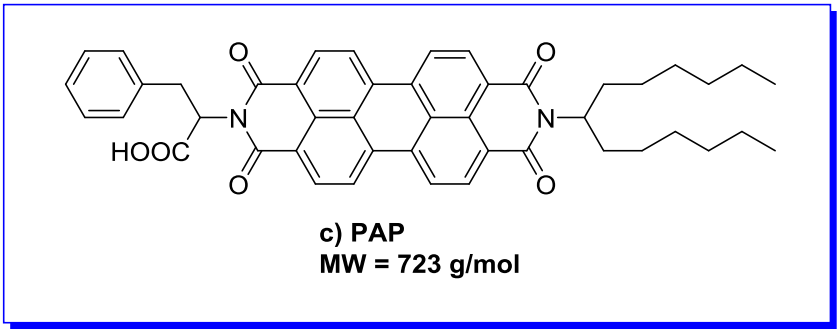

c) PAP
MW = 723 g/mol

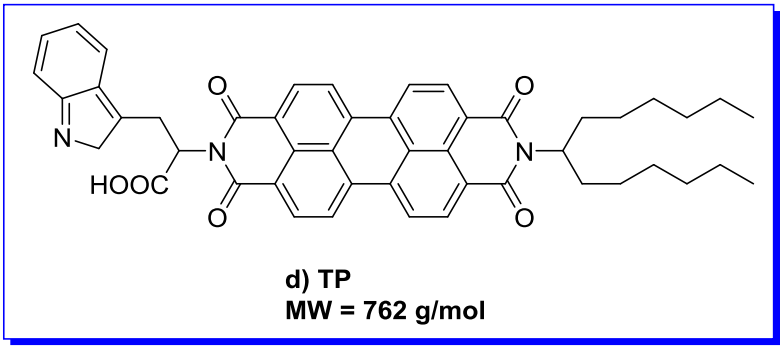

d) TP
MW = 762 g/mol

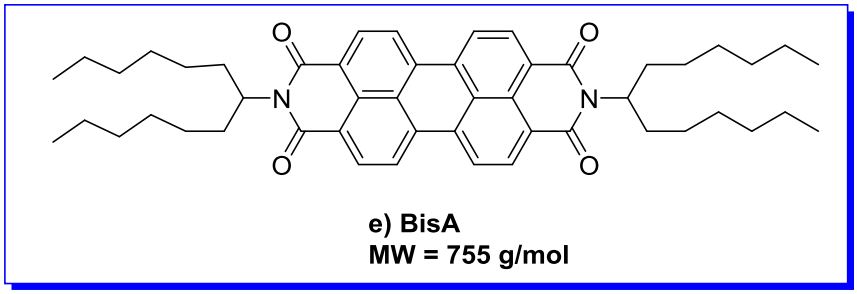

Figure 2.3 A group of polyaromatic model compounds proposed by Nordgard and Sjöblom mimicking asphaltene interfacial properties. The name abbreviations indicate the original names of the head groups (a) (b) hexanoic acid, (c) phenylalanine, (d) tryptophan and (e) perylene aromatic core. Among those, (a) and (b) have similar core structures but different peripheral carbon chain lengths.[23]

The reported solubility tests of the perylene-based model compounds showed the precipitation onset points of TP and PAP were at ~ 20 and ~ 27 vol% of heptane in mixtures of heptane and toluene. The solubility of the model compounds increases when small amount of polar compounds are present. In general, the precipitation behaviors of the model compounds are similar to that of asphaltenes.[102]

The interfacial properties of perylene model compounds were assessed by measuring the interfacial tension at toluene-water interface at elevated pH (~9). All model compounds with polar chains present similar high interfacial activities. The non-acidic BisA do not show any noticeable interfacial activities. Therefore, it can be concluded that the mere presence of carbonyl groups on the central aromatic cores is not enough to induce measureable adsorption at the liquid/ liquid interface.[23] Langmuir trough experiments were also carried out to obtain conformational information of model compounds at the interface.[104] Together with the experimental results from Brewster angle microscopy (BAM) and steady-state fluorescence, the

interfacial arrangements/ orientation of C5Pe, C5PeC11, PAP and BisA at the water-air interface were proposed. C5Pe, C5PeC11 and PAP adopt an up-right orientation with a face-to-face packing of the polyaromatic cores perpendicular to the interface.[23] Strong pH dependence was observed for C5PeC11. As pH is decreased, more carboxylate groups become protonated and the molecules become less surface active, which is consistent with the behaviors observed for C_6-asphaltenes.[103] On the other hand, BisA adopts a flat-on orientation at the interface due to the incorporation of polar groups on the core structures. This study shows the important relationship between interfacial/ surface activity and the presence of polar groups and sheds light on the future design of asphaltene model compounds.

Moreover, the surface force apparatus (SFA) was also used to measure the molecular interactions of C5Pe in toluene and heptane. It was concluded that the repulsions observed between the adsorbed C5Pe molecules on two clay (mica) surfaces was of a pure steric origin. For interactions of pre-adsorbed C5Pe films (C5Pe versus mica and C5Pe versus C5Pe), no significant adhesion was detected in toluene, while strong adhesion was measured in heptane.[105,106] These results suggest polarity plays an important role in determining the model compounds interfacial activities. In addition, the roles of charges, pH and aqueous properties were also determined by measuring the interactions between mica surfaces covered with model compound C5Pe in aqueous phases.[106] Repulsive forces of both steric and electrostatic origins were detected between the two adsorbed C5Pe layers. At short distances, the force can be fitted with Alexander-de Gennes scaling theory and at longer distance with pH > 4, fitted with Derjaguin-Landau-Verway-Overbeek (DLVO) theory.[107] Finally, the effects of divalent ions Ca^{2+} in aqueous phase on the forces acting between two surfaces were investigated.

Results show the presence of divalent cations induce C5Pe aggregation formation on mica surfaces, which leads to longer range steric repulsions.[105]

2.3 Asphaltene Fractionation

In addition to the use of model compounds, another method to study asphaltenes is through fractionation. Over the years, procedures for effective asphaltene fractionation were actively sought to reduce the complexity of whole asphaltenes. In fact, when evaluating model compounds, it is common to compare the various properties of the synthesized molecules with that of the fractionated asphatlenes. In 2007, Sjöblom *et al.* fractionated asphaltenes via a two-step precipitation procedure using *n*-pentane. The first fraction was obtained by mixing 3:1 (volume ratio) of *n*-pentane/ crude oil followed by filtration. In the following step, the second fraction was precipitated from the filtrate using 18:1 (volume ratio) of *n*-pentane/ crude oil. Fraction properties such as the on-set points of precipitation, interfacial tension, and radius of gyration were characterized. The second fraction was found to be more interfacial active and formed aggregates with smaller radius of gyration.[108,109]

Fogler *et al.* divided the asphaltenes into different sub-fractions based on the differences in polarities. It was found that the asphaltenes generated from unstable crude oils and solid deposits contain higher amounts of polar fractions compared to the asphaltenes obtained from crude oils with less stability issues. The dielectric constants and dipole moments measurement showed the more polar asphaltene fraction had a stronger tendency to form aggregates in toluene at low concentrations. The solubility and flocculation experiments confirmed the higher polarity fractions were more likely to form deposits in the field and therefore more difficult to remediate.

Together Fogler *et al.* concluded that the presence of the high-polarity asphaltene was the key factor in determining the stability of asphaltenes in crude oils. [110,111]

Barre *et al.* also reported the use of ultracentrifugation to produce asphaltene fractions with reduced polydispersity. The structure of these fractions was investigated using viscosity and X-ray scattering (SAXS) measurements. The relative viscosities of the solutions were found to be fraction dependent. Both fractal and disc models were used to analyze the obtained structural parameters. The hydrodynamic to gyration radius ratios were found to be more consistent with the fractal description of the aggregates.[112,113]

More recently, Yang *et al*. developed a new procedure for asphaltene fractionation based on their interfacial activities. The most interfacially active asphaltene fraction (IAA) was extracted as an interfacial material from emulsified water droplets in asphaltene solutions. Even though the IAA subfraction only represents less than 2 wt% of whole asphaltenes, it shows profound effect on the interfacial film properties and emulsion stabilities.[114] Measurements using ES-MS, elemental analysis, Fourier transform infrared spectroscopy (FTIR) and nuclear magnetic resonance (NMR) showed IAA molecules have higher molecular weights and contain higher amounts of heteroatoms. Subsequent molecular dynamics (MD) simulation study confirmed the representative IAA molecules had much higher interfacial activities. The results also showed the aggregation of IAA molecules in the bulk oil phase and their adsorption at oil/ water interface were more related to the sulfoxide groups in the molecule. Simulation results also concluded the IAA molecules can self-assemble in solvent forming supramolecular structures and a porous network at the oil/ water interface.[115]

In 2016, Sjöblom *et al.* reported a new asphaltene fractionation method based on adsorption onto calcium carbonate. The detailed fractionation procedure was shown on Fig. 2.4.[22]

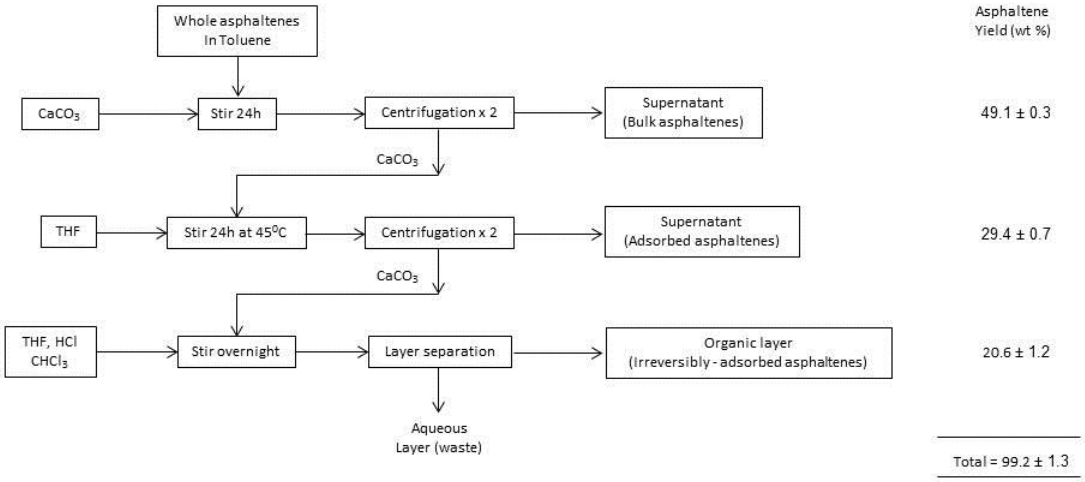

Figure 2.4 Asphaltene fractionation procedures. All data corresponds to Statoil Oil. Centrifugation * 2 refers to centrifugation being performed twice.[22]

In this procedure, 4 g/L asphaltene solution was first prepared by dissolving 1.5 g whole asphaltenes in 375 ml toluene and sonicating for 30 min. $CaCO_3$ 41.4 g was then added to the asphaltene solution which was stirred for 24 h at room temperature. The obtained solution was then centrifuged at 4000 rpm for 20 min. The supernatant was filtered and concentrated to dryness which constitutes the first asphaltene fraction called bulk or non-adsorbed (Non-Ads) asphaltenes. The second fraction was obtained by adding 375 ml THF to $CaCO_3$ from last step.

The mixture was then stirred for 24 h at 45 °C followed by centrifugation at 4000 rmp for 20 min. The second supernatant was recovered, filtered and concentrated to dryness which is called adsorbed (Ads) asphaltenes. Finally, 750 ml mixture of 50/50 (v/v) THF/ $CHCl_3$ was added to the remaining $CaCO_3$ followed by slow addition of 750 ml 4N HCl solution. The mixture was then stirred for 3 h at room temperature. The organic and aqueous layers were separated. The organic layer was then washed with water and concentrated to dryness. This last asphaltene fraction is called the irreversibly – adsorbed (Irr-Ads) asphaltenes. All the asphaltene sub-fractions were dried in a block heater maintained at 70 °C under a stream of nitrogen. [22]

The various fractions obtained were characterized by elemental analysis, Fourier transform infrared spectroscopy (FTIR) and quartz crystal microbalance with dissipation (QCM-D). FTIR results showed the presence of functional groups differs in different subfractions. QCM-D gave direct quantification of the abilities of different fractions to adsorb onto stainless steel. The Non-Ads asphaltenes showed the least adsorption while the Irr-Ads asphaltene subfraction with highest concentration of carbonyl, carboxylic acid or derivative groups showed the highest adsorption. In addition, it is also observed that the Irr-Ads subfraction was able to form visco-elastic layers on metal surfaces, decreasing the calculated adsorption amounts. Taking into account that the Non-Ads asphaltenes showed least adsorption, it can be concluded that different asphaltene subfractions tend to interact with each other reducing the overall adsorption behaviors.[22]

In this research, the aggregation behaviors of the above fractionated asphaltenes were investigated using dynamic light scattering (DLS) and ESI-MS (conducted by Dr. Lan Liu) techniques. Model compounds C5PeC11, C5Pe and BisAC11 were investigated to correlate their aggregation behaviors with that of the various sub-fractions of asphaltenes. An aggregation

inhibitor DBSA was tested to understand its effects on asphaltenes and model compound molecules. Polydispersity effects of model compounds were investigated by mixing together various model compounds and study the mixture's flocculation behaviors in different solvent systems.

2.4 Light Scattering

When a beam of light hits an object, it would interact with the matter in one of the two ways: adsorption and scattering. For adsorption, the photons eventually disappear and the electromagnetic energy is transformed into the internal energy of the absorber. In the case of light scattering, light beam attenuation occurs that deflects the ray from a straight path. In fact, light scattering is the reason that most objects are visible to human eyes. Due to the attenuation of the light beams, their intensities decrease:

$$I = I_0 * e^{-\tau x} \quad (1)$$

, where I_0 is the intensity of incident light; τ is the turbidity; and x is the thickness of the material the light is passing through as shown in Fig. 2.5.[116]

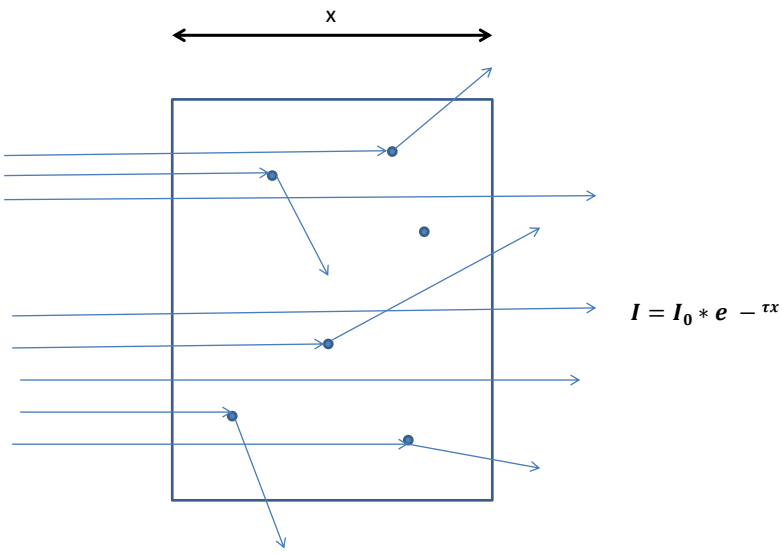

Figure 2.5 The transmitted light is weakened by scattering.[116]

In the scattering theory, there are two forms of particle scattering: elastic and inelastic scattering. For elastic scattering, the kinetic energy of a particle is conserved in the center-of-mass frame while the direction of photon propagation is modified. On the contrary, inelastic scattering represents a fundamental process in which the kinetic energy of the photon is lost. Raman scattering is one of the examples of inelastic scattering in which a small fraction of scattered photons ends up having a frequency lower than that of the incident photons. Raman scattering is mainly used to determine the chemical composition and molecular structures in chemical laboratories.

Rayleigh scattering is the most common form of elastic scattering, in which the scattering of light occurs for molecules or particles smaller than the wavelength of incident light. For Rayleigh scattering, the intensity has a strong dependence on the size of the particles and is inversely proportional to the fourth power of the wavelength of light. Therefore, Rayleigh scattering is responsible for the blue color of sky. Another important type of elastic scattering is Mie scattering which represents a broader class of scattering light by particles of any diameter. In Mie theory, when particles become larger than one tens of the wavelength of incident light, the scattering changes from being isotropic to a distortion in the forward scattering direction. When the size of the particles becomes equivalent or greater than the wavelength of the laser, the scattering can be explained by the maxima and minima in the plot of scattering light intensity with angle. Together the theories behind Rayleigh and Mie scattering constitute basic principles behind dynamic and static light scattering techniques.

2.4.1 Static Light Scattering

Static light scattering is an optical technique that measures the intensity of the scattered light at different scattering angles. Measurement of the scattering intensity at various sample concentrations allows calculation of the root mean square radius R_g, average molecular weight M_w, as well as the second virial coefficient A_2. Static light scattering was based on the principle that when laser light impinges on a macromolecule, the oscillating electric field of the light induces an oscillating dipole within the molecule. The intensity of the radiated light from the oscillating dipole depends on the magnitude of the dipole induced in the macromolecule. Therefore the larger M_w is of the macromolecule, the greater the intensity of its scattered light.

$$I_{scattered} = constant * CM \quad (2)$$

In the above equation, *M* is the molecular weight and *C* is the weight concentration. This simple relationship is the foundation of the famous Zimm's expression developed by Bruno Zimm in 1993.[117,118]

$$\frac{K^*C}{R(\theta,C)} = \frac{1}{M_w P(\theta)} + 2A_2C \quad (3)$$

In this later developed equation, $R(\theta, C)$ is the excess Rayleigh ratio of the solution as a function of the scattering angle θ and sample concentration. Excess Rayleigh ratio is usually regarded as a normalized intensity which is directly proportional to the intensity of the scattered light in excess to the light scattered by pure solvents. C is the concentration of the macromolecule sample. M_w is the molar weight of the sample molecule and $A_2$is the so-called second virial coefficient. If A_2 is positive, the inter-particle forces are repulsive and if negative, the forces are attractive. When the second virial coefficient is zero, the solution is approaching ideal behavior and there are no net interactions between the dissolved particles. K^* is a constant and can be calculated as

$$K^* = \frac{(2\pi n_0)^2(\frac{dn}{dC})^2}{N_A\lambda^4} \quad (4)$$

where n_0 is the refractive index of the pure solvent, $\frac{dn}{dC}$ is the refractive index increment of the solute/ solvent system, λ is the wavelength of the laser and N_A is the Avogadro's number.

The Zimm's equation allows the determination of the molecular weight of dissolved particles by measuring the scattered intensity at many different angles and extrapolate to zero scattering angle (where $P(\theta) = 1$) and measuring several concentrations of the sample for each angle in order to extrapolate to zero concentration. It is not doable to just measure the sample at

extremely low concentrations due to the inherent settings of static light scattering instrument. It is worth mentioning here that the scattered intensity generally decreases with increasing scattering angle. When the particles are extremely small (less than 1/10 of the laser wavelength), the scattered intensity is independent of the scattering angle. Therefore, within the measurement error, it is impossible to distinguish the scattered intensity from a constant value. The typical measuring range of particles for static light scattering is from 10 nm to 1000 nm.

Below in Fig. 2.6 shows a general scheme for the commercially available static light scattering instrument.

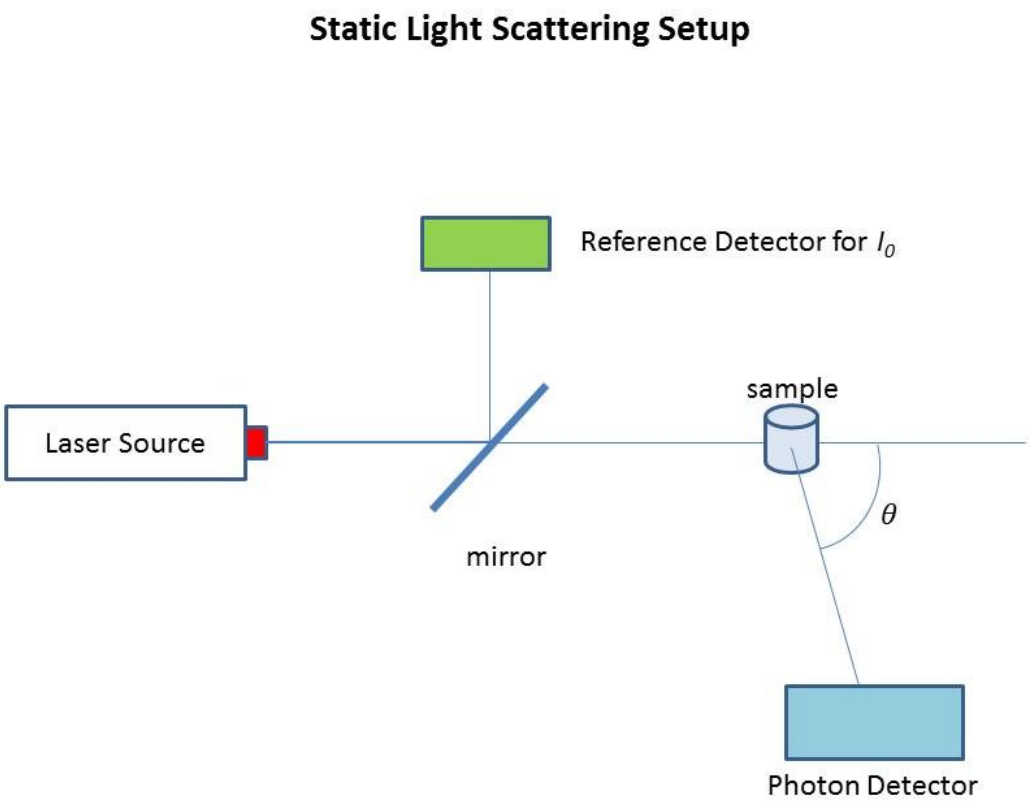

Figure 2.6 Sketch of the setup of static light scattering instrument. The intensity of the scattered light is measured as a function of the scattering angle θ. The reference detector measures the split light intensity as I_0. A more sensitive photon detector is used to measure the much feeble scattered light.

Static light scattering has become a versatile tool for characterizing particles and their in vitro interactions. Due to its non-intrusive nature, static light scattering technique has become a popular instrument covering a broad range of applications in chemistry, engineering, and biological fields. [119] [120] [121][122]

2.4.2 Dynamic Light Scattering

Dynamic light scattering (also known as photon correlation spectroscopy) is a technique used to determine the size distribution of small particles in solution. Unlike static light scattering, dynamic light scattering measurements are normally done at one scattering angle at very short intervals (~200ns). The only information extractable from the measurement is the diffusion coefficients of the dissolved particles, which can be interpreted in terms of particle sizes. The detailed setup of dynamic light scattering used in this research will be discussed in next chapter.

The application of dynamic light scattering is usually focused on the characterization of the sizes of various particles including proteins, polymers, micelles, carbohydrates, and nano-materials. If the system is non-dispersive in size, the mean effective diameter of the particles can be determined. In addition, stability studies can be conducted conveniently using DLS. Continuous DLS measurements of the same sample can be used to determine if particles can aggregate overtime. In some studies, stability tests depending on temperatures can be conducted by linking

a temperature control system to the sample holder. More recently, development of dynamic light scattering instrumental setup has been made that allows one to make absolute measurements of the sizes of particles suspended in liquids in the range from 0.001 to 5 μm.[123] Optical rearrangement of the spectrometer also makes it possible to measure light scattering in opaque systems which are normally characterized by strong light adsorption.[124] However, further development of DLS instrumental setup is not the purpose of this research. A commercial available DLS instrument is used without any further modification.

Chapter 3 Principles of Dynamic Light Scattering

3.1 Theories behind Dynamic Light Scattering Measurement

3.1.1 Brownian Motion of Particles in Solution

Brownian motion is first named after the botanist Robert Brown in 1827 when he noticed the pollen grains move randomly in all directions in water. A decade later Albert Einstein published a paper in 1905 which explains the origin of the random walk as a result of the pollen grains being moved by individual water molecules. Einstein's theory laid the foundation for modern physical chemistry. There are two parts in Einstein's theory: in the first part, the diffusion coefficient is related to the mean squared displacement of particles in Brownian motion; while in the second part, the diffusion coefficient of particles is related to the measurable physical quantities.[125,126] In Einstein's theory, when a free particle is moving in space, the mean square displacement in terms of the elapsed time and diffusivity can be obtained as

$$\lambda^2 = 2D_t t \quad (5)$$

In the above equation, λ is the mean free path and t is the average time between collisions. For liquid systems, the diffusion rate is usually related to the viscosity of the fluid. For less viscous liquids, they diffuse more easily compare with thick ones. More specifically, the viscosity η can be used as a quantitative measure of the liquids' transport momentums. Therefore an equation between the translational diffusion coefficient D_t and the particle size can be obtained through the force balance between osmotic force and the fluid friction.

$$D_t = \frac{kT}{6\pi R_h \eta} \quad (6)$$

The above equation is the famous Stokes-Einstein Equation, where k is the Boltzmann constant, T is the temperature, R_h is the hydrodynamic radius of the spherical particles, and η is the viscosity of the fluid. This equation relates the diffusion rate of a particle in solution to temperature, particle size as well as the fluid viscosity. Therefore, small particles diffuse quickly while larger ones diffuse slowly, which forms the foundation of modern DLS instrumentation.

3.1.2 Hydrodynamic Radius

In the characterization of molecular sizes, different measurement techniques often give different sizes for the same sample. This is because for irregular shaped particles, different equivalent spherical diameters are measured. Depending on the measured diameters, different values such as radii of the same volume, radii of the same maximum/ minimum lengths or hydrodynamic radii can be reported.

The hydrodynamic radius R_h of the particle is defined as the radius of a hard sphere that diffuses at the same speed as the particle being measured. It depends not only on the actual size of the particle, but also its surface structure and the solvent properties in the medium. For particles in a solution, the thickness of the electric double layers (Debye length κ^{-1}) is heavily depended on the ionic concentration in the surrounding medium. At low ionic concentration, the double layer is extended around the particle, reducing the diffusion rate and resulting in a larger R_h. On the contrary, when the solution has higher ionic concentration, the electrical double layer of the particle is compressed, and the measured hydrodynamic radius is reduced.

In addition, when the surface of the particle is changed due to the adsorbed polymer chains, the diffusion rate will also be reduced, resulting in a lower apparent hydrodynamic radii as shown in Fig. 3.1.

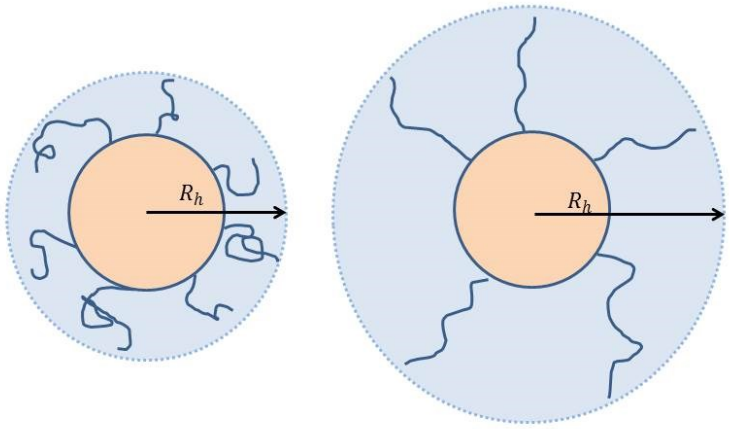

Figure 3.1 The hydrodynamic radius changes due to polymers adsorbed onto particle surface.

For irregular shaped particles, DLS will give the hydrodynamic radius of a sphere that has the same average translational diffusion coefficient as the particle being measured.

3.1.3 Light Scattering Effects

As particles undergo Brownian motion, the amounts of light that can be scattered by these particles vary. The smaller the area of detector, the stronger the light intensity fluctuation can be observed. As shown in Fig. 3.2, small particles move faster than large particles and therefore, the intensity of the scattered light changes more rapidly for smaller particles. The characteristic time of the measured intensity variation is directly related to the diffusion rate of the particle which leads to the calculation of its hydrodynamic radius.

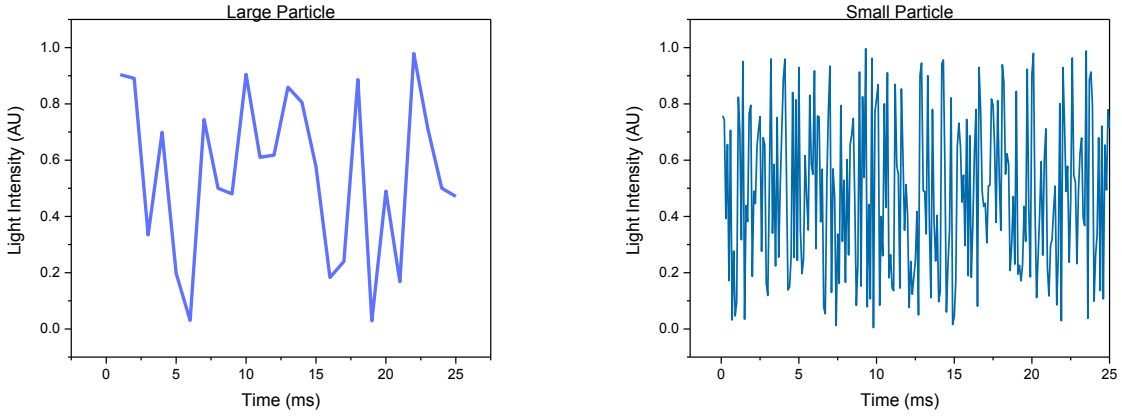

Figure 3.2 The rates at which particles diffuse are related to their sizes. For large particles, the light intensity fluctuates slowly. For small particles, the light intensity changes quickly.

Common laboratory DLS instrumentation uses the procedure of autocorrelation. Instead of cross-correlation, autocorrelation compares two signals, one of which is a time-delayed version of itself. At time zero, the measured intensity stays the same and gives a 100% autocorrelation. As time progress, the autocorrelation diminishes gradually until there's no more similarity between the starting and ending states. For small particles that move fast, the breakdown of the autocorrelation happens quickly. Therefore, by quantifying how fast the correlation takes to breakdown between the starting state and the ending state, one could obtain size information of the particles.

Modern DLS instruments compute the intensity auto-correlation function $G_2(\tau)$ from the measured photon counts as shown in the following equation:

$$G_2(\tau) = \langle I(t)I(t+\tau)\rangle = \lim_{T\to\infty} \int_0^T I(t)I(t+\tau)dt \qquad (7)$$

In this equation, τ is the lag time between the two correlations, T is the total duration of DLS experiments, and the bracket $\langle \quad \rangle$ indicates a time average. Since the lag time is extremely small ~ 10^{-9} s, a special operating device is needed to perform the computations in time. For a dilute suspension of monodisperse spheres, $G_2(\tau)$ can be written as

$$G_2(\tau) = \partial + \beta e^{-2\Gamma\tau} \qquad (8)$$

where ∂ is the baseline at infinite time, β is the amplitude or coherence factor, and Γ is the decay rate. $G_2(\tau)$ can be normalized by dividing the baseline ∂ yielding the normalized intensity auto correlation function $g_2(\tau)$.

$$g_2(\tau) = 1 + b g_1(\tau)^2 \qquad (9)$$

In the above equation, $g_1(\tau)$ and $g_2(\tau)$ are the normalized auto- and field- correlation functions respectively. The parameter b is referred to as the coherence factor which depends on the detector area. Typical values of b have the range 0.9-1. The field correlation function can be related to the particle translational diffusion coefficient, D_t.

$$g_1(\tau) = e^{-D_t q^2 \tau} \tag{10}$$

In the above equation, q is the scattering vector: $q = \left(\frac{4\pi n}{\lambda_0}\right) \sin\left(\frac{\theta}{2}\right)$, where n is the dispersant refractive index, λ_0 is the laser wavelength and θ is the detection angle. Therefore, this equation provides the basis to obtain diffusional properties of the system.

3.2 DLS Instrumentation Setup

Figure 3.3 shows a typical setup of DLS experiment. The sample is usually held in a disposable glass tube inside a fixed sample holder. A coherent monochromatic light source is used and in our experiments, the light source is He-Ne lasers with a wavelength of 632.8 nm. The scattered light is then collected by the photon detector at the constant scattering angle θ.

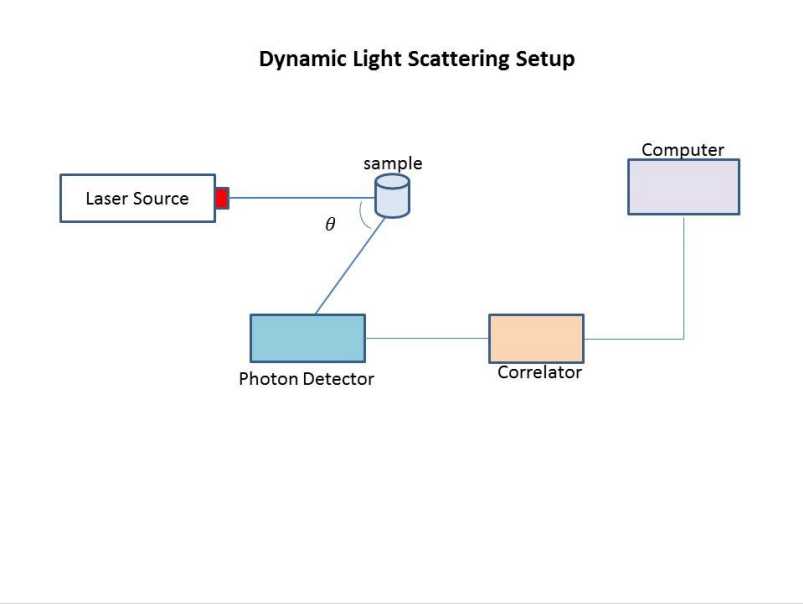

Figure 3.3 Scheme of a typical dynamic light scattering setup. In DLS, the detector has a very small detection area and the laser beam is made as narrow as possible. Weight concentration and refractive index increment $\frac{dn}{dC}$ of the sample are not needed in the measurement. Usually angle θ is kept constant in experiments.

For the detector, either Photomultipliertubes (PMT) or Avalanche Photodiodes (APD) is used for the measurements of the scattered light intensity. The photon counting rate (number of impinging photons per unit time) is taken as an equivalent to the intensity. A correlator is used for fast data treatment and a computer is needed for data acquisition and handling.

3.3 DLS Data Analysis

3.3.1 Mono and Poly-disperse Systems

After the successful acquisition of $g_2(\tau)$, algorithms are needed to convert it to $g_1(\tau)$. However, due to the presence of noise in the measured data, $g_2(\tau)$ could be negative.[127] The most appropriate way to complete the conversion is as follows:

$$g_1(\tau) = \begin{cases} \sqrt{\frac{g_2(\tau)-1}{b}} & for\ g_2(\tau) - 1 \geq 0 \\ -\sqrt{\frac{|g_2(\tau)-1|}{b}} & for\ g_2(\tau) - 1 < 0 \end{cases} \quad (11)$$

For monodisperse systems, the successful obtain of $g_1(\tau)$ can lead to the determination of diffusion coefficients. However, for polydisperse systems, different particles contribute to the normalized field correlation function and therefore $g_1(\tau)$ can only be obtained through the integration of all particles' correlation functions in the system.

$$g_1(\tau) = \int_0^\infty q(D_t) e^{-D_t q^2 \tau} dD_t \quad (12)$$

In the above equation, $q(D_t)$ is the density distribution of translational diffusion coefficients. However, for experimentally obtained field correlation functions, an infinite number of equally probable solutions of $q(D_t)$ exist due to measurement errors. Even small variations in $g_1(\tau)$ gives wildly different hydrodynamic radii distributions for the same sample.[128] Therefore the mathematical nature of the problems limits the use of more direct data analysis algorithms.[129]

There are three main types of data analysis: the method of cumulants, functional fitting and Laplace inversion. For systems with a monomodal distribution, the particles have an average

mean with a tight distribution about the mean. Therefore, a linear cumulant expansion is the most common practice for data analysis. In fact, due to its fast and easy-to-use nature, the cumulant method was incorporated in the International Standard.[129] In the method of cumulants, after the normalization of the obtained autocorrelation function, $\ln|g_1(\tau)|$ is fitted by a polynomial to obtain the cumulants. However, the method of cumulants is only reliable for monodisperse systems. Even with very accurate instrumentation, random errors occur in the fitted cumulants and the uncertainties increase as more cumulants are being calculated. Since the system in this research is composed of particles with various dimensions, the method of cumulants is not suitable for data analysis.

The method of functional fitting is rarely used since a distribution type and adjustable parameters need to be assumed. The parameters are then estimated by a nonlinear optimization procedure. Common model functions include exponential functions, Schulz functions, stretched exponential function (KWW functions) and FCS model functions. This method is tedious and therefore not suitable for continuously collected data analysis. In addition, the optimization results rely heavily on the initial guesses of the variables.

The Laplace inversion method uses algorithms that do not assume a certain type of distribution of diffusion coefficients. Therefore this method is most suitable for applications in polydisperse systems. However, assumptions are needed to deal with the mathematically ill-posed problem of the general inversion of Laplace transformation of $g_1(\tau)$. Since this is the primary method used in the DLS data analysis in this thesis, more details are included below.

3.3.2 The Laplace Inversion Method

Due to the mathematically ill-posed nature of the general Laplace transformation of $g_1(\tau)$, constrains or priori information need to be introduced to obtain a solution. To avoid small variations in the measured data, an algorithm called CONTIN (Constrained Regularization Method for Inverting Data) was developed by Provencher *et al.* In this method, Provenchers used Tikhonov regularization and devised the role of a regularizor to introduce parsimony in the solution.[130–132] The second derivative of the distribution $q(D_t)$ was mostly chosen as a regularizor to penalize the gradient of distribution.[129]

In CONTIN, the regularization parameter α determines the strength of the constraints. If α is chosen as zero, CONTIN acts as a NNLS (Non-Negative Least Squares) system, which turns to be very sensitive to small variations in the measured data as well as measurement errors. However, if α is set a high value, the data are underestimated in the solution and not all extractable information can be achieved.[129] Therefore, the selection of an optimum regularization parameter is extremely important in DLS data analysis. To solve the problem, a Fisher *F*-test is normally used to test whether the probability of the regularization parameter increase for a given value of α is consistent with the noisy data or already mainly due to the regularizing function. The test calculates a probability of rejection if the standard deviation of the smoothed solution differs too much from the reference standard deviation.[129] Provencher recommends using a probability of rejection of 0.5 for reasonable results.[131,132] Introducing a regularization for the inverse problem greatly enhances its solvability as well as the stability of the solution.[129]

However, prior to the CONTIN regularization method can be applied, the ACF needs to be converted to the FCF. The presence of negative values might make the process less reliable. To solve the problem, a nonlinear fit model is implemented into the program. The fitting model used is,

$$g_2(\tau) - 1 = b * [\int \exp(-Dq^2\tau)\, q(D) dD]^2 \quad (13)$$

Compare with the fitting using previously described equation,

$$g_1(\tau) = \int_0^\infty q(D_t) e^{-D_t q^2 \tau} dD_t \quad (14)$$

, the fitting of $g_2(\tau)$ instead of $g_1(\tau)$leads to more smooth distribution functions. In addition, for $g_1(\tau)$ fitting, due to the square root function, the noise of the FCF is no longer symmetric and is more likely to give artifact peaks or features. Therefore, in this research, the nonlinear regularization method is used which offers the best choice available to extract distributions of diffusion coefficients from DLS data.[129]

3.4 DLS Measuring Limits

To conduct DLS measurements, sample preparation is extremely important in obtaining reliable data. The sample particles should be within the measuring limits of DLS with a different refractive index from the dispersant solvents. Generally speaking, DLS has a measuring range of 1 nm - 1000 nm. More specifically, the lower measuring limit of DLS depends on the sample concentration as well as laser power and detector sensitivities of the instrumentation. If the sample concentration is too low, there may not be enough measurable scattered light. Therefore, during the method optimization stage, it is a common practice to measure different

concentrations and compare the obtained results. The hydrodynamic radius from a DLS measurement should be independent of sample concentration. In addition, when measuring large particles, the intensity of scattered light also depends on the number density of particles in the light path. If the number of particles is too low, severe fluctuations occur in the momentary number of particles. This causes large fluctuations in the scattered intensity leading to unrealistic results.

The upper measuring limit of DLS is more complicated to determine. Since DLS is based on the theory of Brownian motion of particles, deviations occur when particle motion is no longer random. The most common reason to cause non-random motion is the onset of sedimentation of particles. In colloidal systems, all particles will sediment. However, the rate of sedimentation varies and depends on particles size and the relative density difference between particles and the surrounding medium. For successful DLS measurements, the rate of particle sedimentation should be much slower than the rate of diffusion. The best practice to make sure no sedimentation has occurred is to look for stable count rate over multiple measurements over the entire measuring period. A decreasing count rate indicates loss of particles due to sedimentation.

Another important factor that limits the measurement range is multiple scattering. For ideal DLS measurements, the incident photon is only scattered once before reaching the detector. However, when the sample is at high concentration, it is possible that the scattered photon is re-scattered by surrounding particles. This multiple scattering phenomenon leads to complications in DLS data analysis due to averaging effects that cannot be easily retrieved.[133] As a result, the coherence factor in the auto correlation function decreases due to the destructive interference of the multiple scattered lights. In addition, the decay of ACF is shifted towards lower lag times and the spectrum is broadened. Overall, the net effect of multiple scattering is the broader distribution of

the obtained diffusion coefficients. The easiest way to correct multiple scattering is to dilute the sample and repeat the measurement.

In addition, at high concentrations, particle interactions also play an important role. Restricted diffusion describes the phenomenon where the presence of other particles hinders the free particle diffusion. The result causes DLS size distribution move towards larger particles sizes when using dispersant viscosity. A good solution to fix the restricted diffusion problem is to use the actual bulk concentration instead of dispersant concentration in the Stokes-Einstein equation.

Chapter 4 Materials and Method Optimization

4.1 Materials

4.1.1 Asphaltene Model Compounds

Three different model compounds were used to mimic asphaltene aggregation behaviors, C5Pe, C5PeC11 and BisAC11. The synthesis of these molecules can be found elsewhere in literature.[101,102,134] The molecular structures and molecular weights of these modeling compounds are shown below. Model compounds were obtained from Prof. Johan Sjöblom group at NTNU.

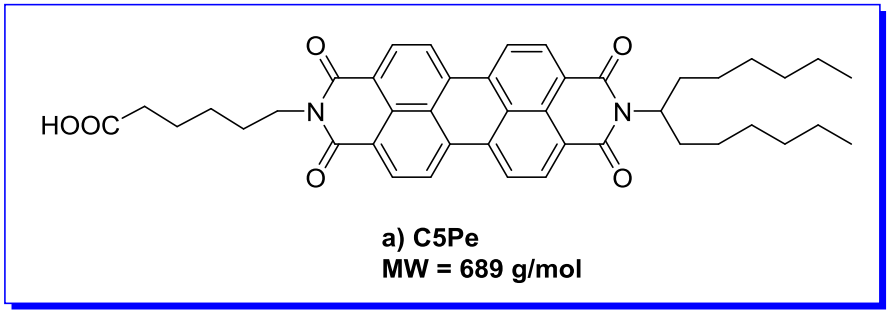

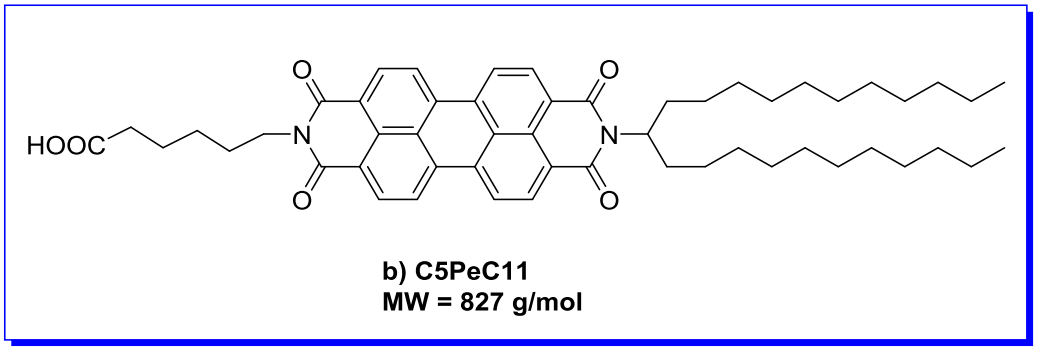

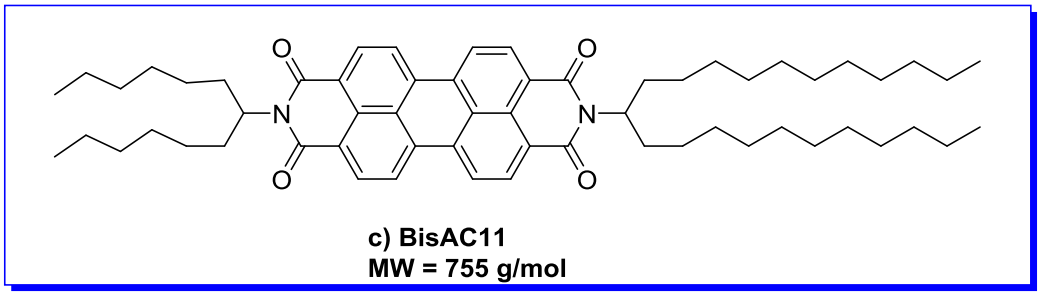

Figure 4.1 Molecular structures and molar weights of perylene based model compounds used in mimicking asphaltene aggregation behaviors.

The perylene bisimide model compounds consist of seven fused ring structures, mimicking the polyaromatic nature of asphaltene molecules. Both C5Pe and C5PeC11 are amphiphilic due to the existence of a terminal carboxylic group and branched alkyl chains. The acidic functional group is important in maintaining the interfacial properties of the model compounds. Previous studies have shown that both C5Pe and C5PeC11 have interfacial activities as asphatlenes

forming monolayer coverages at oil/water interfaces. Model compounds without acidic functionality such as BisAC11, does not stabilize emulsions.[100] These model compounds were chosen so a correlation between structural variations and aggregation behaviors can be established. C5Pe and C5PeC11 have different aliphatic chain length while C5PeC11 and BisAC11 differ in the presence of acid functional groups. The acquired knowledge can be extended to explain and predict asphaltene aggregation behaviors.

4.1.2 Asphaltenes

Asphaltene extraction was performed according to the following procedure by Prof. Sjöblom's group at NTNU.[22] The crude oil was heated to 60 °C for at least one hr. The crude oil was then shaken to ensure homogeneity of the sample. 160 ml *n*-hexane was added to 4 g of crude oil sample and the mixture was stirred overnight. The asphaltene fraction was then recovered using a 45 μm HVLP (Millipore) membrane filter. The obtained asphaltene fraction was then washed with *n*-hexane at 60 °C and then dried in a desiccator purged with nitrogen for 48 hr.

Upon the successful extraction of asphaltenes, fractionation of asphlatenes was performed based on its abilities of being adsorbed onto calcium carbonate. The detailed procedure can be found in Chapter 2.3 in this thesis. Three asphaltene fractions Irr-Ads, Ads and Non-Ads can be obtained. Aggregation behaviors of the three fractions were studied individually.

4.1.3 Asphaltene Aggregation Inhibitors

4-dodecyl benzene sulfonic acid (DBSA) was used as an asphaltene aggregation inhibitor. The chemical structure of DBSA is shown below.

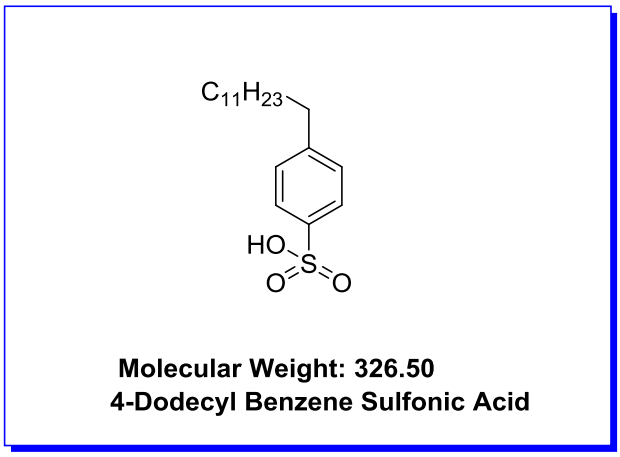

Figure 4.2 Molecular structure of DBSA.

4-Dodecylbenzenesulfonic acid (mixture of isomers, ≥ 95%, Sigma-Aldrich) was used as received. At room temperature, DBSA is a colorless viscous liquid soluble in water, toluene, heptane as well as other organic solvents. The reported literature density of DBSA is 1.06 g/ml at 20 °C. The refractive index of DBSA is 1.51.

4.1.4 Solvents and Solution Preparation

Toluene and heptane was used as organic solvents in this study. Toluene (99.8% min by GC, HPLC grade, Fisher Scientific, Canada), heptane (96% min by GC, HPLC grade, Fisher Scientific, Canada) and methanol (99.9 % min by GC, HPLC grade, Fisher Scientific, Canada) were used as received. The stock solutions of asphaltene fractions and model compounds were prepared by dissolving a known mass of materials in toluene to yield a final concentration of 1 g/L under sonication for 45 min. The stock solutions were sonicated and filtered with 0.2 μm PTFE filter each time before usage. Water used throughout the study was purified with a Millipore system and had a resistivity of 18.2 mΩ/m (Milli-Q water).

To minimize the mixing effects, desired amounts of pure heptane and toluene solvents were first mixed together to obtain a heptol solution of 1800 μl. 200 μl concentrated model compounds or asphaltene fraction in toluene solutions were then added into the heptol mixture. The sample was shaken violently for 30 s before DLS measurement started. The total amount of solution was kept the same as 2000 ml for all runs.

4.2 DLS Experiment Method and Optimization

4.2.1 Refractive Index Measurements

Refractive indexes of various toluene/ heptane solutions were obtained for DLS measurements. Abbe refractometer was used for measuring the refractive index of the solvent mixtures. All measurements were performed at 22 °C. After the prism was cleaned with acetone and dried with

KimWipe, a few drops of the liquid mixture (at various tolene/heptane ratios) were placed on the polished surface of the lower refracting prism. The hinged upper incident prism was closed and locked with a knob. The liquid was therefore evenly distributed on the face of the refracting prism. Scan the lower larger adjustment knob until a light and dark divided image appeared. The dispersion was then adjusted by using the upper smaller dispersion correction knob until a sharp boundary of the image could be seen. Center the boundary in the crosshair of the view and read the refractive indexes from scale. All measured refractive indexes of the liquid mixture were summarized below in Table 4.1.

Table 4.1 Measured refractive indexes of various heptane/tolene solutions at 22 °C.

Volume Ratio heptane:toluene	Refractive index	toluene mass fraction	heptane mass fraction
0.00	1.4972	1.00	0.00
0.10	1.4840	0.88	0.12
0.20	1.4738	0.76	0.24
0.25	1.4709	0.70	0.30
0.30	1.4612	0.65	0.35
0.35	1.4575	0.59	0.41
0.40	1.4506	0.54	0.46
0.45	1.4464	0.49	0.51
0.50	1.4415	0.44	0.56
0.56	1.4340	0.38	0.62
0.60	1.4306	0.34	0.66
0.66	1.4235	0.29	0.71
0.70	1.4209	0.25	0.75
0.72	1.4170	0.23	0.77
0.74	1.4145	0.22	0.78
0.76	1.4120	0.20	0.80
0.78	1.4100	0.18	0.82
0.80	1.4119	0.16	0.84
0.86	1.4013	0.11	0.89
0.90	1.3972	0.08	0.92
1.00	1.3876	0.00	1.00

4.2.2 Kinematic Viscosity Calculations

Kinematic viscosity of the bulk solution was required when calculating the hydrodynamic diameters of particles with Stokes-Einstein equation. Ideally, solution viscosity at varying aggregation stages of the particles should be used. However, since the change in viscosity is small compare with the increase in the measured hydrodynamic radii of particles in solution, the kinematic viscosity of bulk solutions were used. Due to the very dilute nature of the solutions, the viscosities of the mixture were estimated using Refutas equations.[135]

In Refutas method, the Viscosity Blending Number (VBN) of each component is first calculated and then used to determine the VBN of the liquid mixture. Therefore, to calculate VNB of toluene and heptane, the following Eq. 15 was used.

$$VBN_i = 14.534 * \ln(\ln(\nu_i + 0.8)) + 10.975 \quad (15)$$

where ν_i is the kinematic viscosity of each solvent. For toluene, $\nu_{toluene} = 0.678$; for heptane $\nu_{heptane} = 0.568$. The VBN of the liquid mixture is then calculated as,

$$VBN_{mixture} = \sum_{i=0}^{N} x_i * VBN_i \quad (16)$$

,where x_i is the mass fraction of each solvent component in the mixture. The kinematic viscosity of the mixture can then be estimated using the obtained VBN with Eq.17 below.

$$\nu_{mixture} = \exp\left(\exp\left(\frac{VBN_{mixture} - 10.975}{14.534}\right)\right) - 0.8 \quad (17)$$

Using the above method, the calculated kinematic viscosity of the bulk solvents are summarized in Table 4.2 below. Same values were used in DLS data analysis.

Table 4.2 Calculated viscosity of mixture solvents using VNB as indicated above. The densities of the mixtures were also calculated by assuming ideal mixing between toluene and heptane.

heptane:toluene	viscosity(cp)	VBN(mixture)	kinematic viscosity(cSt)	mixture density(kg/m3)
0.00	0.59	-2.68	0.68	870.00
0.10	0.56	-3.08	0.66	850.95
0.20	0.54	-3.46	0.65	831.90
0.25	0.53	-3.64	0.64	822.38
0.30	0.52	-3.82	0.64	812.85
0.35	0.51	-3.99	0.63	803.33
0.40	0.50	-4.16	0.62	793.80
0.45	0.48	-4.32	0.62	784.28
0.50	0.47	-4.48	0.61	774.75
0.56	0.46	-4.67	0.61	763.32
0.60	0.46	-4.79	0.60	755.70
0.66	0.44	-4.97	0.60	744.27
0.70	0.44	-5.08	0.59	736.65
0.72	0.43	-5.14	0.59	732.84
0.74	0.43	-5.20	0.59	729.03
0.76	0.43	-5.25	0.59	725.22
0.78	0.42	-5.31	0.59	721.41
0.80	0.42	-5.36	0.58	717.60
0.86	0.41	-5.53	0.58	706.17
0.90	0.40	-5.63	0.58	698.55
1.00	0.39	-5.89	0.57	679.50

4.2.3 The Scattering Angle

Since the decay rate of auto correlation function in dynamic light scattering depends on the scattering vector (Chapter 3), the scattering angle plays an important role in maintaining the quality of a DLS measurement. Particles of different sizes scatter with different intensities depending on the scattering angle. Therefore, there exists an optimum angle of detection for each particle size. For polydisperse samples with unknown particle sizes, several scattering angles need to be tested before reaching a certain angle with good measuring repeatability.

In order to determine the best detection angle in DLS experiments, both pure solvents and model compounds were tested. 8 ml heptane and 2 ml toluene were mixed well and filtered with a PTFE syringe filter (0.22 μm). The solvent mixture was then transferred to a Fisher disposable borosilicate glass tube which was inserted into the DLS sample holder. Temperature was kept at 22°C during the measurement. After the system is stabilized for 30 min, scattering experiments were carried out at five different angles, 30°, 45°, 60°, 75° and 90°. Each experiment was repeated three times to ensure repeatability. The followings are the generated count rate vs time plots.

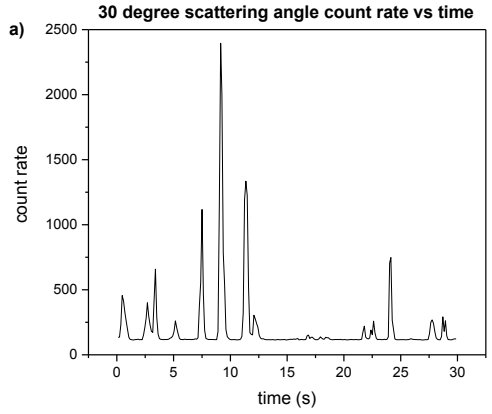

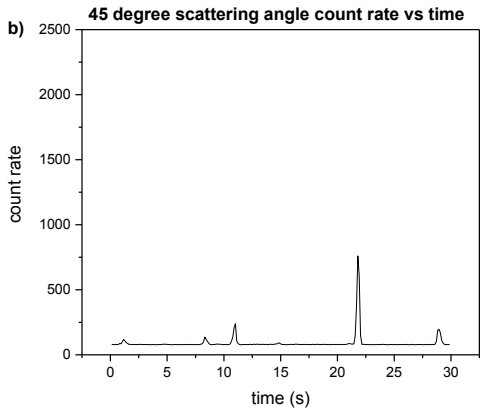

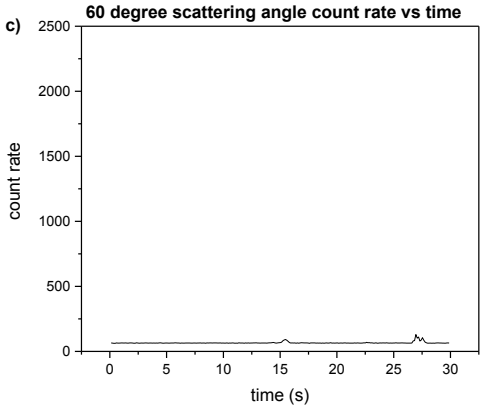

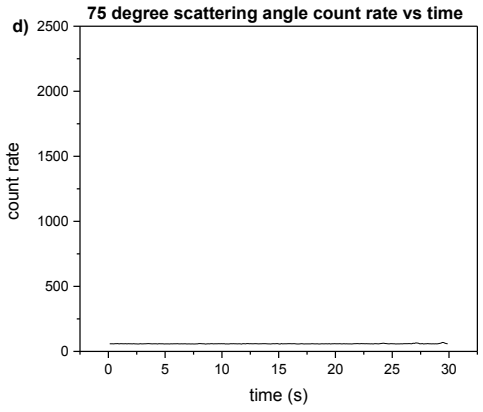

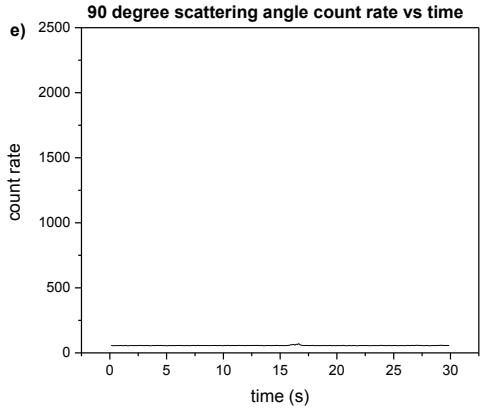

Figure 4.3 Pure heptol solvent light scattering count rate vs time at five different detection angles, a) 30°, b) 45°, c) 60°, d) 75° and e) 90°.

Since pure solvents should not contain any measurable aggregates, the scattering count rate should be consistent over time. Therefore, as shown in Fig. 4.3, the peaks shown in a), b) and c) are associated with non-even scattering level and can be regarded as noise. The noise level decreases with increasing detection angles. This is because at small detection angles, reflection from glass cell contributes more to the obtained count rate signal. This observation is consistent with previous reports in literature.[136,137] Therefore larger detection angles should be used.

In addition to pure solvents, modeling compounds were also used to further determine the noise levels at various scattering angles. The generated auto correlation functions were compared for the same C5PeC11 solution 20 min after aggregation was induced. The concentration for C5PeC11 in the experiment was 0.05 mg/ml and 80 vol% heptol (i.e. 20 vol% toluene and 80 vol% heptane) was used as the bulk solvent. Below in Fig. 4.4 are the count rate vs time plots for the same model compound 20 min after precipitant (heptane) addition.

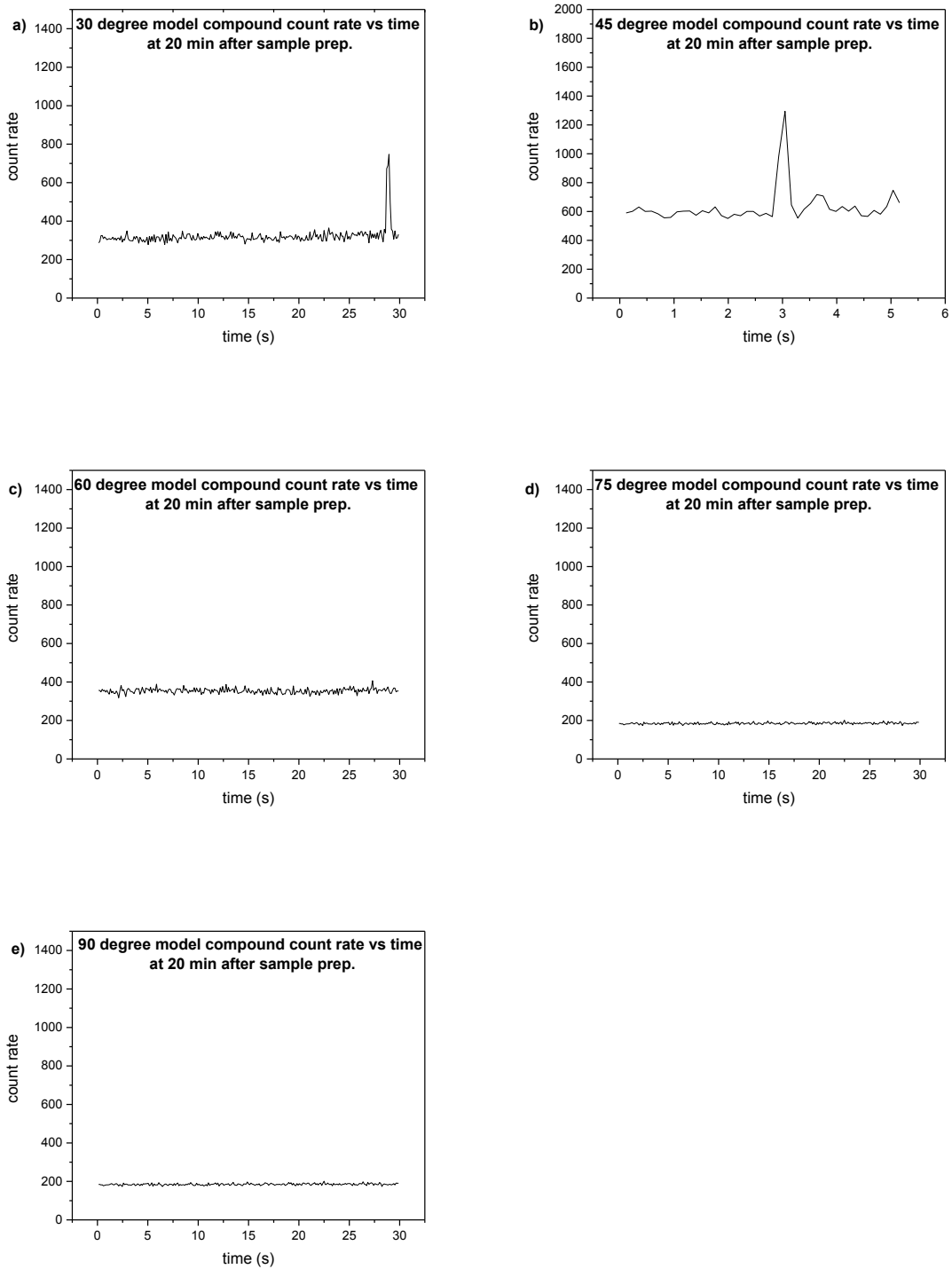

Figure 4.4 C5PeC11 0.05 mg/ml light scattering count rate vs time at 20 min after experiment started. The scattering angles used are: a) 30°, b) 45°, c) 60°, d) 75° and e) 90°.

Figure 4.4 shows that detection at both 75° and 90° angles give consistent count rate between 100-500 kcps during the entire measurement. Unexpected peaks in count rate were observed at smaller scattering angles due to the high probabilities of back scattering. These results confirm both 75° and 90° angles are suitable for DLS measurement. For the following DLS measurements in this research, 75° scattering angle was used as the detection angle.

4.2.4 Experiment Temperature

Since DLS measurements are very sensitive to temperature fluctuations, water bath is used to keep the samples at constant temperatures during measurements. For asphaltenes and model compounds, high temperature inhibits aggregation and low temperature accelerates aggregation significantly. In addition, since sample measurements started immediately upon preparation, no stabilization period is allowed. Therefore, water bath temperature used was close to room temperature at 22 °C. This is also the same temperature used in refractive index measurements.

4.2.5 Sample Concentrations

For DLS experiments, sample concentrations need to be controlled to obtain consistent results. The sample concentration has to be chosen as a compromise between a desirable range of S/N ratios and the minimization of multi-scattering and sedimentation effects within two hr. measurement time. The multi-scattering effect can be identified by observing the obtained ACF. For concentrated samples, ACF is shifted towards smaller lag times with broader distributions

and decreased intercept values, leading to further difficulties in ACF interpretations. For asphaltene fractions, a concentration of 0.1 g/L in heptol leads to repeatable hydrodynamic radius measurements at specific aggregation time. For model compound C5PeC11, a same concentration of 0.1 g/L in heptol as asphaltene fractions was used in all measurements. For C5Pe, due to its low solubility in heptol solution, a concentration of 0.02 g/L was used. For BisAC11, due to its higher solubility in heptol, solutions with concentrations between 0.1 - 0.2 g/L were used depending on experiments. The following Table 4.3 summarizes the concentrations for all compounds used in DLS experiments.

Table 4.3 Optimized measurement concentrations for asphaltene fractions and model compounds in DLS experiments.

Compounds	Irr-Ads Asp.	Ads Asp.	Non-Ads Asp.	C5Pe	C5PeC11	BisAC11
Concentration	0.1 g/L	0.1 g/L	0.1 g/L	0.02 g/L	0.1 g/L	0.1 g/L -0.2g/L

Particle sedimentation interferes with DLS analysis causing decreasing count rate. Once sedimentation occurs, the randomness in Brownian motion is altered and the measured diffusion constant of the particle is no longer valid. One easy way to determine if sedimentation has occurred for a sample is by observing the ACF. Increases in correlation at high delay times indicate non-random movement (sedimentation) of particles.

Figure 4.5 shows a correlation function obtained after 3 hr of continuous measurement of 0.1 g/L C5PeC11in 80 vol% heptol solution. Over time, the concentration of sediment particles increased,

leading to slow growth of a non-exponential tail on the correlation function. After about 3 hr continuous monitoring of the model compound, the ACF became distorted and could no longer be interpreted for hydrodynamic radius. As a result, all measurements were conducted within 120 min measurement time.

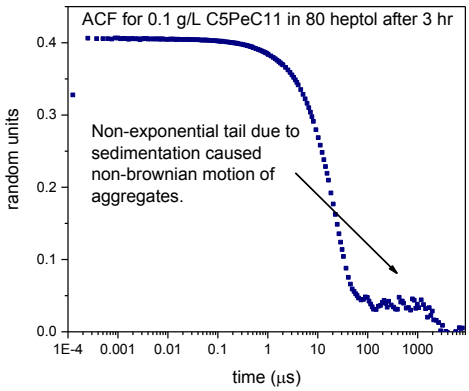

Figure 4.5 ACF obtained for 0.1 g/ L C5PeC11 model compound in 80 vol% heptol solution. The non-exponential tail can be observed after 3 hr continuous measurements due to sedimentation.

4.2.6 DLS Measurement Accumulation Time

For DLS measurement, the optimal accumulation time should be chosen as a compromise between the desire of achieving sufficient statistical accuracy and the requirement of an insignificant variation of the aggregation sizes within the data accumulation period. The accumulation time of the correlation function, depending on the light-scattering intensity, may vary from seconds to hours. The most typical measurement time is between 1-10 min.[138] Since

the total measurement time for our samples were kept below 2 hr., the accumulation time was chosen as 60 s for each run. After each measurement, the system was left for 60 s before the next run started. Therefore, for a 2 hr experiment, a total of 60 runs were completed.

4.2.7 DLS Experimental Methods

For the current research, an ALV-5022 laser light scattering equipment was used. The device uses a cylindrical polarized He-Ne laser (model 1145p-3083; output power = 22mW at λ = 632.8 nm). The detector for the instrumentation is an ALV-High QE Avalanche Photo Diode for single photon detection. The registered photon counts are processed by a multiple Tau digital correlator (ALV SP-86) which is extended on the very fast sampling time limit using ALV-5000/FAST Tau addition. The digital correlator reduces the initial sampling time to just 125 ns to allow the processes of fast measurements. The sample holder includes an external thermostat element that can be used to keep the sample temperature at a fixed value in the range of 8 °C to 55 °C. The cell was filled with high purity, dust-free toluene. Sample volume per measurement was constant at 2000 μl.

Control of the instrument parameters such as cuvette position, measurement time, scattering angle, measurement repetitions and data acquisition and analysis were attained via the ALV correlation software V 3.0.2.4. The software includes cumulant analysis (linear, second and third cumulants), inversion via CONTIN which is a nonlinear regularization method and nonlinear model fitting with model data bases. As discussed in Chapter 3, for this research only nonlinear regularized fitting was used. All dynamic light scattering measurements were taken at 75 ° scattering angle.

The detailed measurement protocol was shown below. Prior to each measurement, the stock solution of model compound or asphaltene fractions were first sonicated and filtered through a 0.2 μm needle filter to remove dust and insoluble impurities. 200 μl filtered solution was then added into a Fisher Disposable Borosilicate Glass tube. 1800 μl filtered heptol solution (various heptane/toluene mass ratios) was then added to induce aggregation. For model compounds C5Pe, C5PeC11, and BisAC11, the solutions were a slightly orange colored clear liquid. Upon addition of heptol, the optical cell was sealed and shaken vigorously for 30 s. Light-scattering experiments started exactly 1 min after the addition of heptol. Similar procedures were used for asphaltene fractions with a final concentration of 0.1 g/L.

Chapter 5 Results and Discussion

5.1 Asphaltene Fractions

5.1.1 Aggregation Behaviors of Three Asphaltene Fractions

The aggregation behaviors of three asphaltene fractions Irr-Ads, Ads and Non-Ads were monitored using DLS. Figure 5.1, 5.2 and 5.3 show the observed ACFs for the three fractions at different heptane concentrations in solution. All ACFs were taken at exactly 30 min after aggregation was allowed to start. All asphaltene fractions are shown sensitive to heptane concentrations. The amplitude of the correlation function increases due to increasing sizes of the scatters with increasing heptane concentrations. This result indicates that for Irr-Ads asphaltenes, heptane is an effective precipitant that induces aggregation. With increasing heptane

concentration, the inflection points also increase in magnitude indicating a decrease in the Brownian diffusion rate due to larger sizes of the aggregates.

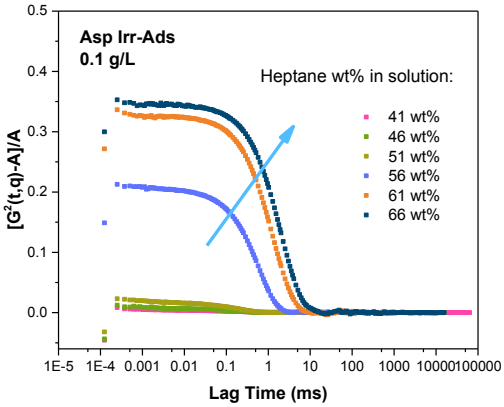

Figure 5.1 DLS correlation functions (in terms of the 'delay' time) for asphaltene Irr-Ads fraction.

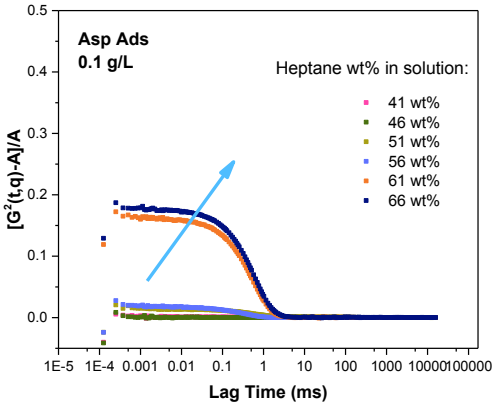

Figure 5.2 DLS correlation functions (in terms of the 'delay' time) for asphaltene Ads fraction.

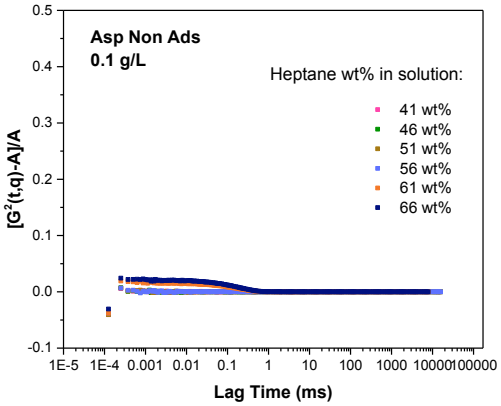

Figure 5.3 DLS correlation functions (in terms of the 'delay' time) for asphaltene Non-Ads fraction.

However, comparing the three figures above, the flocculation tendency varies between different fractions. For Irr-Ads asphaltenes (Fig. 5.1), the decay of the obtained ACFs is more prominent at all heptane concentrations. The amplitude of the correlation function is around 0.35 for Irr-Ads asphaltene in 61 wt% heptol. In general, the faster the decay of the observed ACF, the faster the aggregation rate of the particles in solution. Similar behaviors are found for Ads asphaltene fraction, as heptane concentration increases to 61 wt%, the amplitude of the correlation function reaches around 0.2. However, for the Non-Ads asphaltene, the amplitudes remain low (<0.05) even at high heptane concentrations (> 50 wt%) and the decay of the ACFs is negligible. This suggests in the solution of Non-Ads asphaltenes, only small aggregates/ scatters are present at 30 min after flocculation is allowed to start. It can be concluded that under similar conditions, the aggregation tendency for the asphaltene fractions follows the order: Irr-Ads > Ads > Non-Ads.

Aggregation kinetics of the three asphlatene fractions is then studied under the same condition of 56 wt% heptol. CONTIN analysis is used to obtain hydrodynamic radius distribution every 2 min

for a total of 2 hr. period. The measured hydrodynamic radius as a function of time is shown in Fig. 5.4, which further confirms that Irr-Ads asphaltenes aggregate most easily under the same conditions. For the Non-Ads asphaltenes, the measured hydrodynamic radius stayed almost constant at ~ 60 nm for the entire two hr. suggesting the lowest aggregation tendency.

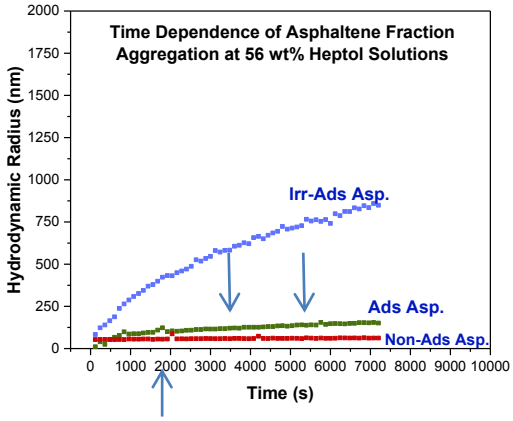

Figure 5.4 Measured time dependence of the aggregation size of three asphaltene fractions. The concentration of heptane is kept constant for three measurements at 56 wt%.

Another advantage of using CONTIN analysis is that the distributions of hydrodynamic radii for multimodel systems such as asphaltenes can be obtained. For the above aggregation profile in Fig. 5.4, the aggregation size distributions are extracted at 30, 60 and 90 min after experiment started (indicated by the arrows) and the results are presented in Fig. 5.5.

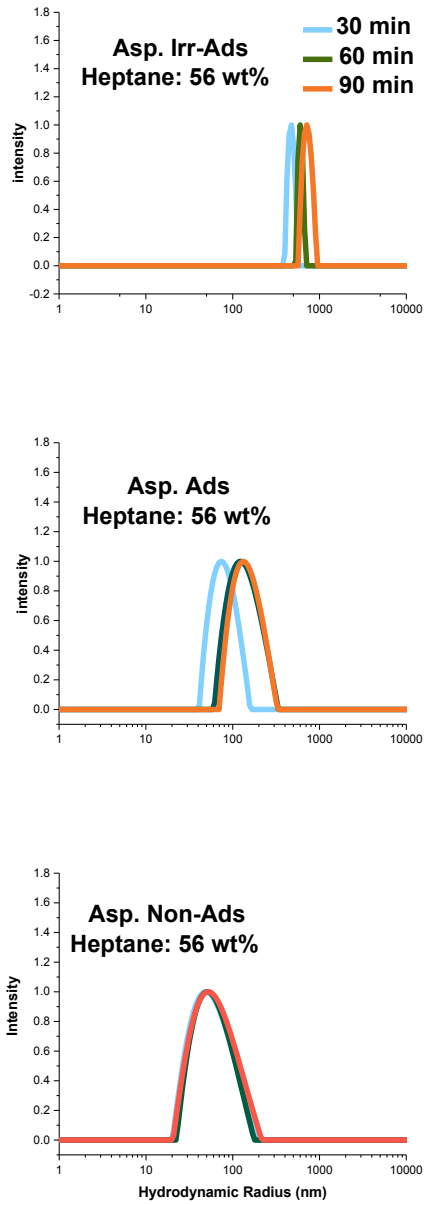

Figure 5.5 Hydrodynamic radii distributions obtained from CONTIN analysis for three asphaltene fractions. The heptane concentration used is 56 wt%. The distribution peaks were obtained at 30, 60 and 90 min after aggregation was induced (indicated with arrows in Fig. 5.4).

As shown on Fig. 5.5, for all asphaltene fractions, the aggregation sizes follow a log-normal distribution in solution. This indicates the size of asphaltene flocs grow in a multiplicative fashion which is typical for three-dimensional structures. For Irr-Ads asphaltene fraction, its hydrodynamic radius increases continuously for the first two hr. For Ads asphaltenes, the 30 min peak is centered at a smaller hydrodynamic radius compare with that of Irr-Ads fraction. After 60 min, the peak for Ads fraction shifts away from the 30 min peak indicating a growth in the hydrodynamic radius. However, for Ads asphaltenes, the 60 min peak and 90 min peak are almost overlapping with each other, suggesting a slow-down in the rate of aggregation. Overall the aggregation tendency for Ads asphaltenes is lower than that of Irr-Ads asphaltenes. For Non-Ads asphaltene fraction, the measured hydrodynamic radii are small at all times. In addition, significant overlaps can be observed for all three peaks taken at different experiment stages for Non-Ads fraction. This suggests Non-Ads asphaltenes have the lowest aggregation rate. The size of aggregates stays almost constant at around 60 nm for the entire experiment, suggesting the lowest aggregation tendency among all fractions.

Same procedures were used to determine the aggregation profiles of three asphaltene fractions at various heptane concentrations from 41 to 61 wt%. Higher heptane concentrations could induce slow sedimentations where the directional motions of particles contribute to the non-exponential decay of the measured correlation functions and complicate the interpretation process. Figure 5.6 shows the measured hydrodynamic radius as a function of time for Irr-Ads asphaltene fraction. At low heptane concentrations, the size of flocs remain small and no obvious fast aggregation can be detected. Higher heptane concentration accelerates the aggregation process. This observation correlates well with previously published results and indicates heptane is an efficient

precipitant that induces asphaltene flocculation.[138][123] With 66 wt% of heptane, distortion of correlation functions occurred after 1 hr., preventing further monitoring of the flocculation. Over the heptane concentration range (< 70 wt%), no upper limit of flocs size was observed for Irr-Ads asphaltenes. For Irr-Ads asphaltenes, the rate of aggregation as well as the size of particles in solution increase with increasing heptane concentrations.

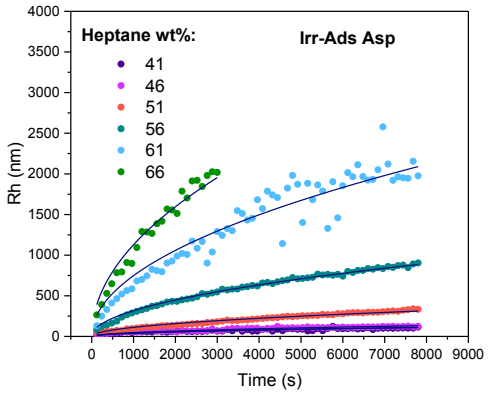

Figure 5.6 Time dependence of Irr-Ads asphaltene aggregation with increasing heptane concentrations.

Figure 5.7 plots the same data from Fig. 5.6 on double logarithmic scales. A linear relationship was observed between the measured hydrodynamic radius and aggregation time, indicating that the size of the aggregates can be approximated by equation

$$R(t) = At^{a}$$

where A is a system-specific constant reflecting the size of aggregates.[138] Upon fitting, values of the exponent constant a were obtained to be 0.36 ± 0.05, which agrees well with the values reported for whole asphaltenes.[138,139] The observed power law dependence indicates that aggregation follows the diffusion-limited aggregation (DLA) kinetics for Irr-Ads asphaltenes.

The DLA of asphaltenes could lead to the formation of fractal structures. The similarities between the current results for Irr-Ads asphaltenes and reported results for whole asphaltenes suggest that the Irr-Ads asphaltenes with very high tendency of molecular aggregation is most likely the fraction of asphaltenes that is responsible for the observed massive aggregation behavior in whole asphaltenes.

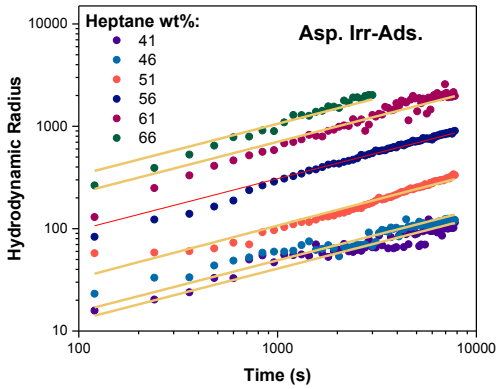

Figure 5.7 Hydrodynamic radii as a function of time plot in logarithmic scales. Slopes after fitting = 0.36 ± 0.05.

Moreover, the three asphaltene fractions were individually tested for their aggregation behaviors in various heptane concentrations. The results are summarized in Fig. 5.8. Compare with Irr-Ads asphaltenes, much lower flocculation tendency was observed for Ads asphaltenes in solutions with up to 61 wt% heptane. At lower heptane concentrations negligible aggregation was shown for Ads asphaltenes. For Non-Ads asphaltenes (Fig 4(b)), no large flocs could be observed in all heptol solutions tested. Even in the heptol with 80 wt% heptane, the measured hydrodynamic

radius of Non-Ads asphaltenes remained small at around 60-80 nm over the entire measurement period.

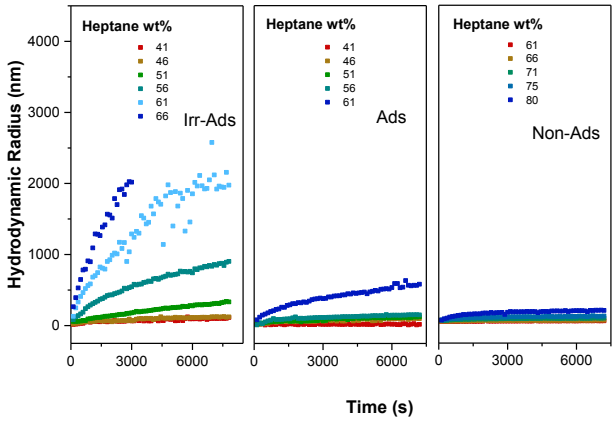

Figure 5.8 Aggregation behaviors for Irr-Ads, Ads, and Non-Ads asphaltene fraction.

These results suggest among the three asphaltene fractions, Irr-Ads asphaltenes has the highest tendency to aggregate, following the diffusion limited aggregation profile. Since the separation of the three asphaltene fractions is quantitative with a recovery of 98-99% (by weight), this result confirms Irr-Ads asphlatenes being the fraction responsible for the massive aggregation in whole asphaltenes.[22] Early studies using FT-IR spectroscopy showed that the primary difference between the three asphaltene subfractions is the higher concentrations of polar groups such as carbonyl and carboxylic acid in the Irr-Ads asphaltenes.[22] It is therefore reasonable to conclude that the binding interactions between various polar groups are one of the dominating forces responsible for the flocculation of whole asphaltenes. Previous results also support the same conclusion that the more polar asphaltene fraction is seen increasingly less soluble in heptane/ toluene solutions. As a result, the addition of more polar resin could disrupt the polar group interactions and destabilize asphaltene aggregation.[140]

In addition, the reported elemental analysis shows the H/C ratios for all the asphaltene fractions remain within a narrow range (1.13-1.20), indicating all fractions have similar degrees of aromaticity.[22] The Irr-Ads asphaltenes even show slightly higher H/C ratios suggesting lower double bond equivalence compare with the remaining fractions. This is in contrast to the common perception that π stacking forces contribute to the aggregation of polyaromatic compounds. π-π interaction is possibly not the dominating factor that induces asphaltene flocculation beyond nanoscales. Other factors exist that control the aggregation of asphaltene molecules. In particular, the higher oxygen levels detected in Irr-Ads asphaltenes contribute greatly to its higher polarity, which increase the binding interactions between nanoaggregates. These results further confirm that the flocculation of asphaltenes in petroleum fluids are mostly driven by polar group interactions such as hydrogen bonding or heteroatom interactions rather than π-π interactions.[141]

5.1.2 Effect of DBSA

Dodecylbenzene sulfonic acid has been identified as an effective precipitation inhibitor for whole asphaltenes. At low concentrations, the 12-carbon chain organic acid has shown to dissolve asphatlenes to molecular scales.[142,143] Several factors are known to determine the effectiveness of DBSA. First, previous research has identified metal content as an important factor. Under the same conditions, removing metals in crude oil can increase the asphaltene dissolution rates by DBSA.[144] Second, molecular modeling has suggested asphaltene dissolution effectiveness is closely related to the non-specific adsorption process of DBSA onto

asphaltene surfaces.[145] In addition, the concentration of DBSA also plays an important role. Turbidity measurements show that low concentrations of DBSA do not prevent the fast sedimentation of asphaltenes.[88] Other studies show that the amount of precipitated asphaltenes increase first with increasing DBSA concentration. Beyond a certain DBSA concentration, a decrease in precipitation can be observed.[146] These observations all suggest the complex nature of the interactions between various species in petroleum fluids. In this study, the effects of DBSA on different asphaltene fractions were individually probed. The role of DBSA concentration was studied in terms of aggregation rates and flocs sizes as well as the amount of precipitant added into the system. Through this study, we want to understand how asphaltene fractionation can play a role in the interactions between asphaltene nanoaggregates and DBSA molecules.

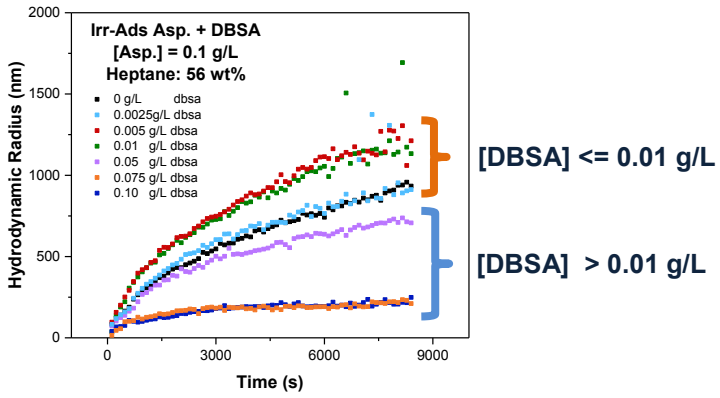

Figure 5.9 Hydrodynamic radii as a function of time for Irr-Ads asphaltene fraction with different DBSA concentrations in solution. Heptane concentration was kept constant at 56 wt%. The concentration for Irr-Ads asphaltene fraction is 0.1 g/L.

As shown on Fig. 5.9, at low DBSA concentrations ([DBSA] <= 0.01 g/L), the hydrodynamic radius actually increases with DBSA concentrations. For the solution when 0.0025 g/L DBSA

was added, the measured sizes of aggregates are almost the same as the case when no DBSA was dosed. When DBSA concentration increases to 0.005 g/L, the rate of aggregation reaches the maximum value and the sizes of flocs peak at ~1250 nm after 2 hr. However, at higher DBSA concentrations, i.e. 0.01 g/L, as shown on Fig. 5.9, no further increase in the rate of aggregation is observed. On the contrary, a dispersive effect can be observed when high amounts of DBSA are dosed into the system and asphaltene flocs remain small and stabilized.

Together these experiments suggest that at low concentrations DBSA can accelerate the aggregation process for Irr-Ads asphaltenes. Similar result was also observed in previous literature.[146,147] Reported MD simulations coupled with high-resolution transmission electron microscopy (HRTEM) experiments reveal the interactions between protonated asphatlenes and DBSA molecules lead to stronger bindings interactions (which can be fifteen times stronger than asphaltene-alkylphenol interactions).[148] These interactions promoted the formation of larger and more compact asphaltene flocs comparing with the small and loose ones formed in the absence of DBSA. [148]

At higher DBSA concentrations, the self-aggregation of DBSA contributes to the full dissolution of asphaltenes in nonpolar solvents.[90,149] Studies suggest that the formation of DBSA hemi-amphiphile micelles at the surface of asphaltene nanoaggregates can prevent the aggregation of asphaltene flocs. Similar behaviors were also observed in the other asphlatene fractions, Ads and Non-Ads asphaltenes.

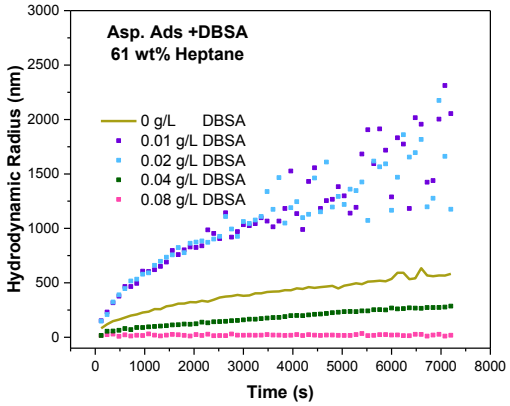

Figure 5.10 Hydrodynamic radii as a function of time for Ads asphaltene fraction with different DBSA concentrations in solution. Heptane concentration was kept constant at 61 wt%. The concentration for Ads asphaltene fraction is 0.1 g/L.

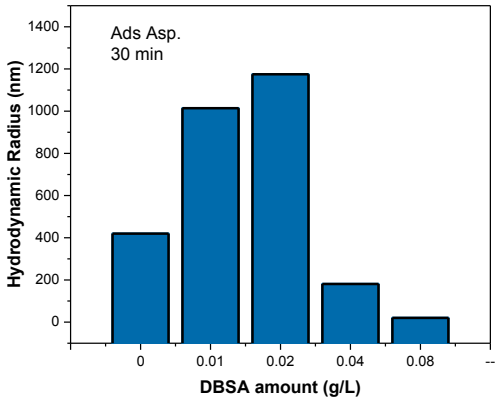

Figure 5.11 The measured hydrodynamic radii for Ads asphaltene fraction as a function of DBSA concentrations in solution 30 min after experiment started. The concentration of Ads asphaltene is 0.1 g/L in 61 wt% heptane/ toluene solution.

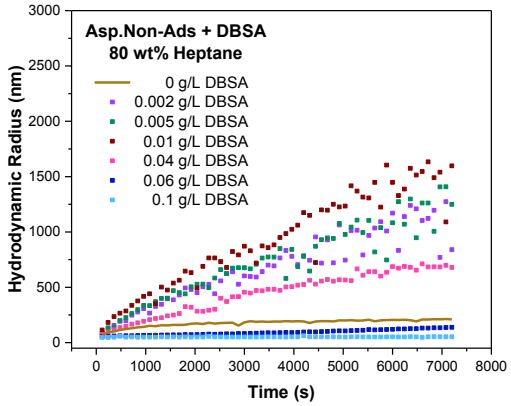

Figure 5.12 Hydrodynamic radii as a function of time for Non-Ads asphaltene fraction with different DBSA concentrations in solution. Heptane concentration was kept constant at 80 wt%. The concentration for Non-Ads asphaltene fraction is 0.1 g/L.

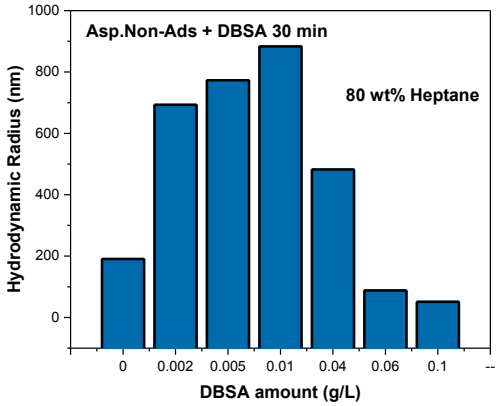

Figure 5.13 The measured hydrodynamic radii for Non-Ads asphaltene fraction as a function of DBSA concentration in solution 30 min after experiment started. The concentration of Non-Ads asphaltene is 0.1 g/L in 80 wt% heptane/ toluene solution.

As shown in Fig. 5.10-13, low DBSA concentrations can cause more prominent aggregations for all asphaltene fractions. As shown in the bar charts (Fig. 5.11 and 5.13), at 30 min after aggregation is allowed to start, the hydrodynamic radius increases first with dosed DBSA amounts before decreases to the point where complete inhibition of aggregation is observed. This behavior is consistent with that of Irr-Ads asphaltene as well as whole asphaltenes. At low concentrations, the self-aggregation and solubility effects of DBSA are competing processes that can prevent the interactions between the inhibitor molecules and asphaltenes. On the other hand, the polar group interaction between DBSA and asphaltenes can act as 'glue' that bind together the small nanoaggregates of asphaltenes inducing aggregation.

In addition, all asphaltene fractions show the presence of saturation points above which the hydrodynamic radius no longer increases with increasing DBSA concentrations. This saturation of aggregate size growth is related to the transition of DBSA coverage on asphaltene nanoaggregates. At the saturation points, the aggregation driving force reaches its maximum and does not change with further increase of the inhibitor concentrations. When DBSA concentration is higher than aggregation threshold, the steric repulsion due to long alkyl chains of DBSA becomes the more dominating force as the number of DBSA on asphaltene nanoagggregate surfaces increases with its solution concentration. Apart from DBSA concentration effects, previous reports also suggest that at high concentrations, the DBSA multilayers on the surface of asphaltenes were a critical factor to stabilize asphaltene aggregates.[85,91,150] These multilayers are formed through association between DBSA molecules and therefore related to the self-aggregation of DBSA.[147] The polar group interactions between asphaltenes are interrupted when DBSA concentrations are higher in solution. This can be explained by two processes, one is the interaction between DBSA and asphaltenes, the other the dissociation of

asphaltene aggregates facilitating the inhibition of asphaltene flocculation. This result suggests all asphaltene fractions interact in similar fashions with DBSA. Lower DBSA concentrations accelerate their aggregation while high DBSA concentrations inhibit aggregation.

5.1.3 Asphaltene Aggregation: Prevention vs. Dispersion

As we have observed in 5.1.2, high DBSA concentrations can inhibit the massive aggregation behaviors of all asphaltene fractions. However one question remains: will the addition of DBSA re-disperse the already formed aggregates of asphaltenes in solution? We designed a group of experiments to test the effect of delayed addition of DBSA into the Irr-Ads asphaltene fraction. The heptane concentration used in the experiments was constant at 56 wt%. DBSA was either added together with Irr-Ads asphaltene at the beginning of the experiments or 30 min later after aggregation started. The experiment results are shown in Fig. 5.14.

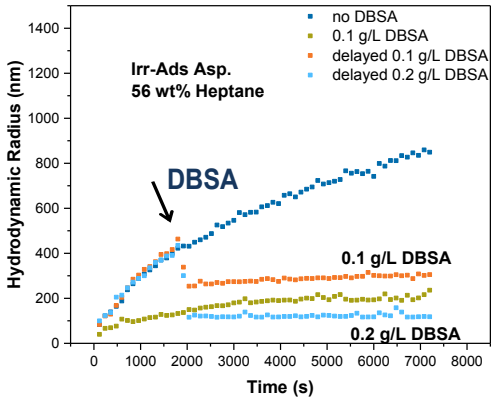

Figure 5.14 Hydrodynamic radii as a function of time for 0.1 g/L Irr-Ads asphaltene. Heptane concentration for all measurements is constant at 56 wt%. DBSA was dosed either in the beginning or 30 min after aggregation was allowed to start.

As shown in Fig. 5.14, with the absence of DBSA, Irr-Ads asphaltenes aggregate fast in 56 wt% heptane/ toluene solution due to the precipitation effect of heptane. After two hr., the measured hydrodynamic radii reach 800 nm. With the addition of DBSA (final DBSA concentration 0.1 g/L) at the beginning, the aggregation process of the mixture is inhibited significantly. The hydrodynamic radius only increases slowly to about 200 nm due to the solvation effects of DBSA. However, if DBSA was added in a delayed fashion 30 min after experiment started, a reduction in size can be observed for the already formed aggregates. The measured hydrodynamic radius decreases from 400 nm to 200 nm within a short time of 6 min upon DBSA addition. The reduced hydrodynamic radius remains small at around 250 nm for the rest of the measurement. This result suggests DBSA could re-disperse the already formed aggregates in heptane/toluene solutions into smaller pieces. However the reduced size of aggregates is still larger than the case when DBSA is mixed into the solution in the beginning. This suggests DBSA could only re-disperse the loosely attached structures. For aggregates that are formed with strong binding forces, the addition of DBSA is less effective. When DBSA is mixed with asphaltenes, sufficient amounts of DBSA are able to surround the nanoaggregates of asphaltenes and inhibit further aggregation. However, after 30 min, strong polar interactions between asphlatene nanoaggregates are formed and the addition of DBSA can only disrupt the weak bondings. By adsorbing on the surface of smaller aggregates, DBSA is able to break down the

loosely attached flocs. Therefore the resulting averaged size of flocs in solution is larger than the case when DBSA is mixed into the solution in the beginning.

More over, an increase in DBSA amounts in a delayed addition manner can further reduce the size of aggregates. As shown in the same Fig. 5.14, when DBSA with a final concentration of 0.2 g/L is added 30 min after aggregation is allowed to start, the measured hydrodynamic radius is reduced to 100 nm, much smaller than the previous case with 0.1 g/L DBSA. This result suggests the interaction between DBSA and asphaltenes is much stronger than that among asphaltene molecules. In solution, asphaltenes preferably interact with DBSA due to polar functional groups. With the presence of long aliphatic chains, these DBSA molecules then stretch themselves into heptol solutions and stabilize the flocculated systems.

5.2 Asphaltene Model Compounds

Since asphlatenes are defined as a solubility class, fractionation of asphaltene is insufficient to understand its aggregation mechanisms on molecular level. The complex and polydisperse nature of asphaltenes significantly limit our abilities to mitigate its adverse effects in crude oil production. Though studying asphaltene chemistry such as polar group concentrations may bring us some insights into its inherent nature, it's likely that fractionation processes involved has modified the interactions between different components. Therefore, to understand how molecular interactions contribute to the aggregation behaviors in asphaltenes, we further studied three model compounds in detail with well-defined molecular structures. The nanoaggregation of the model compounds was investigated using ESI-MS (performed by Dr. Lan Liu) while the

flocculation processes were studied using DLS. This will lead to a better understanding for the more complicated real asphaltenes found in crude oils.

5.2.1 Aggregation Behaviors of C5Pe, C5PeC11 and BisAC11

The flocculation of C5Pe, C5PeC11 and BisAC11 was studied using dynamic light scattering. Similar procedures as in previous measurement of asphaltene fractions were used. However all polyaromatic compounds were individually optimized in terms of solution concentrations based on signal to noise ratios of the scattered light. Figure 5.15-17, show the plots of hydrodynamic radius as a function of time for three polyaromatic compounds, C5Pe, C5PeC11 and BisAC11, respectively. As can be seen, C5Pe exhibits the highest tendency to aggregate due to its short side chains. At concentration as low as 0.02 g/L in 75 wt% heptol, C5Pe aggregates rapidly to form flocs of size between 800 to 1000 nm in less than 30 min. Higher concentrations of C5Pe become insoluble in heptol solutions, resulting in fast sedimentation of precipitated particles/ flocs, leading to distortion of the obtained correlation functions. For C5PeC11, a higher concentration of 0.1 g/L is needed to initiate flocculation at solvent conditions similar to that of C5Pe. For BisAC11, no obvious flocculation was observed even at very high solute concentrations (0.1~0.2 g/L). A possible explanation for the observation is that the longer aliphatic chains in C5PeC11 and BisAC11 are more solvated by interacting with the solvent molecules, resulting in higher solubility of C5PeC11 and BisAC11 in heptane/ toluene mixtures. The observed flocculation behavior of polyaromatic compounds also correlates well with the previous nanoaggregation results from ESI-MS measurements.

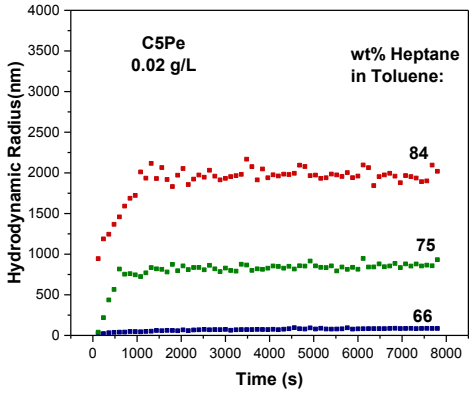

Figure 5.15 Hydrodynamic radii as a function of time for model compound C5Pe. Three different heptane concentrations were tested: 84, 75 and 66 wt%. The optimized concentration for C5Pe is constant at 0.02 g/L in all measurements.

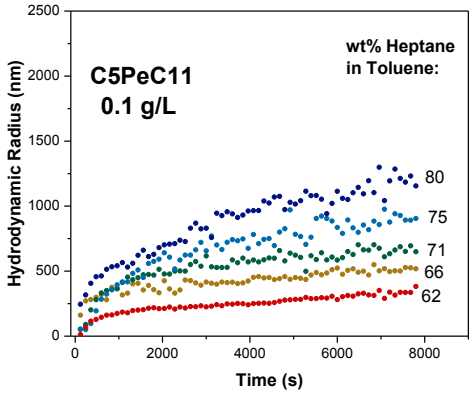

Figure 5.16 Hydrodynamic radii as a function of time for model compound C5PeC11. Various heptane concentrations were used ranging from 62 to 80 wt%. The concentration for C5PeC11 is constant at 0.1 g/L in all measurements.

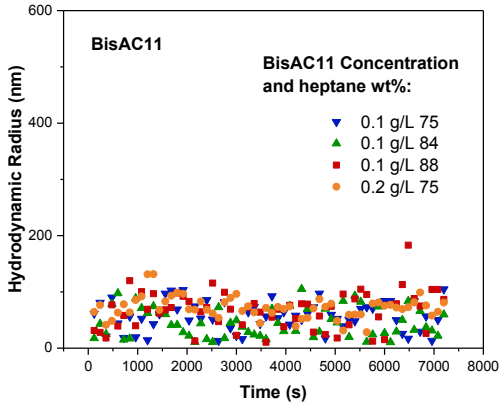

Figure 5.17 Hydrodynamic radii as a function of time for model compound BisAC11. High heptane in toluene concentrations were used at 75, 84 and 88 wt%. The initial concentration of BisAC11 is 0.1 g/L. A higher concentration was also tested at 0.2 g/L. No obvious aggregation behaviors were observed in all cases.

As shown on the ESI-MS spectra in Fig. 5.18 and 5.19, at the same concentration, C5Pe is most likely to aggregate while C5PeC11 do not show significant aggregation behaviors. Under the same conditions, the calculated average nano-aggregation number is 5.14 for C5Pe while for C5PeC11, the number decreases to 1.46. In addition, as shown on the spectra, for C5Pe, large nanoaggregates can be detected formed with 6-17 molecules. However for C5PeC11, dimers and trimes are the most commonly detected species in solution. This suggests that in average C5Pe has larger building blocks comparing with C5PeC11, which explains its fast flocculation observed with DLS. Due to its unstable ionic form, BisAC11 cannot be tested individually using ESI-MS. However the polydispersity effect of BisAC11 combined with either C5Pe or C5PeC11 detected by mass spectrometry are presented in 5.2.4.

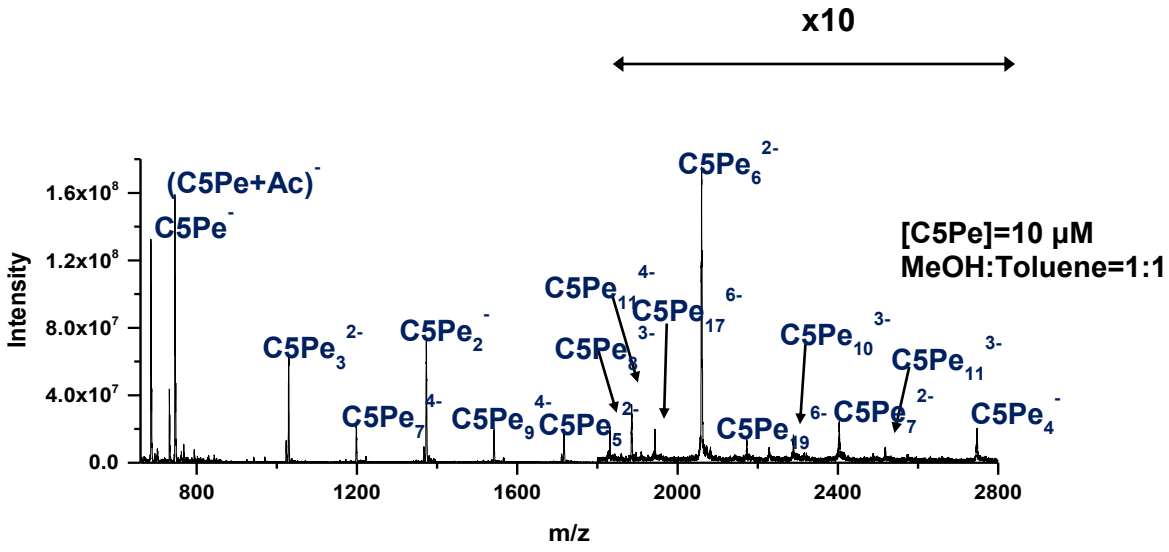

Figure 5.18 ESI-MS spectrum for 1:1 methanol-toluene solution containing 10 µM C5Pe and 5 mM NH_4AC in negative ion mode at 25°.

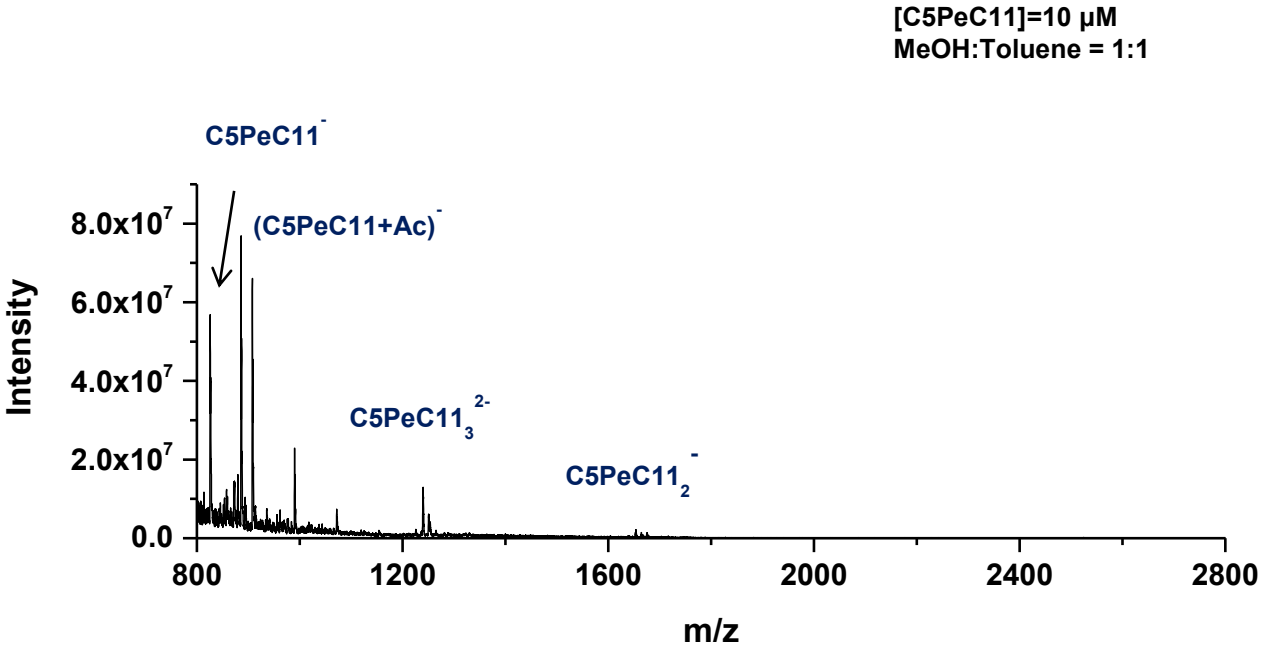

Figure 5.19 ESI-MS spectrum for 1:1 methanol-toluene solution containing 10 µM C5PeC11 and 5 mM NH_4AC in negative ion mode at 25°.

In addition, the aggregation/ flocculation of both C5Pe and C5PeC11 appear to be sensitive to heptane concentrations in solution. For C5Pe, a higher heptane concentration leads to more flocculation within the first 30 min, with the flocs size at the same measurement time doubled with 10 wt% heptane concentration increment. For C5PeC11, 4-5 wt% increments in heptane concentration can lead to a significant variation in the observed flocculation profiles. In the case of BisAC11, the presence of longer aliphatic chains and the lack of polar groups significantly hindered its ability to flocculate. Even at high heptane concentrations over 80 wt%, there is no dramatic change in the flocculation behavior of BisAC11. In addition, a higher concentration of 0.2 g/L BisAC11 in 75 wt% heptane solution also failed to induce appreciable flocculation. The measured hydrodynamic radius of BisAC11 flocs at all solution conditions remained below 200 nm even after 2 hr. of continuous monitoring. These results correspond well with the observed heptane effect on nanoaggregation of the three polyaromatic compounds, suggesting that both molecular structures and functional groups of polyaromatic compounds play important roles in controlling nanoaggregation and flocculation of polyaromatic compounds in bulk solutions.

More specifically, previous results have shown that polar group interaction is one of the dominating factors in controlling the aggregation of PA molecules. Comparing BisAC11 with C5PeC11, the absence of polar functional groups in BisAC11 reduces the binding interactions between molecules in solution. As a result, flocculation of BisAC11 in bulk systems is hindered. Another factor that contributes to the decreased aggregation for BisAC11 is the presence of longer aliphatic chains. The C-C single bonds have higher degrees of freedom and increase the steric hindrance of π-π interactions. As a result, binding processes between molecules and nanoaggregates of BisAC11 become more difficult to occur. To control the aggregation tendency

of PA compounds, the length and number of aliphatic chains as well as polar functional groups in polyaromatic compounds must be controlled to achieve suitable solubility in aliphatic/ aromatic solvents.[151]

Interestingly, as shown in Figure 5.16, the size of C5Pe flocs increases almost linearly with time during the first ten to fifteen minutes. After this fast aggregation period, the measured size of aggregates stayed constant for the rest of the measurement period. Higher heptane concentration in solution gives larger final flocs sizes. This unique property of C5Pe suggests its extremely high tendency to aggregate. In heptane/ toluene bulk solutions, the small nanoaggregates of C5Pe bind together to form larger structures until, with the depletion of nanoaggregates concentrations, the measured aggregate size begins to stay at a relatively constant value.

For C5PeC11, the longer aliphatic chains can better stabilize the polyaromatic molecules and increase its solubility in heptane/ toluene solutions. Notably at the same concentration, C5PeC11 showed similar size ranges of nanoaggregates to that of Irr-Ads asphaltenes. The overall flocculation profile of C5PeC11 is comparable to that of Irr-Ads asphaltenes. This observation indicates that C5PeC11 exhibits similar aggregation behavior to Irr-Ads asphaltenes, demonstrating C5PeC11 to be a potential model compound to study real asphaltene molecules. Moreover, compare with C5Pe, the measured hydrodynamic radius for C5PeC11 increased more slowly with time. Instead of reaching a plateau as in the case of C5Pe, the flocs size continues to increase even after 2 hr. of measurement. The slower and continuous aggregation of C5PeC11 is again similar to that of the Irr-Ads asphaltene fraction as shown in Fig. 5.6. In both cases, the rate of aggregation depends strongly on precipitant (heptane) concentrations. Considering the results obtained previously with ESI-MS, smaller nanoaggregates of C5PeC11 contribute to

smaller building blocks. As a result, the hydrodynamic radius under similar conditions increases in 'smaller steps'; resulting in the observed flocculation characteristics of C5PeC11. This finding confirms the proposed Yen-Mullens' model where small nanoaggregates form first before they bind together to form larger structures.[46]

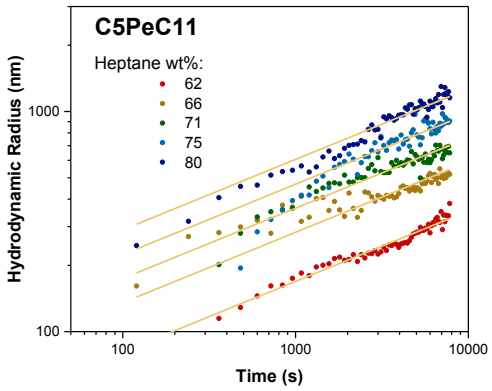

Figure 5.20 Time dependence of the size of C5PeC11 aggregates plotted in double logarithmic scale. The concentration of C5PeC11 is constant at 0.1 g/L, while heptane concentration in solution varies. Same slope = 0.32 was obtained for all data.

Figure 5.20 presents C5PeC11 hydrodynamic radius as a function of time on a double-logarithmic scale. Similar to Irr-Ads asphaltenes, the size of C5PeC11 aggregates, after the initial stabilization period, follows a power law relation showing a linear dependence of time on log-log scale. At different heptane concentrations, aggregate sizes $R(t)$ can be fitted with the same equation of $R(t) = At^a$, where $a = 0.32 \pm 0.04$. This result suggests, at low concentrations C5PeC11 aggregation follows the diffusion limited aggregation kinetics. The rate of diffusion is the limiting factor in determining the flocculation of the model compound. This result is similar to what we have observed for Irr-Ads asphaltenes. However, for mixtures such as asphaltenes, the aggregation behavior is also controlled by polydispersity of molecules. Interactions between

different molecules affect significantly the measured aggregation profiles. A single compound like C5PeC11 is unlikely to mimic complete aggregation behavior of real asphaltenes. This phenomenon was further probed by studying the mixed aggregation behavior of polyaromatic compounds using DLS in 5.2.4.

5.2.2 Effect of DBSA

The flocculation inhibition effects of DBSA on model compounds were also examined using similar methods as in the study with asphaltenes. An increased aggregation tendency at low DBSA concentration would suggest the binding force that drives model compounds aggregation strongly resembles that of pure asphaltenes. This would provide basis for future manipulations of the precipitation of asphaltenes as well as other polyaromatic compounds.

The interactions between DBSA and model compounds C5Pe, C5PeC11 were first studied using ESI-MS (conducted by Dr. Lan Liu). The results are summarized in Fig. 5.21-22 and the calculated averaged aggregation number is presented below in Table 5.1-2.

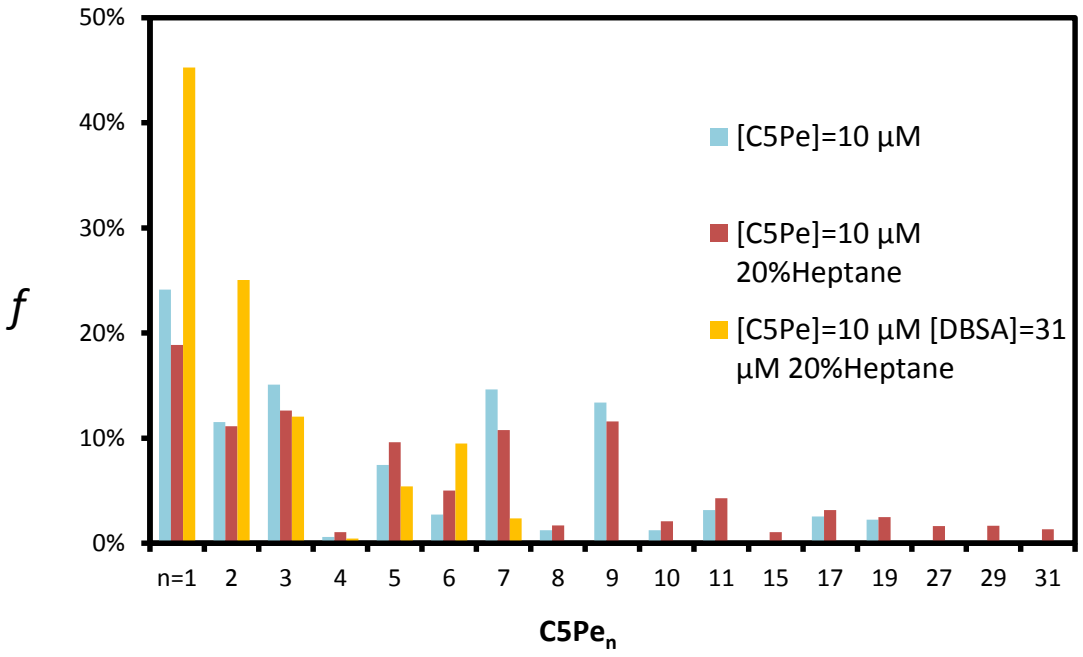

Figure 5.21 C5Pe nanoaggregates fraction in solution as a function of its aggregation number.

Table 5.1 Calculated averaged aggregation number for C5Pe in the presence and absence of DBSA.

System ---------- Aggregation Num.	**[C5Pe]=10µM**	**[C5Pe]=10µM Heptane 20%**	**[C5Pe]=10µM Heptane 20% [DBSA]= 31µM**
n_{avg}	5.14	6.31	2.33

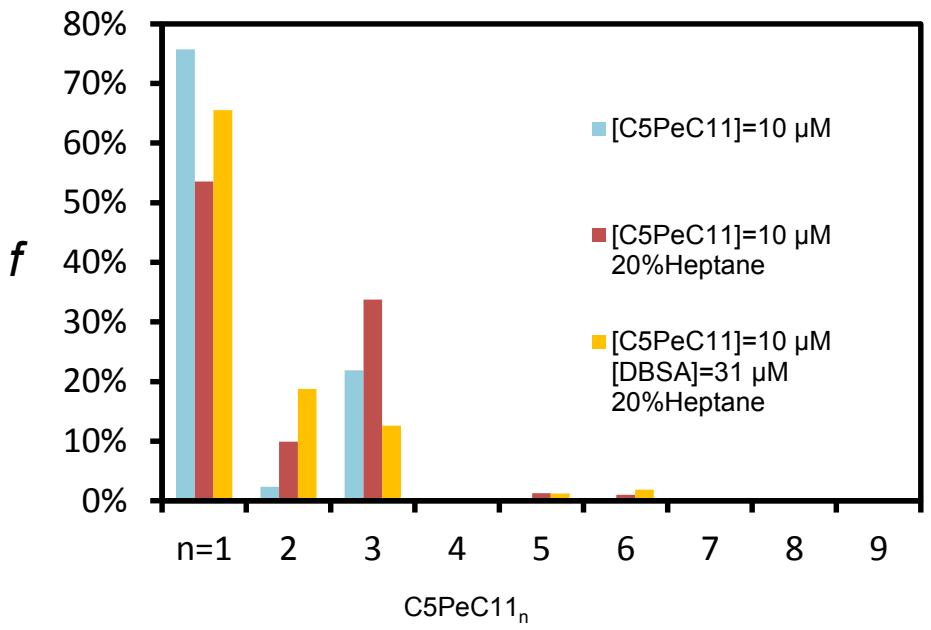

Figure 5.22 C5PeC11 nanoaggregates fraction in solution as a function of its aggregation number.

Table 5.2 Calculated averaged aggregation number for C5PeC11 in the presence and absence of DBSA.

System _____ **Aggregation Num.**	**[C5PeC11]=10µM**	**[C5PeC11]=10µM Heptane 20%**	**[C5PeC11]=10µM Heptane 20% [DBSA]= 31µM**
n_{avg}	1.46	1.91	1.58

Under same conditions, C5Pe shows high aggregation tendencies. For pure C5Pe, the averaged aggregation number is 5.14. When 20 vol% heptane was added, the aggregation number increases to 6.31 and large aggregates composed of up to 31 monomers were observed in

solution. With the presence of DBSA, the fraction of monomers significantly decreases while the averaged aggregation number is reduced to 2.33. This result suggests that on nano-scale, DBSA can disintegrate the aggregation of C5Pe effectively. For C5PeC11, due to its higher solubility, the detected fraction of monomer is high even when 20 vol% heptane was present. The calculated average aggregation number of C5PeC11 is much lower compare with that of C5Pe under same conditions. However similar trend could still be observed. When DBSA was added into the system, a decrease in the concentration of large nanoaggregates was detected. The calculated aggregation number is reduced from 1.91 to 1.58. This suggests DBSA has a similar effect on C5PeC11 that can disperse its aggregates in solution.

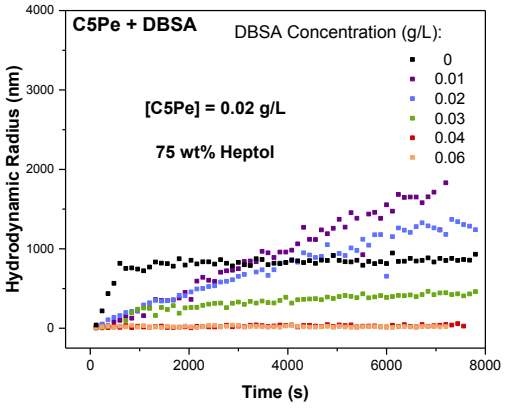

Figure 5.23 DBSA effect on C5Pe aggregation behaviors. The heptane concentration for all measurements was constant at 75 wt%. DBSA concentrations increase from zero to 0.06 g/L. Model compound concentration is constant at 0.02 g/L.

DLS observations are consistent with ESI-MS results. Figure 5.23 shows the hydrodynamic radius of C5Pe in the presence of various concentrations of DBSA. Model compound C5Pe

concentration is constant at 0.02 g/L based on previous optimization results. Upon the addition of DBSA, the aggregation behavior as a function of time changes dramatically. At low DBSA concentrations, the hydrodynamic radius increases almost linearly, reaching 2000 nm after 2 hr. (0.01 and 0.02 g/L DBSA). This behavior contrasts with the situation where no DBSA is added. In that case, a maximum hydrodynamic radius observed for C5Pe is around 800 nm. This suggests DBSA at low concentrations promotes continuous aggregation of C5Pe. It is possible that the long aliphatic chains in DBSA bring C5Pe nanoaggregates close together increasing collision efficiency between nanoaggregates. At high enough concentrations, DBSA inhibit the aggregation of C5Pe and the measured hydrodynamic radius remain low for the entire experiment.

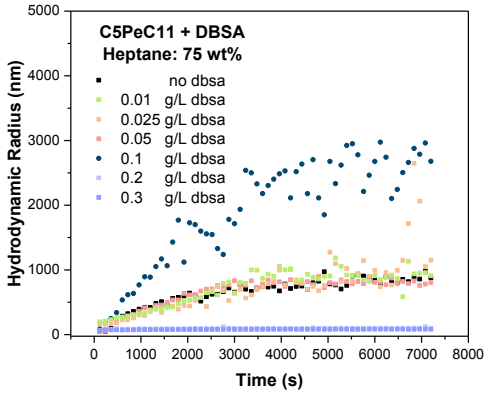

Figure 5.24 DBSA effect on C5PeC11 aggregation behaviors. The heptane concentration for all measurements was constant at 75 wt%. DBSA concentration increases from zero to 0.3 g/L. Model compound C5PeC11 concentration is constant at 0.1 g/L.

Figure 5.24 shows the DBSA effect on the aggregation of C5PeC11, which resembles more to the behaviors of pure asphaltenes. At 75 wt% heptane concentration, pure C5PeC11 aggregate slowly, reaching 900 nm after 2 hr. In the presence of small amount of DBSA (0.01 - 0.05 g/L), the measured aggregation is similar to the case when no DBSA was dosed. Small amounts of DBSA do not alter significantly the aggregation of C5PeC11. Upon the addition of 0.1 g/L DBSA, the measured hydrodynamic radius increases fast reaching 2000 nm within 2 hr. In addition, shortly after the experiment finished, C5PeC11/ DBSA sedimentation was observed. This trend is consistent with what we have observed with asphaltene fractions. In the presence of low DBSA concentrations, the flocculation of model compounds is promoted. Similar reasoning could be used to explain the observed behaviors. At low DBSA concentration, two strong electrostatic interactions exist between DBSA and model compounds. The first one is the interaction between protonated $C5PeC11H^+$ and DBS^- ions, while the second is the interaction between ion-pairs of $C5PeC11H^+$-DBS^-. Similar to the situation with asphlatene molecules, these interactions promote the formation of larger and more compact flocculates. On the other hand, high DBSA concentrations lead to a complete surrounding of DBSA molecules around the nano-aggregates of C5PeC11. The long aliphatic chains of DBSA provide steric hindrance that limits the aggregation rate of model compound. Therefore only small aggregates are detected when high concentrations of DBSA are dosed into the system.

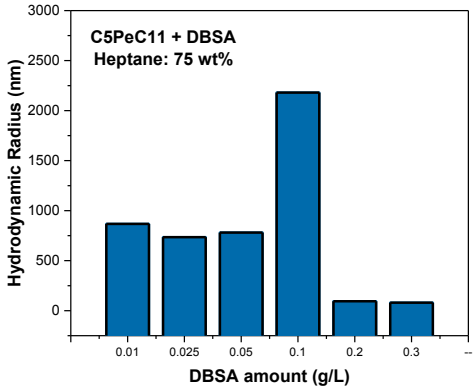

Figure 5.25 Hydrodynamic radius measured by DLS as a function of DBSA concentration in solution 30 min after aggregation is allowed to start. Heptane concentration is constant at 75 wt%. C5PeC11 concentration is 0.1 g/L. DBSA concentration varies from 0.01 g/L to 0.3 g/L.

As shown in Fig. 5.25, at 30 min after aggregation is allowed to start, the aggregation behavior for C5PeC11 resembles that of pure asphaltenes. The observed hydrodynamic radius increases first as the concentration of DBSA in solution until it reaches the maximum hydrodynamic radius. When the concentration of DBSA increases above the fast aggregation threshold, the aggregation of model compound becomes inhibited.

5.2.3 Model Compounds Aggregation: Prevention vs. Dispersion

Similar to asphaltene fractions, the effect of delayed DBSA addition was investigated for model compound C5PeC11. DBSA with a final concentration of 0.1 g/L was either mixed together in the beginning with C5PeC11 or added 30 min after aggregation was allowed to start. Heptane

concentration of 62 wt% was used to induce the aggregation process. Compare with 75 wt% heptane concentration (Fig. 5.24), the lower heptane concentration leads to slower rates of aggregation for pure C5PeC11 and smaller particle sizes in solution. After two hr., the hydrodynamic radius for pure C5PeC11 in the absence of DBSA reaches ~ 400 nm, which is about half the size when 75 wt% heptane is used. This observation is in accordance with the fact that heptane is a good precipitant for perylene bisimide model compounds.

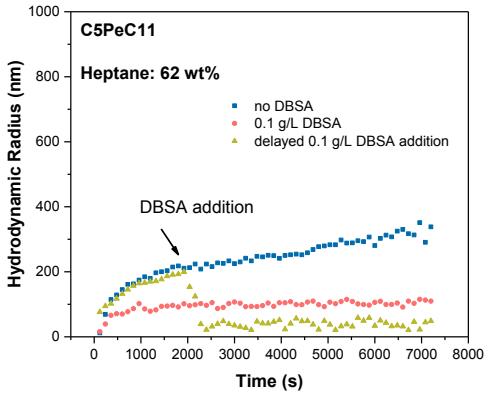

Figure 5.26 Effect of delayed DBSA addition on C5PeC11 aggregation behaviors. Heptane concentration is 62 wt%. Model compound C5PeC11 concentration is 0.1 g/L. DBSA with a final concentration of 0.1 g/L was either mixed with C5PeC11 in the beginning or added 30 min after experiment started.

As shown in Fig. 5.26, premixing C5PeC11 and DBSA leads to decreased aggregation behaviors. The presence of DBSA successfully inhibits the increase in the size of particles in suspension. The detected hydrodynamic radius remains low (<100 nm) even after two hr. of continuous

monitoring. This behavior resembles closely the behavior of asphaltenes and suggests C5PeC11 could be used as a suitable model compound to study the aggregation behaviors of asphaltenes.

As shown on Fig. 5.26, if the addition of DBSA is delayed for 30 min after aggregation is allowed to start, the initial aggregation profile looks exactly the same as the one without DBSA addition. This confirms the accuracy of the measured hydrodynamic radius at the beginning of the experiments. Upon the delayed addition of DBSA, the measured hydrodynamic radius decreases immediately. The final observed size of aggregates is lower than the case when DBSA is dosed in the beginning. This result suggests DBSA is effective in both the prevention and re-dispersion of the flocs formed with C5PeC11 model compound. This is consistent with the results obtained for the Irr-Ads asphaltene fraction. The binding interaction between C5PeC11 and DBSA is stronger than that between pure C5PeC11 molecules, which is possibly due to ion pair interactions. This stronger binding force enables DBSA to dissemble the already formed flocs of C5PeC11 resulting in decreased size of aggregates in solution.

5.2.4 Polydispersity Effects on Aggregation of Model Compounds

In order to understand how molecules with different structures interact to affect their aggregation in bulk solutions, the flocculation of C5Pe, C5PeC11 and BisAC11 binary and tri-mixtures were studied using dynamic light scattering. After dissolving C5PeC11 with either C5Pe or BisAC11 in heptane/ toluene solution, the hydrodynamic radius is measured as a function of time using the same procedure as described in previous experiments.

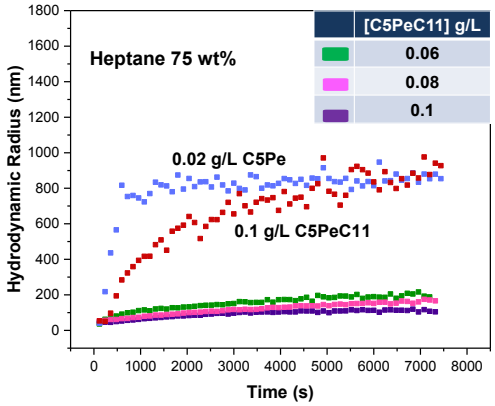

Figure 5.27 Hydrodynamic radius as a function of time for 0.02 g/L C5Pe, 0.1 g/L C5PeC11 and their mixtures of varying C5PeC11 concentrations in 75 wt% heptol solutions.

Figure 5.27 shows hydrodynamic radius R_h for C5Pe, C5PeC11 and their mixtures at different ratios. Heptane amount in all solutions was kept constant at 75 wt%. This heptane concentration was chosen since it induces appreciable amount of aggregation within 2 hr of measurement for pure C5Pe and C5PeC11. As indicated, C5Pe 0.02 g/L and C5PeC11 0.1 g/L by themselves aggregate to less than 1000 nm without any sedimentation being observed. After combining these two compounds together without varying their individual concentrations, the measured hydrodynamic radius decreased significantly. The maximum size of aggregates measured by DLS reduced to below 200 nm after 2 hr. In addition, for mixture systems with 0.02 g/L C5Pe and various amount of C5PeC11, the aggregation rate is much slower than systems with single compounds of 0.02 g/L C5Pe or 0.1 g/L C5PeC11. This behavior corresponds well with previous results from ESI-MS study that the combination of different polyaromatic compounds helps dispersing nanoaggregates as shown by decreasing the nanoaggregation number. Therefore massive flocculation of individual C5Pe or C5PeC11 in bulk solution becomes limited. [151]

Another interesting fact shown on Fig. 5.27 is that in the mixture, C5PeC11 can act as a dispersant for C5Pe. Increasing C5PeC11 concentration from 0.06 g/L to 0.1 g/L leads to decreased hydrodynamic radius as well as the rate of aggregation. This find demonstrates the significant difference between a single compound and a mixture of PAs in aggregation/ flocculation in bulk solutions. The dispersing effect of C5PeC11seems contradictory to concentration effects, but illustrates the importance of inter-molecular interactions. In molecular mixtures like asphaltenes, the interactions between various functional groups are so strong that can sometimes offset the indigenous concentration effects. It can be speculated that in the system of C5Pe + C5PeC11, increasing amount of C5PeC11 can interact with C5Pe molecules. With its longer aliphatic chains, C5PeC11 is able to stabilize the nanoaggregates in heptane/ toluene solutions to a greater extent, and therefore decrease the rate of aggregation. The polar group interactions between C5Pe molecules are no longer exclusive due to the presence of C5PeC11. The polar group interactions between the two types of molecules bring the long aliphatic chains of C5PeC11 to a closer proximity to the nanoaggregates, which carries along steric hindrance for the nanoaggregates to accumulate. Therefore, as a more soluble compound, C5PeC11 disrupt the interactions between C5Pe nanoaggregates. In addition, it is possible that C5PeC11 forms steric layers surrounding C5Pe nanoaggregates leading to decreased aggregation. This result suggests for structurally similar compounds with similar polarity, the more soluble compound could help in the solvation of the less soluble one. Embedded in this observation is the key in understanding the interactions between PA compounds. Similar results were confirmed by MD simulations and previous MS experiments that the addition of C5PeC11 decreases nanoaggregation in solution.

In addition to the average particle size, CONTIN analysis also provides the size distributions of flocs in solutions at a particular aggregation time. Figure 5.28 shows the measured hydrodynamic radius distribution at 30 min (1800 s) after experiment started. In 75 wt% heptane/ toluene solution, the hydrodynamic radius of 0.02 g/L C5Pe is centered around 1000 nm with a R_h breadth of 3165 nm. However with 0.08 g/L C5PeC11 mixed with same amount of C5Pe, the hydrodynamic radius distribution peak shifted and the hydrodynamic radius of aggregation reduced to around 200 nm. The breadth of the size distribution peak for the mixed system also decreased to around 919 nm, which is much smaller than that for the pure C5Pe system. These results suggest that polydispersity effects of different polyaromatic compounds can reduce the aggregates to smaller and more uniformly distributed aggregates. In addition, CONTIN analysis also reveals a log-normal distribution in both cases. This finding confirms that the aggregation of perylene bisimide polyaromatic compounds proceeds in a multiplicative fashion, which results from the three-dimensional structure of aggregates in solution. The concentration of larger aggregates/ flocs increases at the cost of reducing the population of smaller particles, resulting in an increase in the average hydrodynamic radius of the aggregates/ flocs. Our results confirm the Yen-Mullen's model of asphaltene aggregation. [46]

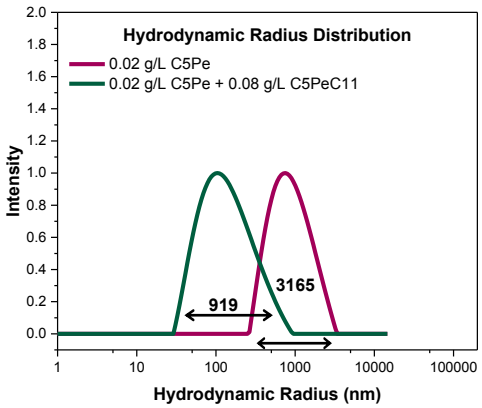

Figure 5.28 The hydrodynamic radius distribution for pure C5Pe and its mixture with C5PeC11 obtained by CONTIN analysis at $t = 1800\ s$ after experiment started.

Due to the lack of polar groups and the presence of longer aliphatic chains, BisAC11 has a higher solubility in heptane/ toluene solutions. It is interesting to know whether BisAC11 can interact with the structurally similar polyaromatic compound C5PeC11 and affect its aggregation. For this purpose, similar experiments were carried out where BisAC11 and C5PeC11 were tested for mutual dispersion.

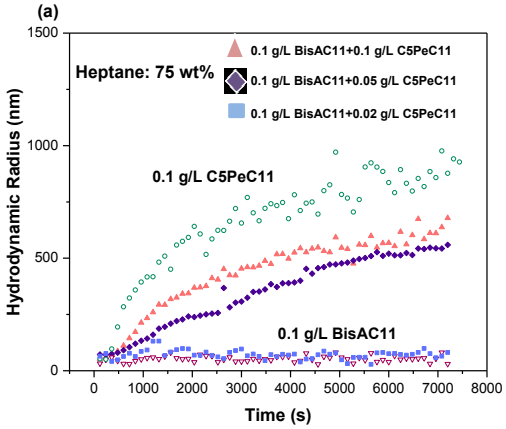

Figure 5.29 Hydrodynamic radius as a function of time for 0.1 g/L C5PeC11, 0.1 g/L BisAC11 and their mixtures of varying concentrations of C5PeC11 in 75 wt% heptol.

As shown in Fig. 5.29, at the same concentrations and solution conditions, pure C5PeC11 and BisAC11 have very different aggregation profiles. In solutions containing 75 wt% heptane, the hydrodynamic radius of 0.1 g/L C5PeC11 increased to ~ 1000 nm after 2 hr. At the same concentration, BisAC11 showed much lower tendency to aggregate and the measured particle sizes in suspension remained below 100 nm at all times. With 0.02 g/L C5PeC11 added into 0.1

g/L BisAC11, the observed hydrodynamic radius remains low. This is probably due to the low concentration of polar groups to induce any substantial association between C5PeC11 and BisAC11. However when the concentration of C5PeC11 was increased to 0.05 g/L in the mixture, substantial increase in the measured hydrodynamic radius was observed. With a further increase in the concentration of C5PeC11 to 0.1 g/L in the mixture, the size of hydrodynamic radius reached ~ 500 nm after 2 hr. Compared with a single component of C5PeC11 at the same concentration, the addition of BisAC11 decreased the aggregation tendency of C5PeC11. It is possible that the long peripheral chains in BisAC11 tangles up with the side chains of C5PeC11, decreasing the degree of interactions among polar groups. These results indicate that adding a compound, which can provide steric hindrance and with high solubility could significantly decrease the flocculation tendency of the mixture.

.

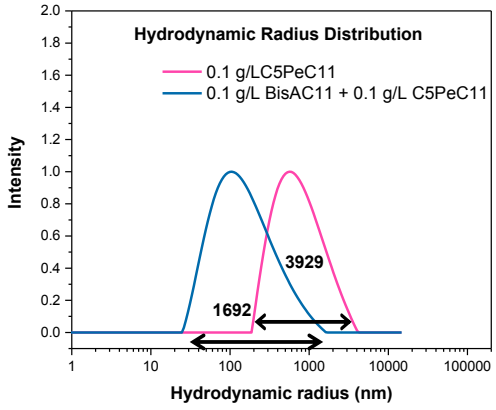

Figure 5.30 The hydrodynamic radius distribution for 0.1 g/L C5PeC11 and its polydisperse mixture with 0.1 g/L BisAC11 in 75 wt% heptol obtained with CONTIN analysis at $t = 1800\ s$ after experiment started.

Particle size distributions for C5PeC11 in the presence and absence of BisAC11 were plotted based on CONTIN analysis results in Fig. 5.30. At exactly 30 min after aggregation is initiated, the hydrodynamic radius for pure C5PeC11 follows a log-normal distribution where the peak of the aggregate size distribution is centered around 700 nm. The breadth of the distribution peak is relatively wide, covering a range of almost 4000 nm. This result suggests vastly different sizes of the aggregates/ flocs were formed. The polydispersity effect as encountered in real asphaltene systems can be observed by mixing C5PeC11 and BisAC11. The hydrodynamic radius for the mixture is reduced to around 200 nm with a breadth of peaks decreased to 1700 nm. This observation suggests a more soluble nature of the C5PeC11+BisAC11 mixture than pure C5PeC11 compound in heptol solutions. BisAC11 is able to increase the solubility of C5PeC11, with the resulting aggregates being more uniformly distributed in solution. However, compared with C5Pe, BisAC11 is less effective in decreasing the aggregation rate and hydrodynamic radius in the mixture with 0.1 g/L C5PeC11. This result confirms the important role of interactions between polar groups in controlling the aggregation of polyaromatic compound mixtures.

In addition to binary mixture systems, C5Pe, C5PeC11 and BisAC11 tertiary mixtures were also investigated to understand how the three compounds interact in heptane/ toluene solutions. For the tertiary mixture, 75 wt% heptol was used as precipitant, which is the same as in single and binary systems. The concentration of individual compounds was kept the same. Figure 5.31 compares the measured hydrodynamic radius of single, binary and tertiary systems as a function of time.

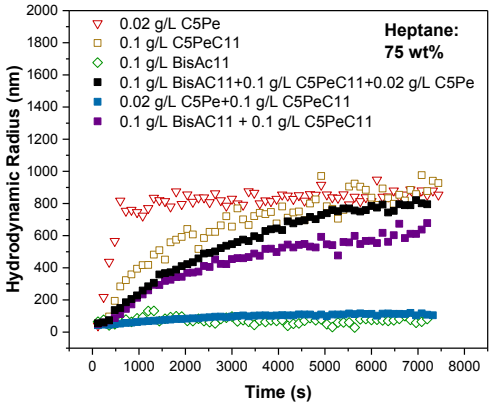

Figure 5.31 Measured hydrodynamic radius as a function of time for 0.02 g/L C5Pe, 0.1 g/L C5PeC11 and BisAC11 in single, bi-and tri-component systems of 75 wt% heptol.

As shown in Fig. 5.31, mixing the three components together caused the aggregation rate increase rapidly exceeding all bi-component systems, reaching 800 nm after 2 hr. In fact, the aggregation profile of the tertiary system is similar to that of the single compound C5PeC11 system. Even though, BisAC11 by itself is less likely to aggregate, its binary and tertiary mixtures with other PA compounds exhibit much higher aggregation tendency. As shown in Fig. 13, the binary mixture of BisAC11 + C5PeC11 aggregates much faster than binary mixture of C5Pe + C5PeC11 reaching 500 nm after 2 hr. Sedimentations in tertiary systems was observed after 2 hr of continuous monitoring. This result further stresses the importance of polar group interactions in the aggregation of PA compounds. For the C5Pe+C5PeC11 binary system, polar group interactions bring C5PeC11 to a close proximity of C5Pe. The long aliphatic chains in C5PeC11 are more effective in causing steric hindrance disrupting the flocculation process for the binary system. In addition, with strong hydrogen binding between C5Pe and C5PeC11, the aliphatic chains in C5PeC11 can stabilize the nanoaggregates formed from C5Pe and C5PeC11

by interacting with the solvent molecules leading to decreased flocculation. On the other hand, for the BisAC11+C5PeC11 binary system, due to the lack of polar group interaction, BisAC11 only binds loosely to C5PeC11, which makes BisAC11 a much less effective dispersant. BisAC11 is unable to stay closely to C5PeC11 nanoaggregates and the aliphatic chains in BisAC11 can only exert partial effects by sterically disrupting the flocculation of C5PeC11 nanoaggregates. This result corresponds well with MS results, where C5Pe-C5PeC11 complexes are common and can be detected in solution, while BisAC11-C5PeC11 complexes are usually absent. For flocculation beyond nanoscale, BisAC11 is less effective and serve more like a 'bystander' in the nanoaggregate solutions of C5PeC11. This result suggests for polydisperse systems, the polarity difference between PA compounds is more important in determining the overall aggregation behaviors. For a PA compound known to aggregate in solution, adding a structurally similar PA compound with similar polarity and higher solubility can successfully decrease the nanoaggregation/ flocculation of the mixture. Similar result is also confirmed for pure asphaltenes. As a more soluble and polar crude oil component, resin is known to decrease the aggregation/ precipitation of asphaltenes. In addition, resins with a high dipole moment are more effective than resins with a low dipole moment in the stabilization of asphaltenes in solution. [146]

For the binary and tertiary systems, in general, there are two reasons that might affect the overall aggregation tendency of polyaromatic compounds in mixture systems. The first is the effect of concentration. Since all polyaromatic compounds were mixed using their original optimized concentrations, the overall concentration of the binary systems is higher than their corresponding single component systems, similar for tertiary mixture in comparison to binary mixtures. The

higher concentration enhances the collision efficiency of different polyaromatic compounds and therefore accelerates the flocculation process. The second contribution to the enhanced aggregation process arises from the inherent chemical properties of polyaromatic compound BisAC11. Due to the absence of polar groups, BisAC11 lacks the ability to bind through polar group interactions. However as shown in MD simulations, the presence of aromatic rings can still facilitate the 'π-π packing' between different polyaromatic compounds. These interactions lead to increased aggregation of the mixture in heptane/ toluene solutions. As a result, the overall flocculation of PA compounds in the mixture system containing BisAC11 compromises between the concentration and polydispersity effect of BisAC11. In addition, structural and functional group interactions also take part in controlling the flocculation. The final observed aggregation behavior of the tertiary mixture closely resembles that of a single compound C5PeC11.

Chapter 6 Conclusions and Future Work

6.1 General Conclusions

In summary, dynamic light scattering results showed that three asphaltene fractions separated based on adsorption on $CaCO_3$ have distinctly different aggregation behaviors. The Irr-Ads asphlatene fraction exhibited the highest aggregation tendency while the Ads and Non-Ads fractions showed significantly less aggregation in heptane/ toluene solutions. Combined with the EI analysis published before,[152] polar groups and heteroatom interactions were identified as important factors in controlling the aggregation of polyaromatic compounds in bulk organic solutions. Higher concentrations of polar functional groups and heteroatoms were considered to increase the collision efficiency of polyaromatic compounds, resulting in accelerated rates of aggregation. In addition, aggregation of three perylene bisimide model compounds was used to

further understand the effect of molecular structural and polydispersity on nanoaggregation of PA molecules and asphaltenes.

For synthesized polyaromatic compounds, DLS studies showed the flocculation potencyin the reverse order of their solubility in heptane/toluene solutions, i.e., C5Pe > C5PeC11 > BisAC11. Increasing heptane concentration in heptane-toluene mixture as solvent was found to increase the rate of aggregation. This observed heptane effect on flocculation agrees very well with the enhanced nanoaggregation by heptane addition observed from previous ESI-MS study.

For polyaromatic compounds, results obtained by DLS showed continuous increase in the hydrodynamic radius measured as a function of time before precipitation started. The analysis on the aggregates size vs. time plot showed a constant slope of 0.32, which led to the conclusion that aggregation of 0.1 g/L C5PeC11 follows a diffusion limited aggregation process. Compared with the results obtained for Irr-Ads asphaltenes, the similarity in the aggregation behavior suggests that C5PeC11 can be used as a model compound to study aggregation mechanisms of asphaltenes.

In order to understand how different molecules interact in bulk solutions, polydispersity effects were studied. For C5Pe + C5PeC11, the binary mixture exhibited decreased aggregation tendencies. The interactions between C5Pe and C5PeC11 altered the binding behavior of the mixtures and hence reduced the flocculation of C5Pe and C5PeC11 molecules. This result is also confirmed by ESI-MS experiments (conducted by Dr. Lan Liu), where the calculated average aggregation number decreases upon mixing of C5Pe with C5PeC11.

Decreased aggregation behavior was also observed for the binary mixture of C5PeC11 + BisAC11. This observed effect can be attributed to the longer aliphatic chains of BisAC11 that are solvated and hence extend themselves into the bulk solutions to prevent further aggregation and hence stabilize nanoaggregates. However, compared with stabilization of C5Pe aggregates by C5PeC11, BisAC11 is less effective in solvating aggregates of C5PeC11. This finding indicates that in addition to steric hindrance, polar group interactions remain a dominating force to drive nanoaggregation and flocculation of model compounds in solution. Furthermore, the tertiary mixture of C5PeC11 + C5Pe + BisAC11 shows an aggregation profile similar to that of pure C5PeC11. The rate of aggregation in the tertiary mixture is fast, reaching 800 nm after 2 hr. It is possible that in the tertiary mixture, the concentration effects, steric hindrance and polar group interactions are competing with each other for the binding between the nanoaggregates. Therefore the observed aggregation behavior is the result of all combined interactions. This result suggests that the interactions responsible for nanoaggregation and flocculation of PA molecules and asphaltenes are of multiple origins. A single type of interaction is not sufficient to explain the complex aggregation behaviors in real asphaltenes.

6.2 Recommendations for Future Work

To obtain a better understanding of the aggregation behavior of polyaromatic compounds including both asphaltenes and synthesized model compounds, the following measurements are recommended.

1. Brewster angle microscope could be used to visualize the aggregation behavior of different asphaltene fractions at heptol-water interfaces. The images obtained from this experiment could provide further support for the observed trend in ESI-MS and DLS experiments.
2. It would be interesting to see how different asphaltene fractions behave when combined together in heptol solutions. To further understand polydispersity effect as well as polar group/ heteroatom interactions, the various binary mixtures of asphatlenes should be studied using DLS.
3. Fractionation of asphaltenes using SiO_2 should be carried out. The chemical properties of different fractions should be collected and compared with that of the asphaltene fractions separated using $CaCO_3$. DLS studies could provide further insight into how different fractionation method affects the inherent aggregation behaviors of real asphaltenes.
4. MD simulation on PA molecules and inhibitors such as DBSA should be carried out to further validate the experiment observations.

Bibliography

[1] G. of Canada, NEB - Estimated production of canadian crude oil and equivalent, Gov. Canada Natl. Energy Board. (2014). https://www.neb-one.gc.ca/nrg/sttstc/crdlndptrlmprdct/stt/stmtdprdctn-eng.html (accessed February 24, 2016).

[2] U.S.E.I. Administration, Canada international analysis - U.S. Energy Information Administration (EIA), https://www.eia.gov/beta/international/analysis.cfm?iso=CAN (accessed February 24, 2016).

[3] G. of Alberta, Conventional crude oil and oil sands, (2013). http://www.albertacanada.com/business/industries/og-conventional-crude-oil-and-oil-sands.aspx (accessed February 24, 2016).

[4] National Energy Board, Canada's energy future 2013: energy supply and demand projections to 2035, (2013) 100. https://www.neb-one.gc.ca/nrg/ntgrtd/ftr/2013/index-eng.html\nhttps://www.neb-one.gc.ca/nrg/ntgrtd/ftr/2013/2013nrgftr-eng.pdf.

[5] R.L. Hirsch, R. Bezdek, R. Wendling, Peaking of world oil production and its mitigation, US Dep. Energy. (2005) 9–27. doi:10.1016/B978-012369495-9/50003-8.

[6] N.R. Canada, Froth treatment, (n.d.). http://www.nrcan.gc.ca/energy/oil-sands/5873 (accessed February 25, 2016).

[7] J. McLean, P. Kilpatrick, Effects of asphaltene aggregation in model heptane-toluene mixtures on stability of water-in-oil emulsions, J. Colloid Interface Sci. 196 (1997) 23–34. doi:10.1006/jcis.1997.4807.

[8] D.N. Madge, W.N. Garner, Theory of asphaltene precipitation in a hydrocarbon cyclone, Miner. Eng. 20 (2007) 387–394. doi:10.1016/j.mineng.2006.10.013.

[9] A.G. Marshall, R.P. Rodgers, Petroleomics: the next grand challenge for chemical analysis, Acc. Chem. Res. 37 (2004) 53–59. doi:10.1021/ar020177t.

[10] A.G. Marshall, R.P. Rodgers, Petroleomics: Chemistry of the underworld, Proc. Natl. Acad. Sci. 105 (2008) 18090–18095. doi:10.1073/pnas.0805069105.

[11] R.P. Rodgers, A.G. Marshall, Petroleomics: advanced characterization of petroleum-derived materials by Fourier Transform Ion Cyclotron Resonance Mass Spectrometry (FT-ICR MS), Asph. Heavy Oils Pet. (2007) 63–93. doi:10.1007/0-387-68903-6_3.

[12] Z. Liao, J. Zhao, P. Creux, C. Yang, Discussion on the structural features of asphaltene molecules, Energy and Fuels. 23 (2009) 6272–6274. doi:10.1021/ef901126m.

[13] T.X. Xia, M. Greaves, In-situ upgrading of Athabasca tar sand bitumen using Thai, Chem. Eng. Res. Des. 84 (2006) 856–864. doi:10.1205/cherd.04192.

[14] H.W. Yarranton, H. Alboudwarej, R. Jakher, Investigation of asphaltene association with

vapor pressure osmometry and interfacial tension measurements, Ind. Eng. Chem. Res. 39 (2000) 2916–2924. doi:10.1021/ie000073r.

[15] L.Y. Zhang, S. Lawrence, Z. Xu, J.H. Masliyah, Studies of Athabasca asphaltene Langmuir films at air-water interface, J. Colloid Interface Sci. 264 (2003) 128–140. doi:10.1016/S0021-9797(03)00355-2.

[16] P. Peng, A. MoralesIzquierdo, A. Hogg, O.P. Strausz, Molecular structure of athabasca asphaltene: Sulfide, ether, and ester linkages, Energy and Fuels. 11 (1997) 1171–1187. doi:10.1021/ef970027c.

[17] D. Zhang, J. Creek, A.J. Jamaluddin, A.G. Marshall, R.P. Rodgers, O.C. Mullins, Asphaltenes-problematic but rich in potential, Oilf. Rev. (2007) 22–43.

[18] L.Y. Zhang, R. Lopetinsky, Z. Xu, J.H. Masliyah, Asphaltene monolayers at a toluene / water interface, Energy and Fuels. 19 (2005) 1330–1336. doi:10.1021/ef0603129.

[19] H. Yarranton, H. Hussein, J. Masliyah, Water-in-hydrocarbon emulsions stabilized by asphaltenes at low concentrations., J. Colloid Interface Sci. 228 (2000) 52–63. doi:10.1006/jcis.2000.6938.

[20] M. a. Anisimov, I.K. Yudin, V. Nikitin, G. Nikolaenko, a. Chernoutsan, H. Toulhoat, et al., Asphaltene aggregation in hydrocarbon solutions studied by photon correlation spectroscopy, J. Phys. Chem. 99 (1995) 9576–9580. doi:10.1021/j100023a040.

[21] L.M. Petrova, N. a. Abbakumova, I.M. Zaidullin, D.N. Borisov, Polar-solvent fractionation of asphaltenes from heavy oil and their characterization, Pet. Chem. 53 (2013) 81–86. doi:10.1134/S0965544113020084.

[22] S. Subramanian, S. Simon, B. Gao, J. Sjöblom, Asphaltene fractionation based on adsorption onto calcium carbonate: Part 1. Characterization of sub-fractions and QCM-D measurements, Colloids Surfaces A Physicochem. Eng. Asp. 495 (2016) 136–148. doi:10.1016/j.colsurfa.2016.02.011.

[23] J. Sjoblom, S. Simon, Z. Xu, Model molecules mimicking asphaltenes, Adv. Colloid Interface Sci. 218 (2015) 1–16. doi:10.1016/j.cis.2015.01.002.

[24] G.A. Mansoori, Remediation of asphaltene and other heavy organic deposits in oil wells and in pipelines, Proceedings. (2010) 12–23. doi:10.5510/OGP20100400039.

[25] F. Alvarez-Ramírez, Y. Ruiz-Morales, Island versus archipelago architecture for asphaltenes: Polycyclic aromatic hydrocarbon dimer theoretical studies, Energy and Fuels. 27 (2013) 1791–1808. doi:10.1021/ef301522m.

[26] J.M. Sheremata, M.R. Gray, H.D. Dettman, W.C. McCaffrey, Quantitative molecular representation and sequential optimization of Athabasca asphaltenes, Energy and Fuels. 18 (2004) 1377–1384. doi:10.1021/ef049936+.

[27] O.P. Strausz, P. Peng, J. Murgich, About the colloidal nature of asphaltenes and the MW of covalent monomeric units, Energy and Fuels. 16 (2002) 809–822.

doi:10.1021/ef0002795.

[28] O.P. Strausz, T.W. Mojelsky, F. Faraji, E.M. Lown, P. Peng, Additional structural details on Athabasca asphaltene and their ramifications, Energy and Fuels. 13 (1999) 207–227. doi:10.1021/ef980274w.

[29] O.P. Strausz, T.W. Mojelsky, E.M. Lown, I. Kowalewski, F. Behar, Structural features of Boscan and Duri asphaltenes, Energy and Fuels. 13 (1999) 228–247. doi:10.1021/ef980245l.

[30] O.P. Strausz, T.W. Mojelsky, E.M. Lown, The molecular structure of asphaltene: an unfolding story, Fuel. 71 (1992) 1355–1363. doi:10.1016/0016-2361(92)90206-4.

[31] A.H. Alshareef, A. Scherer, X. Tan, K. Azyat, J.M. Stryker, R.R. Tykwinski, et al., Formation of archipelago structures during thermal cracking implicates a chemical mechanism for the formation of petroleum asphaltenes, Energy and Fuels. 25 (2011) 2130–2136. doi:10.1021/ef200170a.

[32] H. Groenzin, O.C. Mullins, S. Eser, J. Mathews, M.G. Yang, D. Jones, Molecular size of asphaltene solubility fractions, Energy and Fuels. 17 (2003) 498–503. doi:10.1021/ef010239g.

[33] H. Groenzin, O.C. Mullins, Asphaltene molecular size and structure, J. Phys. Chem. A. 103 (1999) 11237–11245. doi:10.1021/jp992609w.

[34] H. Sabbah, A.L. Morrow, A.E. Pomerantz, R.N. Zare, Evidence for island structures as the dominant architecture of asphaltenes, Energy and Fuels. 25 (2011) 1597–1604. doi:10.1021/ef101522w.

[35] H. Groenzin, O.C. Mullins, Molecular size and structure of asphaltenes from various sources, Energy and Fuels. (2000) 677–684. doi:10.1021/ef990225z.

[36] A. Sharma, H. Groenzin, A. Tomita, O.C. Mullins, Probing order in asphaltenes and aromatic ring systems by HRTEM, Energy and Fuels. 16 (2002) 490–496. doi:10.1021/ef010240f.

[37] Y. Bouhadda, D. Bormann, E. Sheu, D. Bendedouch, A. Krallafa, M. Daaou, Characterization of Algerian Hassi-Messaoud asphaltene structure using Raman spectrometry and X-ray diffraction, Fuel. 86 (2007) 1855–1864. doi:10.1016/j.fuel.2006.12.006.

[38] I. Merdrignac, D. Espinat, Physicochemical characterization of petroleum fractions: the state of the art, Oil Gas Sci. Technol. Rev. lIFP. 62 (2007) 7–32. doi:10.2516/ogst:2007002.

[39] O.C. Mullins, B. Martínez-Haya, A.G. Marshall, Contrasting perspective on asphaltene molecular weight. This comment vs the overview of A. A. Herod, K. D. Bartle, and R. Kandiyoti, Energy and Fuels. 22 (2008) 1765–1773. doi:10.1021/ef700714z.

[40] O.C. Mullins, Review of the molecular struction and aggregation of asphaltenes and

petroleomics, SPE J. 13 (2008) 48–57. doi:10.2118/95801-PA.

[41] A.R. Hortal, B. Martínez-Haya, M.D. Lobato, J.M. Pedrosa, S. Lago, On the determination of molecular weight distributions of asphaltenes and their aggregates in laser desorption ionization experiments, J. Mass Spectrom. 41 (2006) 960–968. doi:10.1002/jms.1056.

[42] B. Martínez-Haya, A.R. Hortal, P. Hurtado, M.D. Lobato, J.M. Pedrosa, Laser desorption/ionization determination of molecular weight distributions of polyaromatic carbonaceous compounds and their aggregates, J. Mass Spectrom. 42 (2007) 701–713. doi:10.1002/jms.1226.

[43] M.R. Gray, Consistency of asphaltene chemical structures with pyrolysis and coking behavior, Energy and Fuels. 17 (2003) 1566–1569. doi:10.1021/ef030015t.

[44] P. Peng, J. Fu, G. Sheng, A. Morales-Izquierdo, E.M. Lown, O.P. Strausz, Ruthenium-ions-catalyzed oxidation of an immature asphaltene: Structural features and biomarker distribution, Energy and Fuels. 13 (1999) 266–277. doi:10.1021/ef980235k.

[45] L. Barre, J. Eyssautier, O.C. Mullins, The asphaltenes, Annu. Rev. Anal. Chem. 4 (2011) 393–418. doi:10.1146/annurev-anchem-061010-113849.

[46] O.C. Mullins, H. Sabbah, A.E. Pomerantz, L. Barre, A.B. Andrews, Y. Ruiz-Morales, et al., Advances in asphaltene science and the Yen − Mullins Model, Energy and Fuels. 26 (2012) 3986−4003. doi:10.1021/ef300185p.

[47] C.W. Dwiogins, A small angle X-Ray scattering study of the colloidal nature of petroleum, J. Phys. Chem. 69 (1965) 3500–3506.

[48] B. Roux, Jean-Noel, Broseta, D., Deme, SANS study of asphaltene aggregation: concentration, Langmuir. 17 (2001) 5085–5092. doi: 10.1021/la0101651.

[49] G. Andreatta, N. Bostrom, O.C. Mullins, High-Q ultrasonic determination of the critical nanoaggregate concentration of asphaltenes and the critical micelle concentration of standard surfactants, Langmuir. 21 (2005) 2728–2736. doi:10.1021/la048640t.

[50] H. Zeng, Y.-Q. Song, D.L. Johnson, O.C. Mullins, Critical nanoaggregate concentration of asphaltenes by direct-curretn (DC) electrical conductivity, Energy and Fuels. 23 (2009) 1201–1208. doi: 10.1021/2f800781a.

[51] D.E. Freed, N. V Lisitza, P.N. Sen, Y.Q. Song, A study of asphaltene nanoaggregation by NMR, Energy and Fuels. 23 (2009) 1189–1193. doi: 10.1021/ef800631a.

[52] L. Goual, M. Sedghi, H. Zeng, F. Mostowfi, R. McFarlane, O.C. Mullins, On the formation and properties of asphaltene nanoaggregates and clusters by DC-conductivity and centrifugation, Fuel. 90 (2011) 2480–2490. doi:10.1016/j.fuel.2011.02.025.

[53] F. Mostowfi, K. Indo, O.C. Mullins, R. McFarlane, Asphaltene nanoaggregates studied by centrifugation, Energy and Fuels. 23 (2009) 1194–1200. doi:10.1021/ef8006273.

[54] J. Orbulescu, O.C. Mullins, R.M. Leblanc, Surface chemistry and spectroscopy of UG8 asphaltene langmuir film, part 2, Langmuir. 26 (2010) 15265–15271. doi:10.1021/la1017642.

[55] K.L. Gawrys, G.A. Blankenship, P.K. Kilpatrick, Solvent entrainment in and flocculation of asphaltenic aggregates probed by small-angle neutron scattering, Langmuir. 22 (2006) 4487–4497. doi:10.1021/la052509j.

[56] M.H. Schneider, A.B. Andrews, S. Mitra-Kirtley, O.C. Mullins, Asphaltene molecular size by fluorescence correlation spectroscopy, Energy and Fuels. 21 (2007) 2875–2882. doi:10.1021/ef700216r.

[57] I.K. Yudin, Mikhail A. Anisimov, Asphaltenes, Heavy Oils, and Petroleomics, Springer New York, New York, NY, 2007. doi:10.1007/0-387-68903-6.

[58] K. Oh, M.D. Deo, Near Infrared Spectroscopy to study asphaltene aggregation in solvents, in: Asph. Heavy Oils, Pet., Springer New York, New York, NY, 2007: pp. 469–488. doi:10.1007/0-387-68903-6_18.

[59] J.S. Buckley, G.J. Hirasaki, Y. Liu, S. V. Drasek, J.-X. Wang, B.S. Gill, Asphaltene precipitation and solvent properties of crude oils, Pet. Sci. Technol. 16 (1998) 251–285. doi:10.1080/10916469808949783.

[60] O.C. Mullins, The modified yen model, Energy and Fuels. 24 (2010) 2179–2207. doi:10.1021/ef900975e.

[61] Y. Ruiz-Morales, Aromaticity in pericondensed cyclopenta-fused polycyclic aromatic hydrocarbons determined by density functional theory nucleus-independent chemical shifts and the Y-rule - Implications in oil asphaltene stability. Can. J. Chem. 87 (2009) 1280–1295. doi:10.1139/V09-052.

[62] R.B. de Boer, K. Leerlooyer, M.R.P. Eigner, A.R.D. van Bergen, Screening of crude oils for asphalt precipitation: theory, practice, and the selection of inhibitors, SPE Prod. Facil. 10 (1995) 55–61. doi:10.2118/24987-PA.

[63] E.B. Sirota, M.Y. Lin, Physical behavior of asphaltenes, Energy and Fuels. 21 (2007) 2809–2815. doi:10.1021/ef060634c.

[64] N.B. Joshi, O.C. Mullins, A. Jamaluddin, J. Creek, J. McFadden, Asphaltene precipitation from live crude oil, Energy and Fuels. 15 (2001) 979–986. doi:10.1021/ef010047l.

[65] K. Karan, A. Hammami, M. Flannery, B. Artur Stankiewicz, Evaluation of asphaltene instability and a chemical control during production of live oils, Pet. Sci. Technol. 21 (2003) 629–645. doi:10.1081/LFT-120018543.

[66] K. Oh, T.A. Ring, M.D. Deo, Asphaltene aggregation in organic solvents, J. Colloid Interface Sci. 271 (2004) 212–219. doi:10.1016/j.jcis.2003.09.054.

[67] J. Wang, J.S. Buckley, Asphaltene stability in crude oil and aromatic solvents - the influence of oil composition, Energy and Fuels. 17 (2003) 1445–1451.

doi:10.1021/ef030030y.

[68] E. Rezaee Nezhad, F. Heidarizadeh, S. Sajjadifar, Z. Abbasi, Dispersing of petroleum asphaltenes by acidic ionic liquid and determination by UV-Visible spectroscopy, J. Pet. Eng. 2013 (2013) 1–5. doi:10.1155/2013/203036.

[69] K.D. Mannistu, H.W. Yarranton, J.H. Masliyah, Solubility modeling of asphaltenes in organic solvents, Energy and Fuels. 11 (1997) 615–622. doi:10.1021/ef9601879.

[70] A. Hirschberg, L.N.J. DeJong, B.A. Schipper, J.G. Meijer, Influence of temperature and pressure on asphaltene flocculation, Soc. Pet. Eng. J. 24 (1984) 283–293. doi:10.2118/11202-PA.

[71] J.X. Wang, J.S. Buckley, A two-component solubility model of the onset of asphaltene flocculation in crude oils, Energy and Fuels. 15 (2001) 1004–1012. doi:10.1021/ef010012l.

[72] T. Maqbool, A.T. Balgoa, H.S. Fogler, Revisiting asphaltene precipitation from crude oils: A case of neglected kinetic effects, Energy and Fuels. 23 (2009) 3681–3686. doi:10.1021/ef9002236.

[73] S. Subramanian, S. Simon, J. Sjöblom, Asphaltene precipitation models: a review, J. Dispers. Sci. Technol. 2691 (2015) 92. doi:10.1080/01932691.2015.1065418.

[74] M. Agrawala, H.W. Yarranton, An asphaltene association model analogous to linear polymerization, Ind. Eng. Chem. Res. 40 (2001) 4664–4672. doi:10.1021/ie0103963.

[75] G. Scatchard, Equilibria in non-electrolyte solutions in relation to the vapor pressures and densities of the components, Chem. Rev. 8 (1931) 321–333. doi:10.1021/cr60030a010.

[76] O.C. Mullins, E.Y. Sheu, A. Hammami, A.G. Marshall, Asphaltenes, heavy oils, and petroleomics, Springer Science+Business Media, 2007. ISBN 10:0-387-31734-1.

[77] Z. Novosad, T.G. Costain, Experimental and modeling studies of asphaltene equilibria for a reservoir under CO2 injection, Proc. SPE Annu. Tech. Conf. Exhib. (1990) 599–607. doi:10.2523/20530-MS.

[78] H. Rassamdana, B. Dabir, M. Nematy, M. Farhani, M. Sahimi, Asphalt flocculation and deposition: I. The onset of precipitation, AIChE J. 42 (1996) 10–22. doi:10.1002/aic.690420104.

[79] H.W. Yarranton, J.H. Masliyah, Molar mass distribution and solubility modeling of asphaltenes, AIChE J. 42 (1996) 3533–3543. doi:10.1002/aic.690421222.

[80] K. Akbarzadeh, H. Alboudwarej, W.Y. Svrcek, H.W. Yarranton, Regular solution model for asphaltene precipitation from bitumen-alkane systems, Thermodynamics. 49 (2003) 2948–2956.

[81] L.N.V. De Bataafsche, P. Maatschappij, Asphaltic bitumen as colloid system', Sixt. Colloid. Symp. (1939) 139–149. doi:10.1021/j150398a001.

[82] K.J. Leontaritis, G.A. Mansoori, Asphaltene flocculation during oil production and

processing: a thermodynamic colloidal model, SPE Soc. Pet. Eng. (1987) 149–158. doi:10.2118/16258-MS.

[83] E.Y. Sheu, D.A. Storm, M.M. De Tar, Asphaltenes in polar solvents, J. Non. Cryst. Solids. 131-133 (1991) 341–347. doi:10.1016/0022-3093(91)90326-2.

[84] C.-L. Chang, H.S. Fogler, Stabilization of asphaltenes in aliphatic solvents using alkylbenzene-derived amphiphiles. 1. effect of the chemical structure of amphiphiles on asphaltene stabilization, Langmuir. 10 (1994) 1749–1757. doi:10.1021/la00018a022.

[85] C.-L. Chang, H.S. Fogler, Stabilization of asphaltenes in aliphatic solvents using alkylbenzene-derived amphiphiles. 2. study of the asphaltene-amphiphile interactions and structures using Fourier Transform Infrared Spectroscopy and small-angle X-ray scattering techniques, Langmuir. 10 (1994) 1758–1766. doi:10.1021/la00018a023.

[86] G. Dennis Miller, Kelkheim; Axel Vollmer, Kriftel; Michael Feustel, Kongernheim; Peter Klug, Ethercarboxylic acids as asphaltene dispersants in crude oils, US 6,063,146, 1998. https://docs.google.com/viewer?url=patentimages.storage.googleapis.com/pdfs/US6063146.pdf.

[87] C. Rodney J. Gochin, Tadworth; Alec Smith, Method of controlling aphsltene precipitation in a fluid, US 6,270,653 B1, 2001.

[88] K. Kraiwattanawong, H.S. Fogler, S.G. Gharfeh, P. Singh, W.H. Thomason, S. Chavadej, Effect of asphaltene dispersants on aggregate size distribution and growth, Energy and Fuels. 23 (2009) 1575–1582. doi:10.1021/ef800706c.

[89] K. Safaie, A.R.S. Nazar, Evaluation of asphaltene inhibitors effect on aggregation coupled sedimentation process, J. Dispers. Sci. Technol. 35 (2014) 329–337. doi:10.1080/01932691.2013.778782.

[90] O. León, E. Rogel, A. Urbina, A. Andújar, A. Lucas, Study of the adsorption of alkyl benzene-derived amphiphiles on asphaltene particles, Langmuir. 15 (1999) 7653–7657. doi:10.1021/la9812370.

[91] E. Rogel, Effect of inhibitors on asphaltene aggregation: A theoretical framework, Energy and Fuels. 25 (2011) 472–481. doi:10.1021/ef100912b.

[92] M. Barcenas, P. Orea, E. Buenrostro-gonzález, L.S. Zamudio-rivera, Y. Duda, Study of medium effect on asphaltene agglomeration inhibitor efficiency, Energy and Fuels. 22 (2008) 1917-1922. doi:10.1021/ef700773m

[93] L. Goual, M. Sedghi, X. Wang, Z. Zhu, Asphaltene aggregation and impact of alkylphenols, Langmuir. 30 (2014) 5394–5403. doi:10.1021/la500615k.

[94] F. Rakotondradany, H. Fenniri, P. Rahimi, K.L. Gawrys, P.K. Kilpatrick, M.R. Gray, Hexabenzocoronene model compounds for asphaltene fractions: Synthesis & characterization, Energy and Fuels. 20 (2006) 2439–2447. doi:10.1021/ef060130e.

[95] X. Tan, H. Fenniri, M.R. Gray, Pyrene derivatives of 2,2’-bipyridine as models for

asphaltenes: synthesis, characterization, and supramolecular organization, Energy and Fuels. 22 (2008) 715–720. doi:10.1021/ef700395g.

[96] T. Kuznicki, J.H. Masliyah, S. Bhattacharjee, Molecular dynamics study of model molecules resembling asphaltene-like structures in aqueous organic solvent systems, Energy and Fuels. 22 (2008) 2379–2389. doi:10.1021/ef800057n.

[97] T. Kuznicki, J.H. Masliyah, S. Bhattacharjee, Aggregation and partitioning of model asphaltenes at toluene-water interfaces: Molecular dynamics simulations, Energy and Fuels. 23 (2009) 5027–5035. doi:10.1021/ef9004576.

[98] A.H. Alshareef, A. Scherer, J.M. Stryker, R.R. Tykwinski, M.R. Gray, Thermal cracking of substituted cholestane-benzoquinoline asphaltene model compounds, Energy and Fuels. 26 (2012) 3592–3603. doi:10.1021/ef300438j.

[99] A.H. Alshareef, A. Scherer, X. Tan, K. Azyat, J.M. Stryker, R.R. Tykwinski, et al., Effect of chemical structure on the cracking and coking of archipelago model compounds representative of asphaltenes, Energy and Fuels. 26 (2012) 1828–1843. doi:10.1021/ef300035p.

[100] E.L. Nordgård, G. Sørland, J. Sjöblom, Behavior of asphaltene model compounds at W/O interfaces, Langmuir. 26 (2010) 2352–2360. doi:10.1021/la902801c.

[101] E.L. Nordgård, J. Sjöblom, Isoprenoid tetraacids. Part I: synthesis and interfacial activities, J. Dispers. Sci. Technol. 29 (2008) 1114–1122. doi:10.1080/01932690701817818.

[102] E.L. Nordgåd, E. Landsem, J. Sjöblom, Langmuir films of asphaltene model compounds and their fluorescent properties, Langmuir. 24 (2008) 8742–8751. doi:10.1021/la800945m.

[103] D. Pradilla, S. Simon, J. Sjöblom, J. Samaniuk, M. Skrzypiec, J. Vermant, Sorption and interfacial rheology study of model asphaltene compounds, Langmuir. (2016) acs.langmuir.6b00195. doi:10.1021/acs.langmuir.6b00195.

[104] P. Dynarowicz-Łątka, A. Dhanabalan, O.N. Oliveira, Modern physicochemical research on Langmuir monolayers, Adv. Colloid Interface Sci. 91 (2001) 221–293. doi:10.1016/S0001-8686(99)00034-2.

[105] J. Wang, N. Van Der Tuuk Opedal, Q. Lu, Z. Xu, H. Zeng, J. Sjöblom, Probing molecular interactions of an asphaltene model compound in organic solvents using a surface forces apparatus (SFA), Energy and Fuels. 26 (2012) 2591–2599. doi:10.1021/ef201366y.

[106] J. Wang, Q. Lu, D. Harbottle, J. Sjoblom, Z. Xu, H. Zeng, Molecular interactions of a polyaromatic surfactant C5Pe in aqueous solutions studied by a surface forces apparatus, J. Phys. Chem. B. 116 (2012) 11187–11196. doi:10.1021/jp304444d.

[107] V. E. J. W., O. J.Th.G., Theory of the stability of lyophobic colloids, Symp. Stabliity Colloid. Dispersions. (1946) 631–636. doi:10.1038/162315b0.

[108] M. Fossen, H. Kallevik, K.D. Knudsen, J. Sjoblom, Asphaltenes precipitated by a two-step precipitation procedure. 1. Interfacial tension and solvent properties, Energy and

Fuels. 21 (2007) 1030–1037. doi:10.1021/ef060311g.

[109] M. Fossen, J. Sjoblom, H. Kallevik, J. Jakobsson, A new procedure for direct precipitation and fractionation of asphaltenes from crude oil, J. Dispers. Sci. Technol. 28 (2007) 193–197. doi:10.1080/01932690601034415.

[110] V. Nalwaya, V. Tantayakom, P. Piumsomboon, S. Fogler, Studies on asphaltenes through analysis of polar fractions, Ind. Eng. Chem. Res. 38 (1999) 964–972. doi:10.1021/ie9804428.

[111] P. Wattana, H.S. Fogler, A. Yen, M. Del Carmen Garcia, L. Carbognani, Characterization of polarity-based asphaltene subfractions, Energy and Fuels. 19 (2005) 101–110. doi:10.1021/ef0499372.

[112] D. Fenistein, L. Barre, Experimental measurement of the mass distribution of petroleum asphaltene aggregates using ultracentrifugation and small-angle X-ray scattering, Fuel. 80 (2001) 283–287. doi:10.1016/S0016-2361(00)00072-7.

[113] L. Barré, S. Simon, T. Palermo, Solution properties of asphaltenes, Langmuir. 24 (2008) 3709–3717. doi:10.1021/la702611s.

[114] F. Yang, P. Tchoukov, E. Pensini, T. Dabros, J. Czarnecki, J. Masliyah, et al., Asphaltene subfractions responsible for stabilizing water-in-crude oil emulsions. Part 1: interfacial behaviors, Energy and Fuels. 28 (2014) 6897–6904. doi:10.1021/ef501826g.

[115] F. Yang, P. Tchoukov, H. Dettman, R.B. Teklebrhan, L. Liu, T. Dabros, et al., Asphaltene subfractions responsible for stabilizing water-in-crude oil emulsions. Part 2: molecular representations and molecular dynamics simulations, Energy and Fuels. 29 (2015) 4783–4794. doi:10.1021/acs.energyfuels.5b00657.

[116] L. Øgendal, Light Scattering: A brief introduction, (2015) 45. http://igm.fys.ku.dk/~lho/personal/lho/LS_brief_intro.pdf.

[117] W. Technolog, Understanding multi-angle static light scattering, http://www.wyatt.com/library/theory/understanding-multi-angle-static-light-scattering.html. (accessed March 20, 2016).

[118] B.H. Zimm, Apparatus and methods for measurement and interpretation of the angular variation of light scattering; preliminary results on polystyrene solutions, J. Chem. Phys. 16 (1948) 1099. doi:10.1063/1.1746740.

[119] D. Some, Light-scattering-based analysis of biomolecular interactions, Biophys. Rev. 5 (2013) 147–158. doi:10.1007/s12551-013-0107-1.

[120] S.R. Forrest, T.A. Witten, Long-range correlations in smoke-particle aggregates, J. Phys. A. Math. Gen. 12 (1979) L109–L117. doi:10.1088/0305-4470/12/5/008.

[121] J.L. Burns, Y. Yan, G.J. Jameson, S. Biggs, A light scattering study of the fractal aggregation behavior of a model colloidal system, Langmuir. 13 (1997) 6413–6420. doi:10.1021/la970303f.

[122] A.Y. Kim, J.C. Berg, Fractal aggregation: Scaling of fractal dimension with stability ratio, Langmuir. 16 (2000) 2101–2104. doi:10.1021/la990841n.

[123] Y.G. Burya, I.K. Yudin, V. a Dechabo, M. a Anisimov, Colloidal properties of crude oils studied by dynamic light scattering, Int. J. Thermophys. 22 (2001) 1397–1410. doi:10.1023/A:1012888819743.

[124] I.K. Yudin, G.L. Nikolaenko, V.I. Kosov, V. a. Agayan, M. a. Anisimov, J. V. Sengers, A compact photon-correlation spectrometer for research and education, Int. J. Thermophys. 18 (1997) 1237–1248. doi:10.1007/BF02575258.

[125] L.S. Uhlenbeck,G.E.; Ornstein, On the theory of the Fermi-liquid, Phys. Rev. 36 (1930) 823-841.

[126] A. Einstein, On the movement of small particles suspended in stationary liquids required by the molecular-kinetic theory of heat, Ann. Phys. 322 (1905) 549–560. doi:10.1002/andp.19053220806.

[127] N. De Jaeger, R. Sneyers, E. Gelad, Particle sizing by photon correlation spectroscopy. Part III: Mono and bimodal distributions and data analysis, Part. Part. Syst. Charact. 9 (1992) 125–137.

[128] H. Ruf, Data accuracy and resolution in particle sizing by dynamic light scattering, Adv. Colloid Interface Sci. 46 (1993) 333–342. doi:10.1016/0001-8686(93)80047-F.

[129] U. Kätzel, Dynamic light scattering for the characterization of polydisperse fractal systems by the example of pyrogenic silica, Thesis. (2007). http://nbn-resolving.de/urn:nbn:de:swb:14-1197634640783-66357.

[130] S.W. Provencher, P. Štêpánek, Global analysis of dynamic light scattering autocorrelation functions, Part. Part. Syst. Charact. 13 (1996) 291–294. doi:10.1002/ppsc.19960130507.

[131] S.W. Provencher, A constrained regularization method for inverting data represented by linear algebraic or integral equations, Comput. Phys. Commun. 27 (1982) 213–227. doi:10.1016/0010-4655(82)90173-4.

[132] S.W. Provencher, CONTIN: A general purpose constrained regularization program for inverting noisy linear algebraic and integral equations, Comput. Phys. Commun. 27 (1982) 229–242. doi:10.1016/0010-4655(82)90174-6.

[133] K. Schätzel, Suppression of multiple scattering by photon cross-correlation techniques, J. Mod. Opt. 38 (1991) 1849–1865. doi:10.1080/09500349114551951.

[134] M.W. Holman, R. Liu, D.M. Adams, Single-molecule spectroscopy of interfacial electron transfer, J. Am. Chem. Soc. 125 (2003) 12649–12654. doi:10.1021/ja0343104.

[135] R.E. Maples, Petroleum refinery process economics (2nd Edition), PennWell, 2000. https://app.knovel.com/web/toc.v/cid:kpPRPEE001/viewerType:toc/root_slug:petroleum-refinery-process/url_slug:petroleum-refinery-process?b-cat-name=Oil %26 Gas Engineering&b-cat-slug=oil-gas-engineering&b-cat-id=203&b-topic-name=Refining %26

Other Processing&b-topic-slug=refining-other-processing&b-order-by=name&b-sort-by=ascending&b-off-set=0&b-filter-by=all-content&b-sub-cat-id=110 (accessed April 18, 2016).

[136] K. Takahashi, H. Kato, S. Kinugasa, Development of a standard method for nanoparticle sizing by using the angular dependence of dynamic light scattering, Anal. Sci. 27 (2011) 751.

[137] S. Gao, J. Shen, J.C. Thomas, Z. Yin, X. Wang, Y. Wang, et al., Effect of scattering angle error on particle size determination by multiangle dynamic light scattering, Applied Optics. 54 (2015) 2824-2831.

[138] M.A. Anisimov, Y.M. Ganeeva, E.E. Gorodetskii, V.A. Deshabo, V.I. Kosov, V.N. Kuryakov, et al., Effects of resins on aggregation and stability of asphaltenes, Energy and Fuels. 28 (2014) 6200–6209. doi:dx.doi.org/10.1021/ef501145a.

[139] A.S. Almusallam, M. Shaaban, K. Nettem, M. a. Fahim, Delayed aggregation of asphaltenes in the presence of alcohols by dynamic light scattering, J. Dispers. Sci. Technol. 34 (2013) 809–817. doi:10.1080/01932691.2012.704737.

[140] P.M. Spiecker, K.L. Gawrys, C.B. Trail, P.K. Kilpatrick, Effects of petroleum resins on asphaltene aggregation and water-in-oil emulsion formation, Colloids Surfaces A Physicochem. Eng. Asp. 220 (2003) 9–27. doi:10.1016/S0927-7757(03)00079-7.

[141] C.R. Martinez, B.L. Iverson, Rethinking the term “pi-stacking,” Chem. Sci. 3 (2012) 2191. doi:10.1039/c2sc20045g.

[142] S.M. Hashmi, A. Firoozabadi, Self-assembly of resins and asphaltenes facilitates asphaltene dissolution by an organic acid, J. Colloid Interface Sci. 394 (2013) 115–123. doi:10.1016/j.jcis.2012.11.069.

[143] L. Goual, A. Firoozabadi, Effect of Resins and DBSA on Asphaltene Precipitation from Petroleum Fluids, AIChE J. 50 (2004) 470–479. doi:10.1002/aic.10041.

[144] T.J. Kaminski, H.S. Fogler, N. Wolf, P. Wattana, A. Mairal, Classification of asphaltenes via fractionation and the effect of heteroatom content on dissolution kinetics, Energy and Fuels. 14 (2000) 25–30. doi:10.1021/ef990111n.

[145] H.H. Ibrahim, R.O. Idem, Interrelationships between asphaltene precipitation inhibitor effectiveness, asphaltenes characteristics, and precipitation behavior during n-heptane (light paraffin hydrocarbon) -induced asphaltene precipitation, Energy and Fuels. (2004) 1038–1048. doi:10.1021/ef0340460.

[146] L. Goual, A. Firoozabadi, Effect of resins and DBSA on asphaltene precipitation from petroleum fluids, AIChE J. 50 (2004) 470–479. doi:10.1002/aic.10041.

[147] D. Wei, E. Orlandi, S. Simon, J. Sjoblom, M. Suurkuusk, Interactions between asphaltenes and alkylbenzene-derived inhibitors investigated by isothermal titration calorimetry, J. Therm. Anal. Calorim. 120 (2015) 1835–1846. doi:10.1007/s10973-015-4542-z.

[148] L. Goual, M. Sedghi, Role of ion-pair interactions on asphaltene stabilization by alkylbenzenesulfonic acids, J. Colloid Interface Sci. 440 (2015) 23–31. doi:10.1016/j.jcis.2014.10.043.

[149] E. Rogel, O. Leo, Study of the adsorption of alkyl-benzene-derived amphiphiles on an asphaltene surface using molecular dynamics simulations, Energy and Fuels. (2001) 1077–1086.

[150] S.M. Hashmi, K.X. Zhong, A. Firoozabadi, Acid–base chemistry enables reversible colloid-to-solution transition of asphaltenes in non-polar systems, Soft Matter. 8 (2012) 8778-8785. doi:10.1039/c2sm26003d.

[151] L. Liu, J. Sjoblom, Z. Xu, Nanoaggregation of polyaromatic compounds probed by electrospray ionization mass spectrometry, Energy and Fuels. 30 (2016) 3742–3751. doi:10.1021/acs.energyfuels.5b02390.

[152] S. Subramanian, S. Simon, B. Gao, J. Sjöblom, Asphaltene fractionation based on adsorption onto calcium carbonate: Part 1: Characterization of sub-fractions and QCM-measurements, Colloids Surfaces A Physicochem. Eng. Asp. 495 (2016) 136–148. doi:10.1016/j.colsurfa.2016.02.011.